

PERFORMANCE ANALYSIS OF A TURBO-TYPE  
ENERGY ABSORBER FOR AN AIRCRAFT  
CARRIER ARRESTING GEAR

Leo Stanley Rolek



# United States Naval Postgraduate School



## THESIS

PERFORMANCE ANALYSIS OF A TURBO-TYPE ENERGY  
ABSORBER FOR AN AIRCRAFT CARRIER ARRESTING GEAR

by

Leo Stanley Rolek, Jr.

7140751

June 1971

*Approved for public release; distribution unlimited.*

LIBRARY

NAVAL POSTGRADUATE SCHOOL

MONTEREY, CALIF. 93940

Performance Analysis of a Turbo-Type Energy  
Absorber for an Aircraft Carrier Arresting Gear

by

Leo Stanley Rolek, Jr.  
Ensign, United States Navy  
B.S.A.E., United States Naval Academy, 1970

Submitted in partial fulfillment of the  
requirements for the degree of

MASTER OF SCIENCE IN AERONAUTICAL ENGINEERING

from the

NAVAL POSTGRADUATE SCHOOL  
June 1971



## ABSTRACT

The increasing weight and speed of carrier based aircraft are taxing the limit of conventional piston type energy absorbers which are used for arresting gear. Turbo-type absorbers have been proposed as an alternative. This study investigates a turbo-type energy absorber for an aircraft arresting gear under development by the Naval Air Engineering Center. A mathematical analysis, computer simulation and performance prediction are given for each mode of operation. It was initially expected that the absorber could operate in just two modes, forward and reverse, but the analysis shows that four distinct modes are possible, since not only shaft rotation but the path of fluid flow can be reversed. Theoretical performance predictions are also compared with test data from an existing smaller scale version of the absorber. The agreement is excellent. An approximation of scaling effects on power absorption is also presented. It is concluded that the turbo-type absorber is basically adequate to meet the demands of carrier operation for the foreseeable future.





## TABLE OF CONTENTS

I.	INTRODUCTION - - - - -	12
II.	DESIGN VALUES AND CONSIDERATIONS - - - - -	15
III.	ANALYSIS OF THE PROBLEM - - - - -	21
	A. MODES OF OPERATION - - - - -	21
	B. DIMENSIONAL ANALYSIS - - - - -	29
	C. ENERGY BALANCE AT EQUILIBRIUM - - - - -	31
	D. MODEL TESTING - - - - -	34
	E. ASSUMPTIONS AND LIMITATIONS OF THE ANALYSIS - - - - -	35
IV.	RESULTS AND DISCUSSION - - - - -	38
V.	CONCLUSIONS AND RECOMMENDATIONS - - - - -	47
APPENDIX A	Detailed Analysis of the Energy Absorber with the Fluid Circulating in the Normal Direction, Mode 1 and 2 - - - - -	48
APPENDIX B	Detailed Analysis of the Energy Absorber with the Fluid Circulating in the Reverse Direction, Modes 1 and 2 - - - - -	82
APPENDIX C	Program NORMAL - - - - -	88
APPENDIX D	Program REVERSE - - - - -	110
	LIST OF REFERENCES - - - - -	129
	INITIAL DISTRIBUTION LIST - - - - -	130
	FORM DD 1473 - - - - -	131



# LIST OF TABLES

Table		Page
I	Parameters of the Absorber - - - - -	18
II	Modes of Operation - - - - -	21
III	Detailed List of Results for All Modes of the Absorber - - - - -	42
IV	Flow Chart for Computer Programs NORMAL and REVERSE - - - - -	90



# LIST OF FIGURES

Figure		Page
1.	Overall Schematic, Programmed Drum Arresting Gear - - -	14
2.	Schematic of Energy Absorber - - - - -	16
3.	Diagram of Absorber Bladings - - - - -	17
4.	Velocity Diagrams for Mode 1 - - - - -	23
5.	Velocity Diagrams for Mode 2 - - - - -	24
6.	Velocity Diagrams for Mode 3 - - - - -	25
7.	Velocity Diagrams for Mode 4 - - - - -	26
8.	Total Enthalpy-Entropy Diagram for Modes 1 and 2 - - -	27
9.	Total Enthalpy-Entropy Diagram for Modes 3 and 4 - - -	28
10.	Energy Balance for Equilibrium for Normal Flow - - - -	32
11.	Energy Balance for Equilibrium for Reverse Flow - - -	33
12.	Power Coefficient versus Rotational Speed - - - - -	39
13.	Power versus Shaft Speed - - - - -	40
14.	Maximum Power Coefficient versus Maximum Reynolds Number - - - - -	41
15.	Estimate of Loss Coefficient $\xi$ - - - - -	75
16.	Estimated Channel Wall Friction Factor $\lambda_f$ - - - - -	77



TABLE OF SYMBOLS

<u>Symbol</u>	<u>FORTTRAN</u>	<u>Definition</u>	<u>Units</u>
<u>Latin</u>			
a	- - - -	Opening at blade exit	ft
b	B	Blade height	ft
$c_f$	CF	Local skin friction coefficient	- - - -
$c_l$	CL	Pressure loss coefficient for lower passage	- - - -
$c_p$	CP	Specific heat of fluid	BTU/lb/°R
$C_u$	CU	Pressure loss coefficient for upper passage	- - - -
$D_h$	- - - -	Hydraulic diameter	ft
h	- - - -	Static enthalpy	ft-lb/slug
H	H	Total head	ft-lb/slug
$H_T$	- - - -	Total enthalpy	ft-lb/slug
$i_R$	IR	Rotor incidence angle	degree
$i_S$	IS	Stator incidence angle	degree
$K_B$	KB	Blockage factor	- - - -
$L_l$	LL	Length of meridional contour of lower passage	ft
$L_u$	LU	Length of meridional contour of upper passage	ft
$\dot{m}$	- - - -	Mass flow rate	slugs/sec
$M_f$	- - - -	Frictional moment	lb-ft
p	SP	Static pressure	lb/ft <sup>2</sup>
$P_E$	- - - -	Equivalent relative total enthalpy	ft <sup>2</sup> /sec <sup>2</sup>





Symbol	FORTTRAN	Definition	Units
$\dot{P}$	-----	Power	lb-ft/sec
$\dot{P}_{ref}$	POWREF	Reference power	lb-ft/sec
$P_T$	TP	Total pressure	lb/ft <sup>2</sup>
$R$	R	Radius	ft
$r_i$	RI	Radius of curvature of inner contour of passage	in
$R_{Ne}$	-----	Effective Reynolds number	-----
$R_{Nl}$	REL	Reynolds number lower passage	-----
$R_{NR}$	RER	Reynolds number rotor	-----
$R_{NS}$	RES	Reynolds number stator	-----
$R_{Nu}$	REU	Reynolds number upper passage	-----
$s$	-----	Blade spacing	ft
$r_o$	-----	Radius of curvature of outer contour of passage	in
$T_R$	TORQUE	Torque exerted on fluid by rotor	lb-ft
$T_{Rref}$	TORREF	Reference torque	lb-ft
$T_S$	-----	Torque exerted on fluid by stator	lb-ft
$u$	-----	Internal energy	ft-lb/slug
$U$	-----	Peripheral velocity of blade	ft/sec
$V$	V	Absolute velocity	ft/sec
$V'$	-----	Useful absolute velocity	ft/sec
$V_M$	VM	Meridional component of absolute velocity	ft/sec
$V_u$	VU	Peripheral component of absolute velocity	ft/sec
$W$	W	Relative velocity	ft/sec
$W'$	-----	Useful relative velocity	ft/sec



<u>Symbol</u>	<u>FORTTRAN</u>	<u>Definition</u>	<u>Units</u>
$W_i$	- - - -	Relative velocity lost due to incidence	ft/sec
$W_u$	WU	Peripheral component of relative velocity	ft/sec
$Y_R$	YR	Rotor blade loss factor	- - - -
$Y_S$	YS	Stator blade loss factor	- - - -
<u>Greek</u>			
$\alpha$	ALPHA	Absolute flow angle	degree
$\alpha_{3B}$	A3B	Tangent to stator blade mean camber line at station 3	degree
$\Lambda_R$	AAR	Aspect ratio of rotor	- - - -
$\Lambda_S$	ARS	Aspect ratio of stator	- - - -
$\alpha_{4B}$	A4B	Tangent to stator blade mean camber line at station 4	degree
$\beta$	BETA	Relative flow angle	degree
$\beta_{1B}$	B1B	Tangent to rotor blade mean camber line at station 1	degree
$\beta_{2B}$	B2B	Tangent to rotor blade mean camber line at station 2	degree
$\Delta$	DEL	Change	- - - -
$\xi_l$	ZETAL	Channel bending loss coefficient for lower passage	- - - -
$\xi_u$	ZETAU	Channel bending loss coefficient for upper passage	- - - -
$\eta_{Mu}$	ETAMU	Friction efficiency for upper passage	- - - -
$\eta_{Ml}$	ETAML	Friction efficiency for lower passage	- - - -
$\eta_R$	- - - -	Rotor efficiency	- - - -



<u>Symbol</u>	<u>FORTTRAN</u>	<u>Definition</u>	<u>Units</u>
$\lambda_f$	LMBD	Wall friction factor in straight ducts	- - - -
$\lambda_l$	LAMDAL	Friction coefficient for lower passage	- - - -
$\lambda_u$	LAMDAU	Friction coefficient for upper passage	- - - -
$\nu$	NU	Kinematic viscosity	ft <sup>2</sup> /sec
$\Pi_H$	- - - -	Dimensionless head	- - - -
$\Pi_P$	PIPOWR	Reference power	lb-ft/sec
$\Pi_T$	PITORQ	Dimensionless Torque	- - - -
$\Pi_\omega$	PIOM	Reference rotational speed	- - - -
$\rho$	RHO	Fluid density	slugs/ft <sup>3</sup>
$\tau_R$	TAUR	Dimensionless torque coefficient	- - - -
$\tau_o$	- - - -	Wall shear stress	lb/ft <sup>2</sup>
$\Phi$	PHI	Flow coefficient used in Program NORMAL	- - - -
$\Phi'$	PHI	Convenient flow coefficient used in program REVERSE	- - - -
$\Psi$	PSI	Velocity coefficient	- - - -
$\omega$	OM	Rotational speed	rad/sec
$\omega_{ref}$	OMREF	Reference rotational speed	rad/sec



## Subscripts

R	Rotor
S	Stator
<i>l</i>	Lower passage
u	Upper passage
o	Outer passage
i	Inner passage
TH	Theoretical
MAX	Maximum value
ref	Reference value
1	Rotor inlet
2	Rotor discharge
3	Stator inlet
4	Stator discharge

## Superscript

'	Useful component
---	------------------





## ACKNOWLEDGEMENTS

The author gratefully acknowledges the assistance provided in this investigation by the following persons:

Professor T. H. Gawain of the Naval Postgraduate School, the thesis advisor, whose understanding and patience made the learning process most gratifying. His insight and guidance insured the worth of this thesis.

Professor Michael H. Vavra of the Naval Postgraduate School who developed the original analysis of the absorber. Without his help and inspiration this thesis would not have been possible.

Mr. Wayne Gallant and the staff of Section SI of the Naval Air Engineering Center in Philadelphia, Pennsylvania. These men kindly provided the background material, supporting information on the M-21 absorber, test data, and the original computer simulation of the analysis. Their full cooperation was most beneficial.



## I. INTRODUCTION

Over the years, the speed, size, and weight of carrier based aircraft have steadily increased, thus demanding an ever larger energy absorption capacity from the shipboard arresting gear. Up to now, design improvements to meet these increasing demands have been limited to mere enlargement of the basic linear hydraulic energy absorber, which has been of the piston type. Modern aircraft, however, have loaded this system to its upper limit, and make any further development along these lines impractical due to weight and space limitations. The need exists for a new concept which will minimize space and weight demands while providing the necessary increase in energy absorption capacity.

The solution proposed involves the use of a turbo-type rotary hydraulic energy absorber. In essence the fluid is put into motion by a suitably designed rotor and is retarded by a stator and by the resistance of the flow passage. The power input to the rotor is absorbed by the hydraulic resistance of the system, and is eventually dissipated as heat.

The energy absorber is directly coupled to a cable storage drum. The drum profile is programmed to match drum rotational velocity to that required for optimum retarder performance. A device of this type was introduced in 1968, and is known as the M-21 energy absorber. The initial design gives satisfactory performance, but is of rather limited capacity, thirty million ft.lbs. Therefore, a program has been undertaken to redesign the absorber to increase the capacity to fifty-five million ft.lbs.



A development program was initiated by the Naval Air Engineering Center (NAEC) (Ref. 1). A full scale test of the programmed drum coupled with the M-21 absorber was conducted to determine the feasibility of the overall concept and to obtain performance data needed in the redesign program. A schematic diagram of the proposed system is shown in Figure 1.

A theoretical approximation of the flow conditions in a machine of this type was derived by Professor Michael H. Vavra (Ref. 2). To facilitate investigation of the effects of various design parameters NAEC formulated a computer program. From the computer analysis, a workable combination of design parameters was chosen such that torque and energy requirements were satisfied at the design point, the condition at which the absorber is expected to perform most often.

Professor Vavra has also been commissioned to develop and test a flow model of the new design. This model will be useful for refining losses, checking for flow separation, and obtaining information that is not available from the mean streamline analysis.

In this paper, a theoretical simulation and performance analysis of the energy absorber in all modes of operation is presented in terms of dimensionless parameters that facilitate comparisons of various designs and interpretation of model tests. The retraction problem is also studied, and preliminary estimates of the power needed to retract the programmed drum are given.

A throttling system is incorporated into the design to aid in arresting aircraft of various sizes. The discussion and analysis presented here are concerned with the condition of open throttle only.



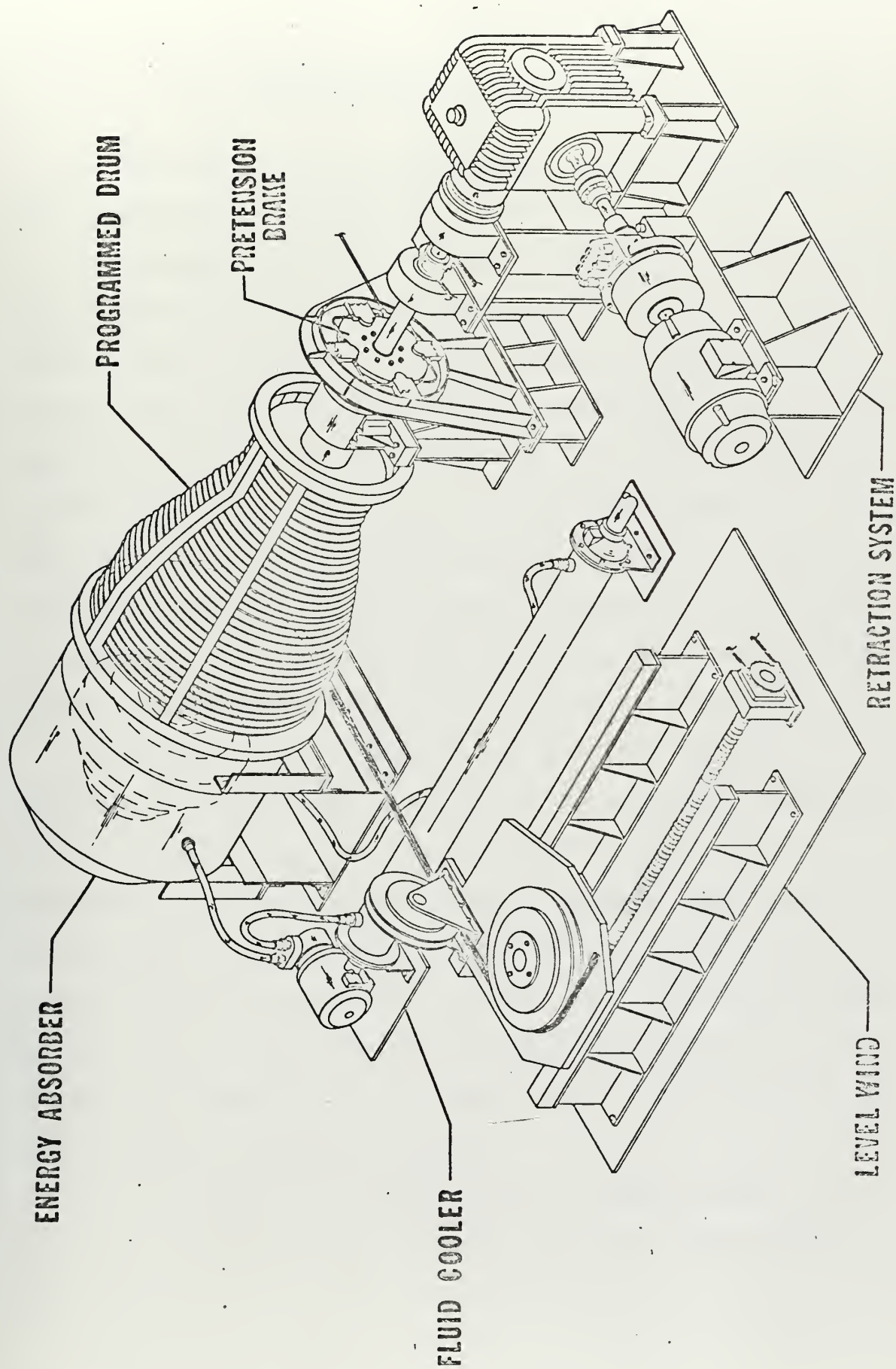


FIGURE I. PROGRAMMED DRUM ARRESTING GEAR







## II. DESIGN VALUES AND CONSIDERATIONS

The main features of the energy absorber design that is analyzed here are summarized in Figures 2 and 3, and Table I.

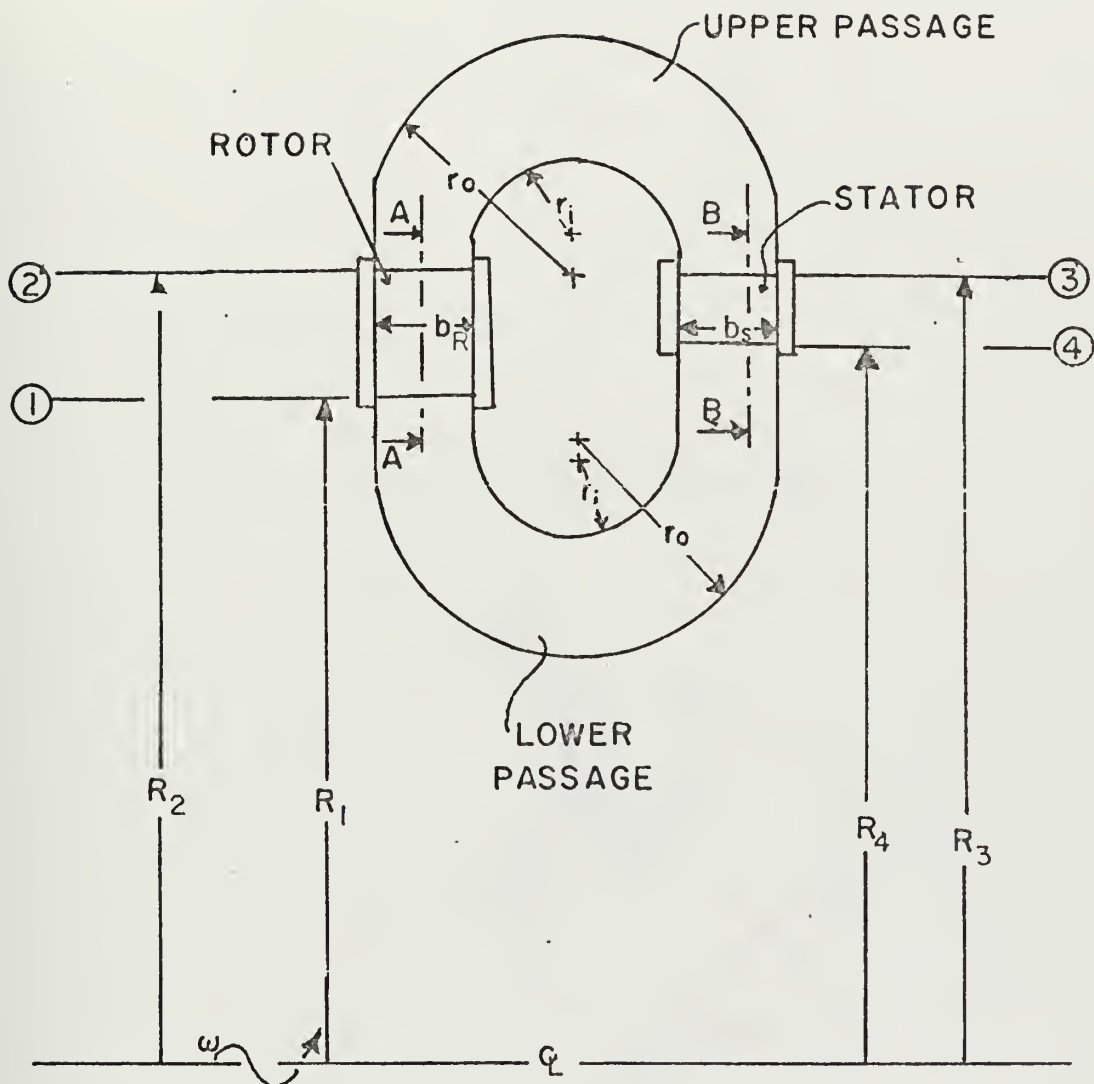
The customary approach in the design of turbomachinery is first to optimize conditions with respect to a single specified design point. The resulting performance over a broad range of off-design conditions is then investigated to determine overall acceptability. The condition at which the absorber is expected to operate most often is naturally chosen as the design point. Specifically, a design torque of 340,000 ft.lbs. is required at a rotational speed of 76 rad./sec.

The maximum rotational speed the cable will impart to the drum, and consequently to the rotor, is about 83 rad./sec. This limit is fixed by the allowable landing speed of the aircraft, and by drum design.

The mechanical power imparted to the rotor is continuously converted to thermal energy of the fluid. The temperature rise of the fluid is significant and imposes a constraint on the design. The temperature limit is the maximum allowable temperature the fluid may attain without causing cavitation. Obviously, heat must be removed to maintain equilibrium conditions. For this reason, provisions are made to bleed off a portion of the circulating fluid continuously and to replace it by fresh cool fluid. During a rapid series of arrests, the cooling problem is especially critical.

The fluid used in the absorber is an ethyl glycol mixture. This fluid is acceptable because it remains usable over a wide range of temperatures.

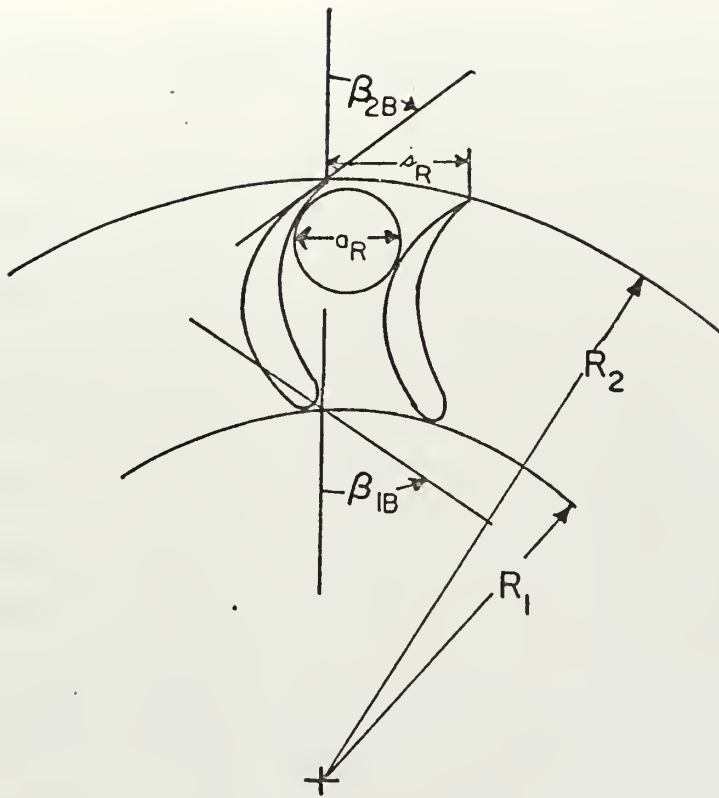




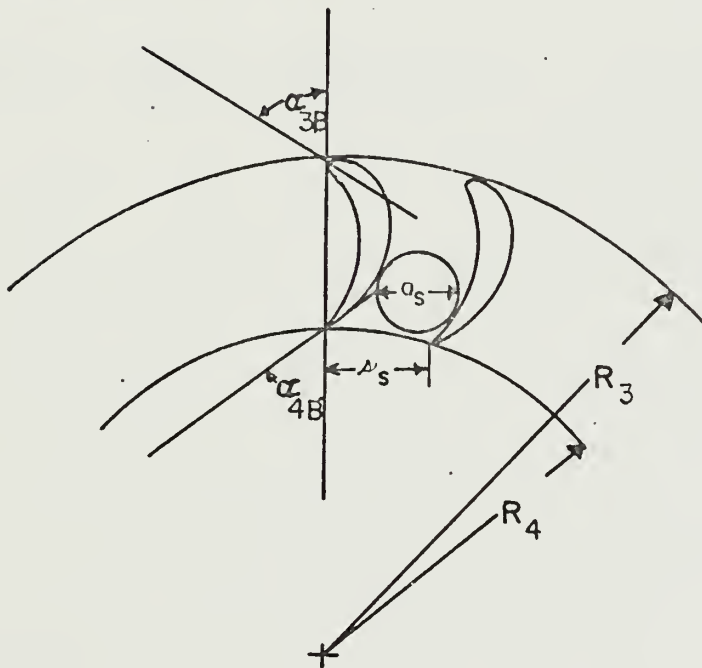
SCHEMATIC DIAGRAM OF ENERGY ABSORBER

FIGURE 2





Section A-A of Figure 2 Through Rotor



Section B-B of Figure 2 Through Stator

Figure 3 DIAGRAM OF ABSORBER BLADING



Table I PARAMETERS OF THE ABSORBER

$$R_1 = 13.61 \text{ inches}$$

$$R_2 = 16.25 \text{ inches}$$

$$R_3 = 16.07 \text{ inches}$$

$$R_4 = 14.93 \text{ inches}$$

$$b_R = 2.02 \text{ inches}$$

$$b_S = 2.02 \text{ inches}$$

$$r_o = 4.18 \text{ inches}$$

$$r_i = 2.02 \text{ inches}$$

$$\frac{(L_{ui} + L_{uo})}{2} = 10.26 \text{ inches}$$

$$\frac{(L_{li} + L_{lo})}{2} = 10.26 \text{ inches}$$

Number of blades for rotor and stator: 72

$$\beta_{1B} = 57^\circ$$

$$\beta_{2B} = 53^\circ$$

$$\alpha_{3B} = 57^\circ$$

$$\alpha_{4B} = 53^\circ$$

$$K_{B1} = .95$$

$$K_{B2} = .87$$

$$K_{B3} = .90$$

$$K_{B4} = .87$$

$$\omega_{MAX} = 83 \text{ rad./sec.}$$

Fluid properties:

$$\rho = 2.095 \text{ slugs/ft.}^2$$

$$c_f = .016$$

$$v = 3.76 \times 10^{-5} \text{ ft.}^2/\text{sec}$$

$$c_p = .7$$





A detailed discussion of the effects of various parameters and loss coefficients is undertaken in the analysis section. A few words, however, are in order here. The radius of curvature  $r_i$  of the inner contour of both the upper and lower passage must not be smaller than the blade height. This insures that the flow does not separate, and it also increases absorption capacity. Estimates of losses in this machine are obtained through various empirical turbomachinery correlations as is shown in the analysis. Enthalpy losses in the passages are significant. Much of this loss is due to the bending of the passage with friction responsible for the remainder. However, a change in the coefficient of friction  $c_f$  which expresses the direct wall friction losses in the passages has little influence on overall performance. A value of  $c_f = 0.016$  was chosen since it gives best agreement with M-21 test data.

The blade shapes first optimized by Professor Vavra from a performance standpoint were found by NAEC to be unacceptable on a stress basis. Blade thickness, spacing and angles were accordingly revised by NAEC, and a blade of sufficient strength was found; its characteristics are listed in Table 1.

The reliability of this analysis can only be judged experimentally by correlation with test data. The theory correlates very well with actual test results on the M-21 design. From this it appears that the theoretical analysis is reasonable and that the new design should be workable, if not optimum.

Naval carrier operations often require a series of rapid and repeated arrests. The drum must be retracted thus reversing the



rotational direction of the rotor. This process is investigated to obtain preliminary estimates of the power required to retract the absorber.



### III. ANALYSIS OF THE PROBLEM

#### A. MODES OF OPERATION

The energy absorber is capable of operation in four modes. These modes are summarized in Table II.

Table II MODES OF OPERATION

<u>Flow Direction</u>	<u>Shaft Rotation</u>	
	Normal	Reverse
Normal	Mode 1	Mode 2
Reverse	Mode 3	Mode 4

Mode 1 corresponds to design point conditions. In this mode, the fluid passes successively through stations 1, 2, 3, 4 and back to 1, in that order. Note that the flow leaving the rotor at station 2 is moving radially outward. See Figures 2 and 3. For fluid circulation in this sense, conditions at stations 2 and 4 are particularly significant. At the rotor exit, station 2, the direction of the flow with respect to the rotor, is assumed to remain constant at all flow rates. At stator exit, station 4, the direction of the flow with respect to the stator is likewise assumed to remain constant. While this assumption of fixed relative and absolute flow directions is not exact, it represents an excellent approximation when the blades are closely spaced as in the present design.

In Mode 2, the sense of the fluid circulation is exactly as described above. However, the direction of shaft rotation is reversed.



Naturally, stations 2 and 4 are still governing in the sense that flow directions at these stations are known.

In Mode 3, the shaft rotation is the same as for Mode 1, but the direction of fluid circulation is reversed. Consequently, the fluid passes successively through stations 2, 1, 4, 3 and back to 1, in that order. Note that the rotor exit is now at station 1, and the direction of flow at this station is radially inward. In this case, stations 1 and 3, are controlling. The relative flow direction at rotor exit, station 1, and the absolute flow direction at stator exit, station 3, are now assumed to remain fixed.

In Mode 4, the sense of fluid circulation is the same as in Mode 3, but the direction of shaft rotation is reversed. Of course, stations 1 and 3 still govern flow direction as in the previous case.

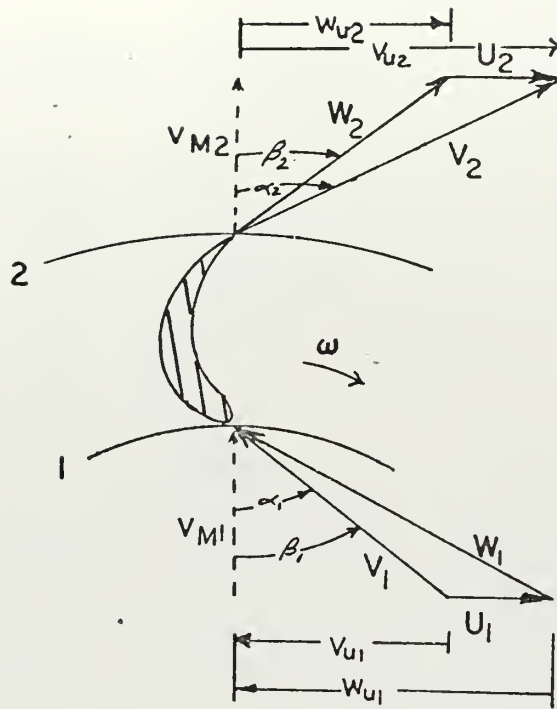
The same set of equations describe Modes 1 and 2, but a separate set of equations is needed to describe the reverse flow Modes, 3 and 4. Note that only two sets of equations are needed for the four Modes, and each set is governed by the flow direction relative to the blade exits. Two separate computer programs are needed since one program will be used to solve each set of equations. Program Normal finds the solution for Modes 1 and 2, and program Reverse finds the solution for Modes 3 and 4. Both programs will be discussed in the appendix. All quantities and results discussed throughout the paper are obtained from these programs.

The velocity diagrams for each mode are presented in Figures 4, 5, 6, and 7. All angles and velocities are drawn to scale.

The thermodynamic processes in the absorber are shown on the enthalpy-entropy diagrams, Figures 8 and 9. The process for normal







Scale: 0.5 inch = 100 ft/sec

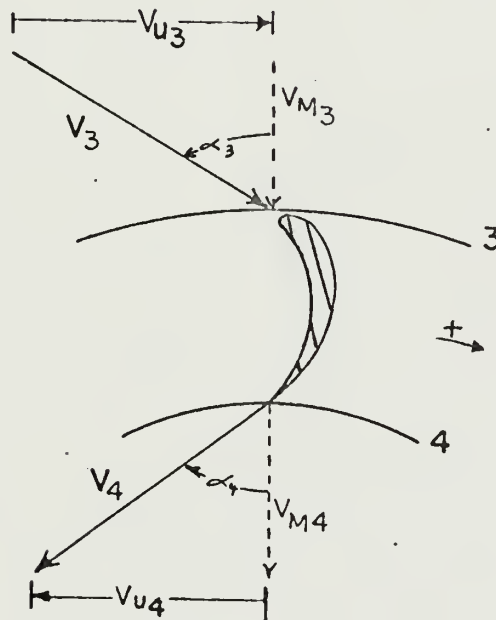
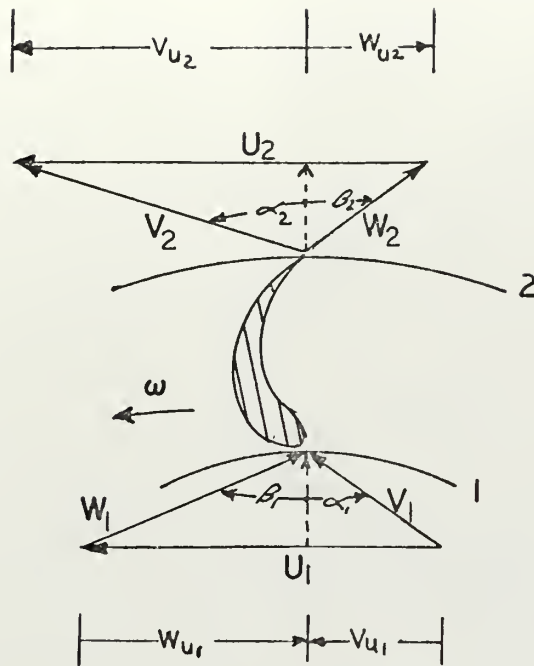


Figure 4 Velocity Diagrams for Mode 1 Operation at

$$R_{Ne} = \frac{\omega_{MAX} R_2^2}{v} = 4.8 \times 10^6$$





Scale: 0.5 inch = 25 ft/sec

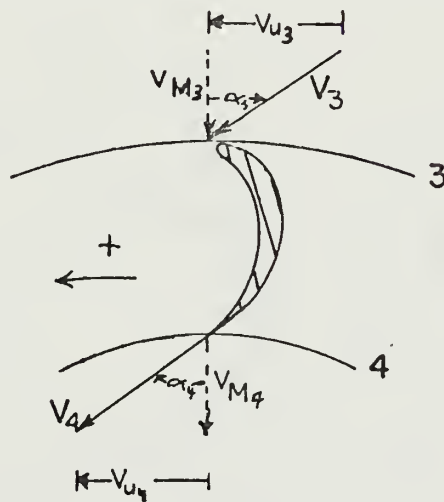
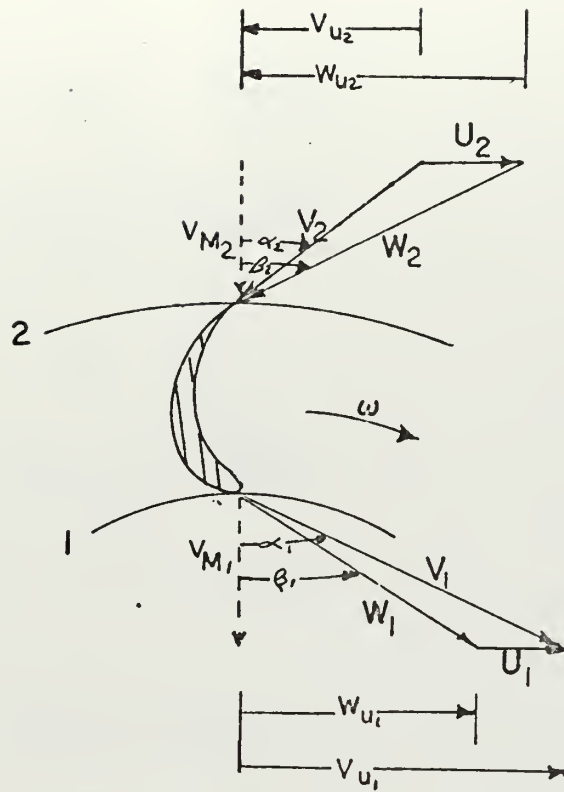


Figure 5 Velocity Diagrams for Mode 2 Operation at

$$R_{Ne} = \frac{\omega_{MAX} R_2^2}{v} = 4.8 \times 10^6$$





Scale: 0.5 inch = 100 ft/sec

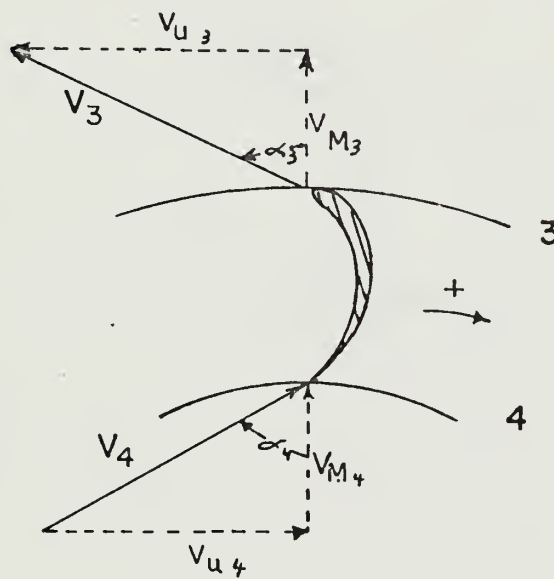
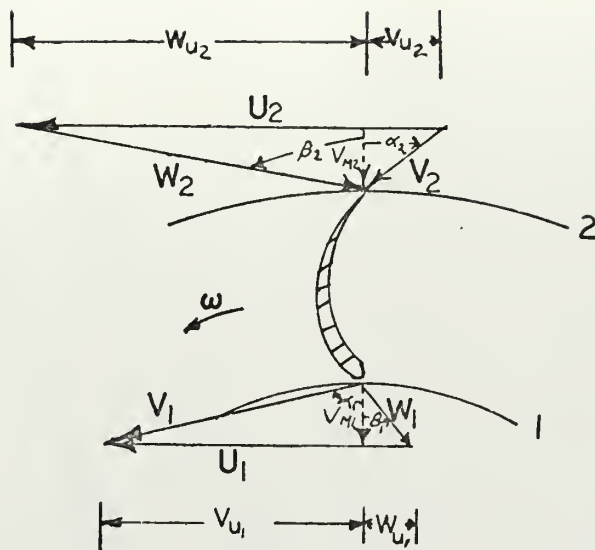


Figure 6 Velocity Diagrams for Mode 3 Operation at

$$R_{Ne} = \frac{\omega_{MAX} R_2^2}{v} = 4.8 \times 10^6$$





Scale: 0.5 inch = 25 ft/sec

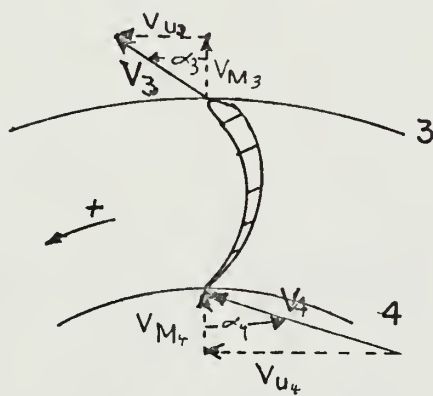


Figure 7 Velocity Diagrams for Mode 4 Operation at

$$R_{Ne} = \frac{\omega_{MAX} R_2^2}{\nu} = 4.8 \times 10^6$$





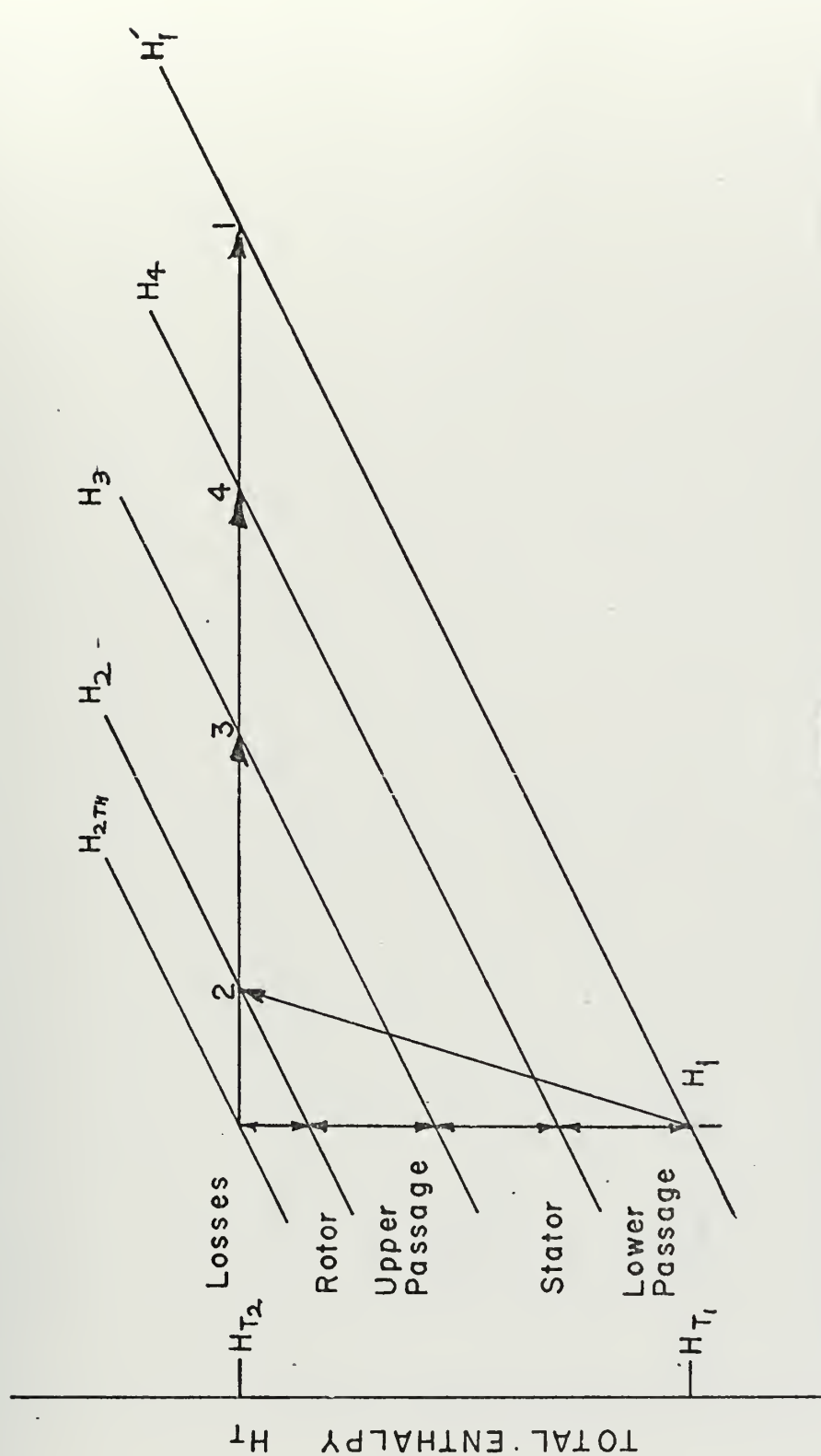


Figure 8 Total Enthalpy-Entropy Diagram of the Thermodynamic Process in the Absorber for Normal Circulation, Modes 1 and 2







circulation, Modes 1 or 2, is shown in Figure 8, while that for reverse circulation, Modes 3 or 4, is shown in Figure 9. The direction of shaft rotation affects the exact quantitative enthalpy values. The graphs, however, are merely qualitative.

A "total head"  $H$  (per unit mass) is used which differs from the standard total enthalpy  $H_T$ . This is discussed in greater depth in the analysis section, but a few words are needed at this point to clarify the discussion.

The fluid is considered incompressible which allows the thermal and mechanical effects to be uncoupled. A "total head" is conveniently defined as

$$H = \frac{P_T}{\rho} = \frac{p}{\rho} + \frac{v^2}{2}$$

Henceforth  $H$  is referred to simply as head. The head and total enthalpy are linked by the simple relation

$$H = H_T - u$$

where  $u$  represents internal energy per unit mass.

## B. DIMENSIONAL ANALYSIS

Results are presented in terms of appropriate dimensionless quantities. The use of non-dimensional terms simplifies the correlation of data, the comparison of various designs, and the interpretation of model tests.

The three quantities chosen as consistent dimensional reference parameters are the radius of the rotor outlet  $R_2$ , the fluid density  $\rho$ , and the shaft rotational speed  $\omega$  or  $\omega_{MAX}$ , whichever is appropriate.



Using these parameters, one defines the effective Reynolds number for this design to be

$$R_{N_e} = \frac{\omega R_2^2}{\nu}$$

where  $\nu$  is the kinematic viscosity. And the dimensionless total head is

$$\Pi_H = \frac{H}{\omega^2 R_2^2}$$

In the discussion of results, it is convenient to define the flow coefficient  $\Phi$  in the following specific way, namely,

$$\Phi = \frac{|V_{M2}|}{\omega R_2}$$

where the algebraic signs of  $\omega$  and  $\Phi$  are always positive for normal shaft rotation and negative for reversed shaft rotation. This sign convention for shaft rotation is maintained regardless of the direction of the fluid circulation, hence the use of the absolute magnitude  $|V_{M2}|$  in the definition.

In the actual computer programs NORMAL and REVERSE, however, somewhat different sign conventions are more convenient. All equations are written in such a way that the three quantities  $V_{M2}$ ,  $\omega R_2$  and  $\Phi$  are always positive. For this reason the four modes are computed as separate cases.

For comparison of various modes and designs the dimensionless torque, power and rotational speed coefficients are respectively

$$\Pi_T = \frac{T_R}{\omega_{MAX}^2 R_2^5 \rho}$$





$$\Pi_{\phi} = \frac{\rho}{\omega_{MAX}^3 R_2^5}$$

$$\Pi_{\omega} = \frac{\omega}{\omega_{MAX}}$$

The detailed analysis considered later also uses various dimensionless quantities for convenience in the derivations. The parameters used to facilitate the non-dimensionalization in that case are not necessarily the same as introduced in the present section, and the separate cases should not be confused.

### C. ENERGY BALANCE AT EQUILIBRIUM

In general the rotor adds energy to the fluid. In traveling through the passages and returning to its initial state the fluid dissipates this mechanical energy through various losses. Under equilibrium these losses exactly cancel the original energy input.

It turns out that the energy input of the rotor can be expressed in terms of the flow coefficient  $\phi$  in the form

$$\Delta H_{IN} = A + B \phi$$

where A and B are true constants. The losses can be expressed as

$$\Sigma \Delta H_{LOSS} = A' + B' \phi + C' \phi^2$$

where A', B', and C' may be considered constant to a first approximation. Actually these quantities are weak functions of  $\phi$ , a fact which must be considered in the exact solution. The energy relations which fix the equilibrium state are shown in Figures 10 and 11. Figure 10 represents the two modes which correspond to normal flow direction.



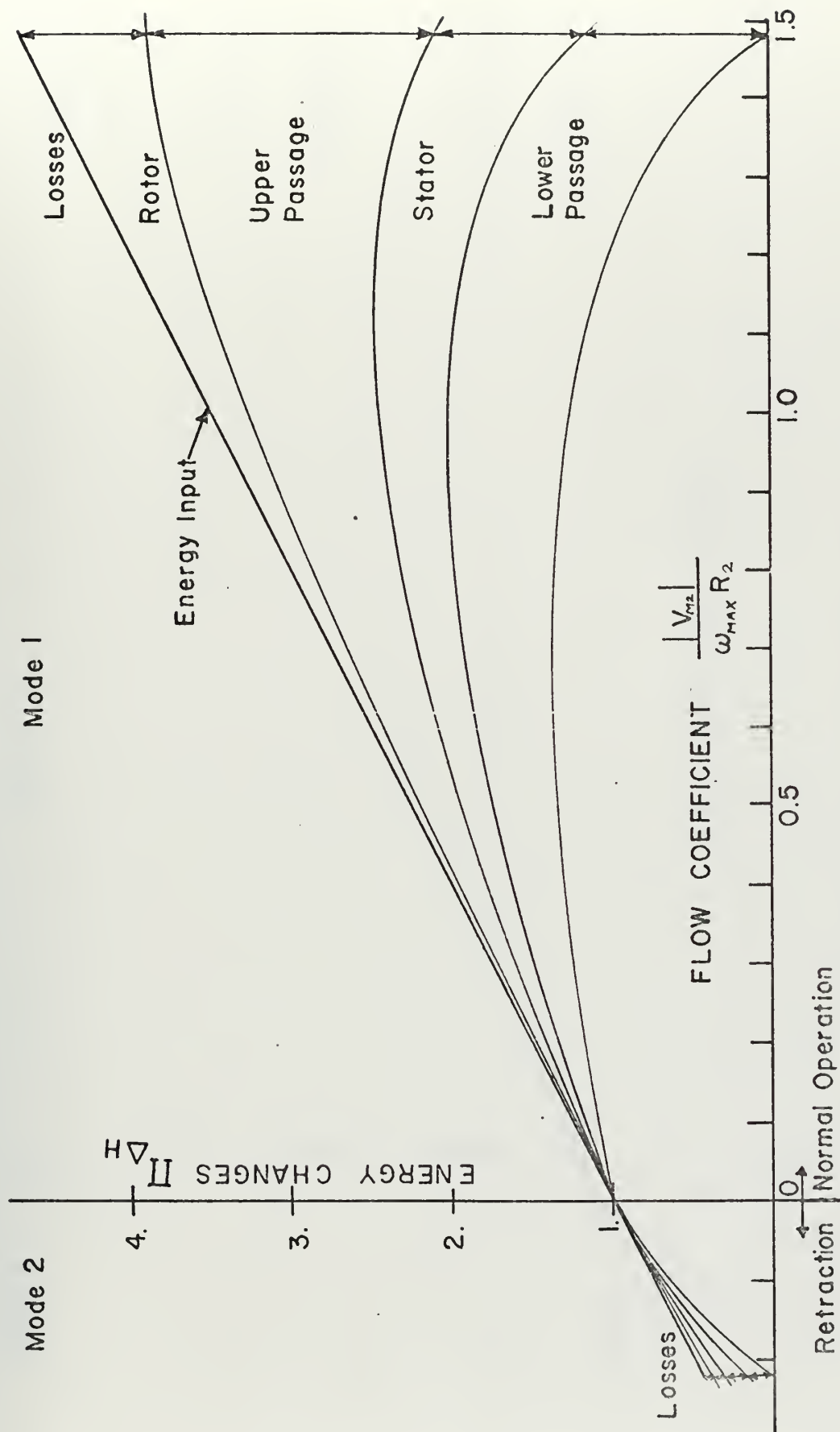


Figure 10 The Energy Balance for Equilibrium Under the Conditions

$$\text{of Normal Circulation at } R_{Ne} = \frac{w_{MAX} R_2^2}{v} = 4.8 \times 10^6$$



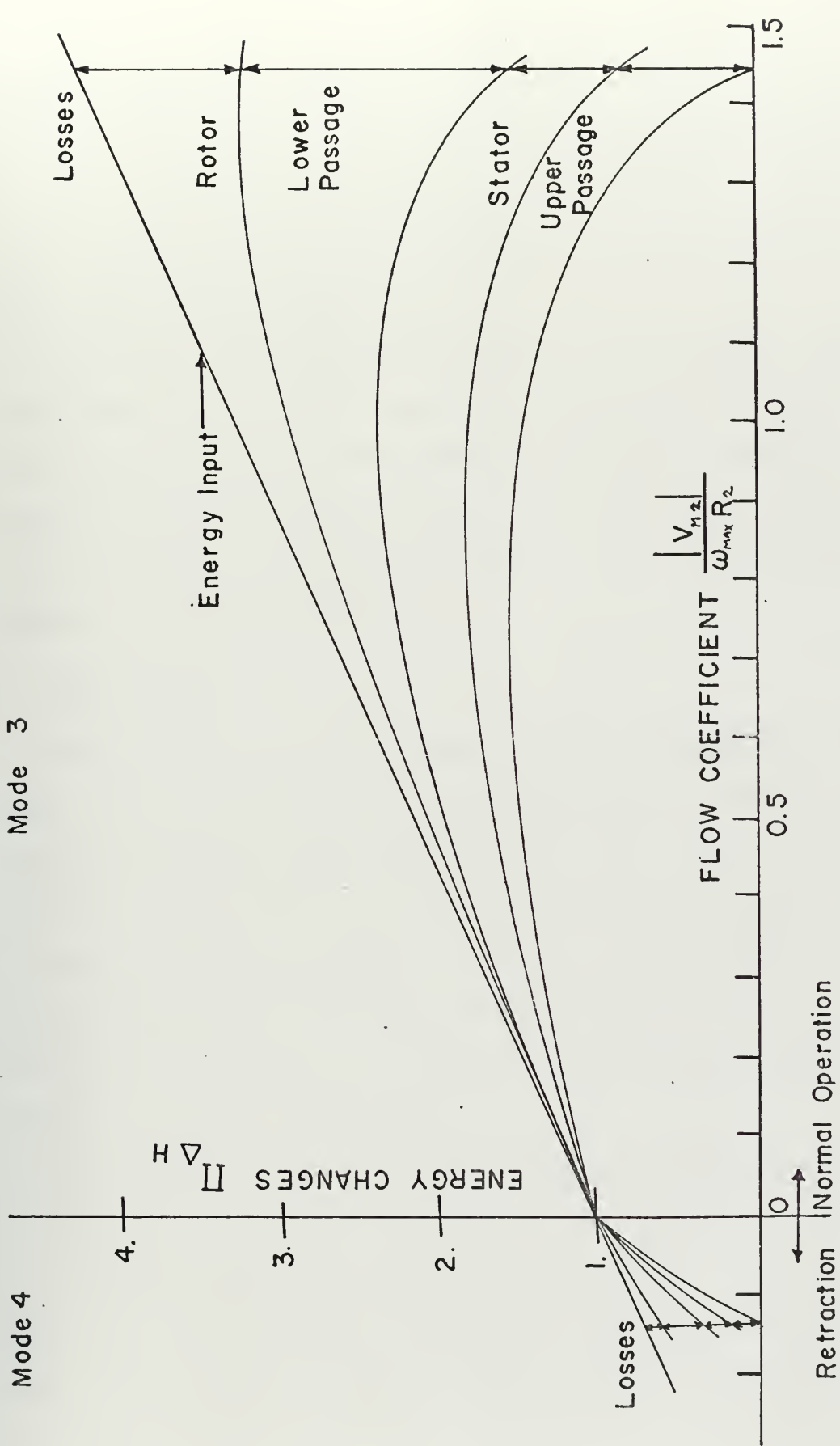


Figure 11 The Energy Balance for Equilibrium Under the Conditions

$$\text{of Reverse Circulation at } R_{Ne} = \frac{\omega_{MAX} R_2^2}{v} = 4.8 \times 10^6$$



Figure 11 shows the two modes for reverse flow. These results are drawn to scale, except that the parabolic lines are only approximate. The final equilibrium points, where the losses balance the energy input, however, and the relative distribution of losses at these points are in correct scale.

Initially, it was thought that only two of the above four modes would prove to be physically possible, one corresponding to normal shaft rotation, the other corresponding to retraction. Surprisingly enough, the present analysis has demonstrated that operation in all four of the modes is theoretically possible. This point is clearly indicated in Figures 10 and 11.

#### D. MODEL TESTING

Professor Vavra has proposed that a model testing program be undertaken. The model will not be a true dynamic model, but will be a purely static device that uses air as the working fluid. Construction of the model will constrain the air flow to the normal direction only. However, the scale model should be useful in checking for flow separation through the passages and refining the loss coefficients for the analysis of the absorber. The effects of the tangential component of velocity will also be investigated.

The discussion of the above static model is not within the scope of this thesis. However, a hypothetical model is considered which is a true dynamic model of the actual full scale device. The size of the hypothetical model is taken as identical to that of the static model. The model is scaled to 0.569 of the size of the actual absorber. In both cases the fluid is air. When expressed in dimensionless terms,





the performance of the hypothetical model is basically the same as that of the full scale machine, except for Reynolds number effects. The full scale machine operates at a maximum Reynolds number, as defined above, of  $4.88 \times 10^6$  while the maximum Reynolds number of the model is  $3.70 \times 10^5$ . The results for this model are presented along with the results for the real absorber.

#### E. ASSUMPTIONS AND LIMITATIONS OF THE ANALYSIS

A one-dimensional mean streamline analysis is obviously only a crude approximation of the actual performance of any turbomachine, but is a starting point necessary in most development programs. The validity of the assumptions used are very important to the reliability of the analysis. The primary assumptions used in this report are summarized below.

The fluid is treated as incompressible. This assumption is excellent as long as the provisions to maintain the fluid at a temperature lower than the cavitation temperature are adequate. This conveniently uncouples mechanical and thermal effects and allows a form of "total head"  $H$  to be defined which is independent of internal energy.

If the velocity distribution across every section were truly uniform, the meridional component  $V_{M_{TH}}$  at the mean streamline could be computed simply from a continuity relation of the form

$$V_{M_{TH}} = \frac{Q}{A_M}$$

where  $Q$  is the volumetric flow rate and  $A_M$  is the meridional cross-section area. The actual velocity distribution, however, is non-



uniform because of the effect of streamline curvature, boundary layers and so on. To allow for these effects, approximately, the actual meridional velocity  $V_M$  is assumed to be governed by a relation of the form

$$V_M = K_B \frac{Q}{A_M}$$

where the so-called blockage factor  $K_B$  is treated as a constant. The blockage factors were extrapolated from M-21 test data. Their reliability in the reverse flow modes is doubtful, however, since all test data were obtained only from Mode 1 operation. An extension of these data to all modes would be very useful.

The present analysis treats operation of the absorber as a steady state phenomenon. Strictly speaking, the operation is actually unsteady. However, the arrest and retraction processes require a sufficient number of drum revolutions that the steady state assumption provides a fair approximation.

A major assumption is that the relative flow direction at the rotor outlet and the absolute flow direction at the stator outlet are constant. For the case of normal flow this is an excellent approximation. However, the validity is reduced for the reverse flow modes. In Modes 3 and 4, the flow encounters a sharp leading edge, and exits past a blunt trailing edge. The implication is that the flow is not as well guided as in the normal flow case. Thus the actual turning angle of the flow is undoubtedly less than predicted by the theoretical analysis. The power absorbed in both reverse flow modes would consequently be less than predicted.



Losses, in general, are approximated by various empirical correlations and are reasonable as shown by test results. They are discussed in depth in the detailed analysis section.

Incidence losses, however, pose a problem. The incidence loss approximations introduced in the analysis section are reasonable as long as the incidence angles remain small. This is obviously not the case for the retraction modes as shown in Figures 5 and 7. The approximations break down physically at these severe incidence angles.

It was thought earlier that two of the four theoretical modes might show themselves to be physically impossible. For example, a large incidence loss might conceivably preclude the attainment of the necessary energy balance. This has not proved to be the case, however. It appears from the present analysis that operation in all four modes remains possible physically. It is true, of course, that the predicted performance for the two retraction modes, Modes 2 and 4, will be inaccurate because of these large incidence effects, but this in itself does not eliminate the existence of these modes.

At extreme angles of incidence, a distinct possibility of stalling exists. In normal operation, this limits the attainable power absorption. In a retraction mode, however, stalling would not be totally undesirable. If the rotor stalls, the energy absorbed by the device is greatly reduced, and the power necessary to retract the rotor is minimal.

All of the foregoing assumptions are thought to be reasonable. Refinements of various points would be useful, especially for large incidence angles and blunt trailing edges.



#### IV. RESULTS AND DISCUSSION

The discussion of the problem up to this point has already included a number of significant results reached in the analysis as shown in Figures 4 through 11.

Additional detailed results for all modes of the absorber are presented in Figures 12, 13, 14, and in Table III. The results for Mode 1 of the dynamic model are also included.

The main results of this investigation are summarized concisely in Figure 12. This is a logarithmic plot of the dimensionless power  $\Pi$  as a function of the dimensionless shaft speed  $\omega/\omega_{MAX}$ . Performance of the proposed absorber, of the hypothetical model, and of the existing M-21 machine are compared on this graph. Note that the theoretically predicted performance of the M-21 version as shown by the continuous line is in excellent agreement with the actual measured performance as shown by the data points.

The actual horsepower is plotted as a function of absolute shaft speed for all four modes of the proposed absorber in Figure 13. The power absorbed during arrest and the power expended during retraction are presented for a range of possible operating speeds.

The maximum dimensionless power is also shown as a function of Reynolds number  $R_{N_e}$  in Figure 14. This graph, although based on only three computed points, does correctly portray, approximately, how scaling affects power absorption. It would be a simple matter to calculate additional points on this curve from program NORMAL.





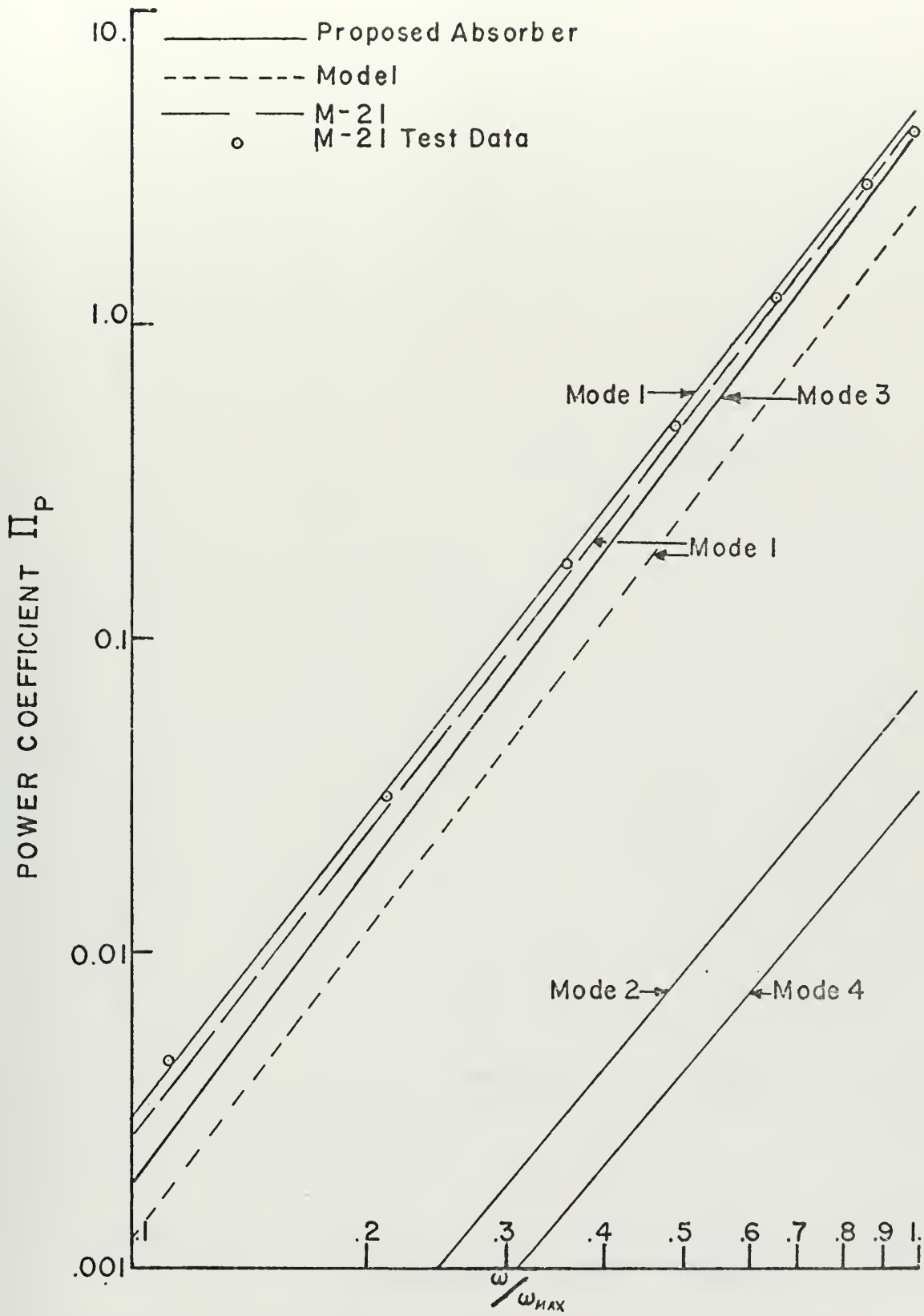


Figure 12 Non-dimensional Power vs. Non-dimensional Rotational Speed



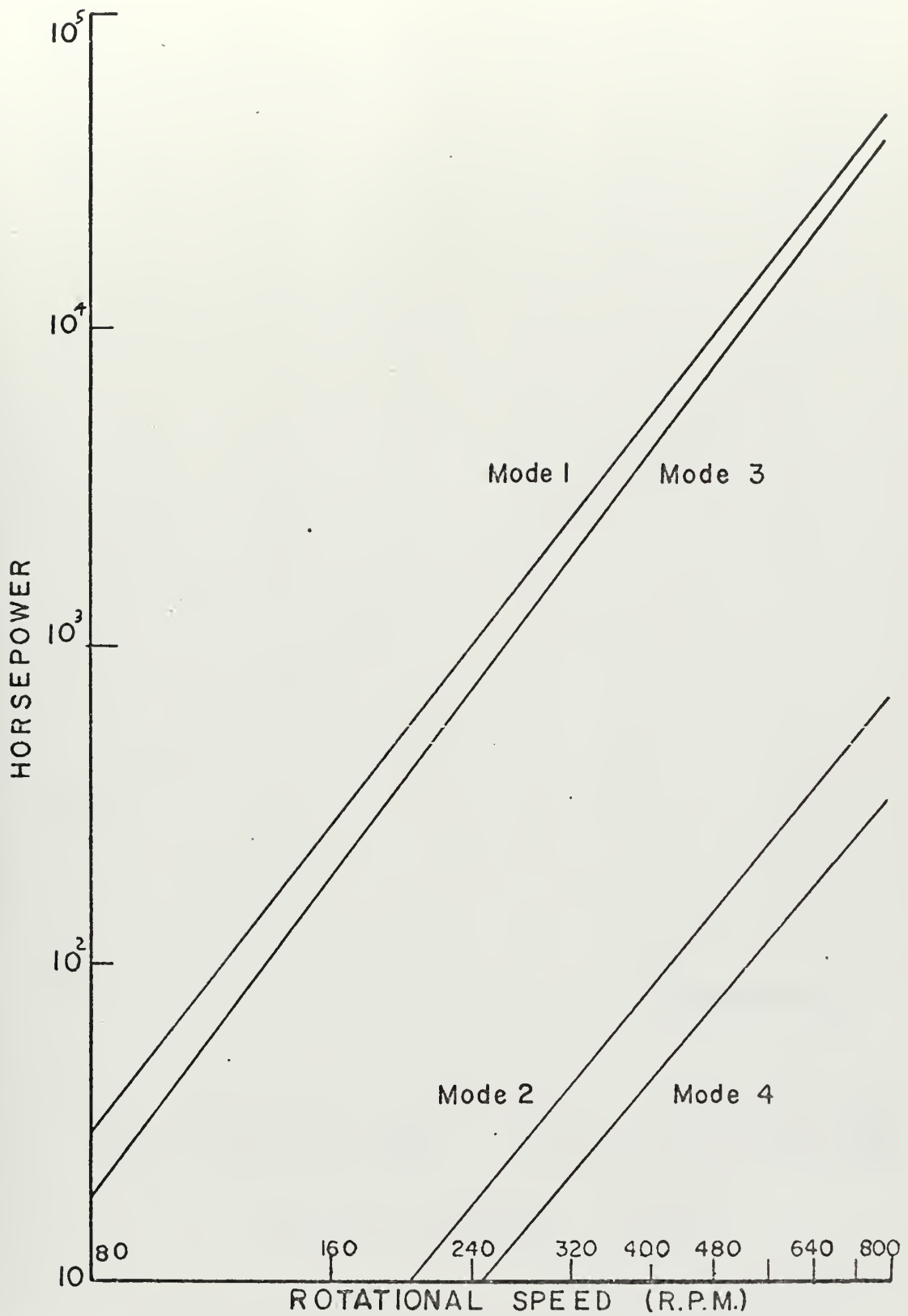


Figure 13 Absolute Power vs. Shaft Speed for the Four Operating Modes of the Proposed Energy Absorber



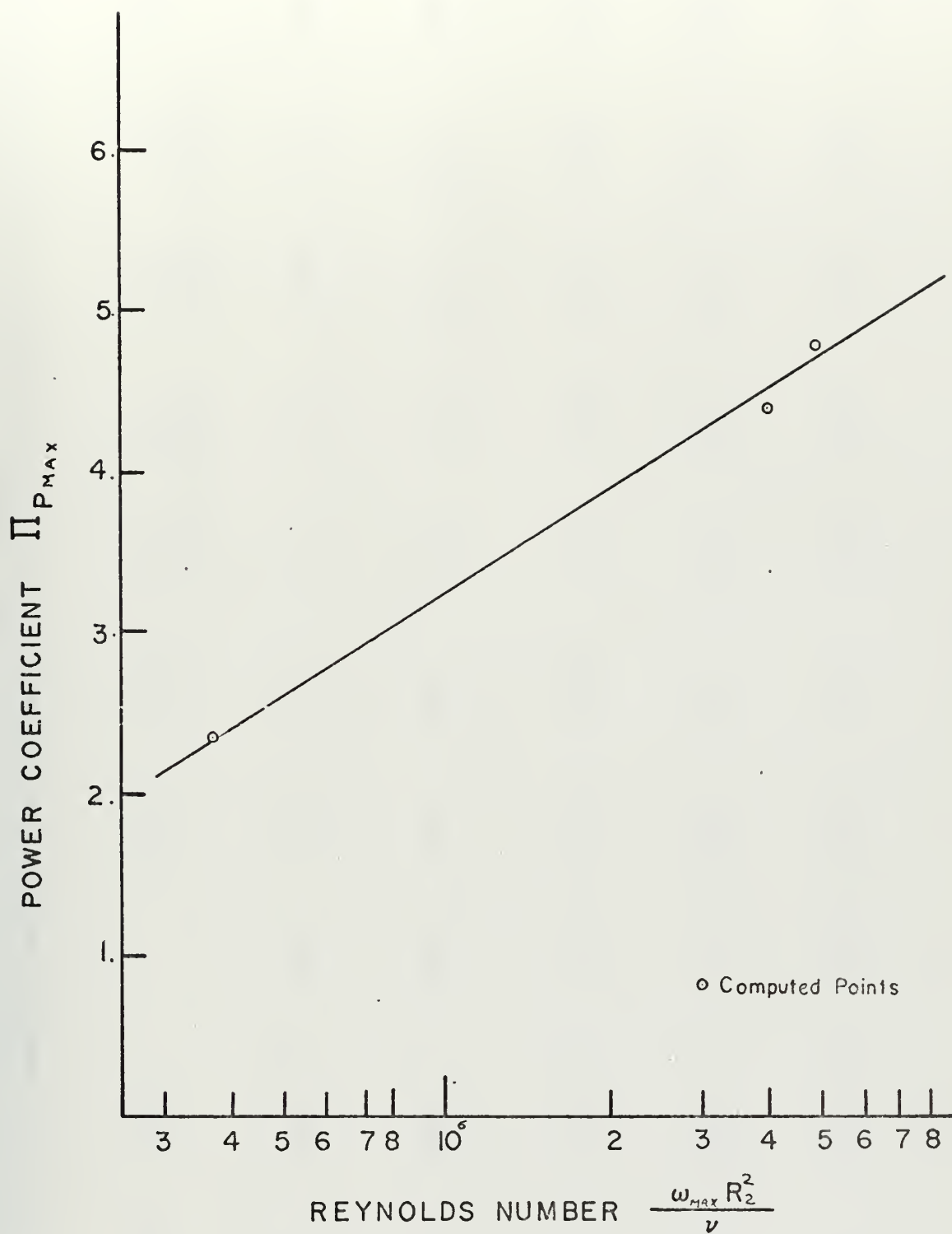


Figure 14 Maximum Power Coefficient vs. Maximum Reynolds Number for the 3 Designs Considered



Table III: Detailed results of the proposed energy absorber for the four modes and the dynamic model for Mode 1. All results are for the case of  $\omega = \omega_{\max}$ .

Operating Mode	$N_{\text{Re}}$	$\phi$	Torque (lb-ft)	Horsepower Absorbed	$\frac{\Delta H_R}{\text{slug}} \left( \frac{\text{ft-lbs}}{\text{slug}} \right)$	$\frac{\Delta H_u}{\text{slug}} \left( \frac{\text{ft-lbs}}{\text{slug}} \right)$	$\frac{\Delta H_S}{\text{slug}} \left( \frac{\text{ft-lbs}}{\text{slug}} \right)$	$\frac{\Delta H_L}{\text{slug}} \left( \frac{\text{ft-lbs}}{\text{slug}} \right)$	$\pi \phi$
1	$4.88 \times 10^6$	1.489	318730.	48551.	51313.	24304.	11658.	15351.	4.765
2	$4.88 \times 10^6$	0.223	4512.	687.	4026.	2694.	981.	351.	0.067
3	$4.88 \times 10^6$	1.450	271770.	41050.	41999.	10558.	8822.	22620.	4.063
4	$4.88 \times 10^6$	0.136	2194.	334.	1895.	115.	1174.	607.	0.033
Model Mode 1	$3.70 \times 10^5$	0.995	10.65	1.62	11054.	5315.	3715.	2475.	2.352





Table III. Continued

Operating Mode	$\Pi_{TR}$	$\Pi_{\Delta H in}$	$i_R$ (degrees)	$i_S$ (degrees)	$\Delta\beta_R$ (degrees)	$\Delta\alpha_S$ (degrees)	$\gamma_R$	$\gamma_S$	$C_U$	$C_I$	$\eta_{Mu}$
1	4.765	4.71	-3.73	2.26	113.7	-112.3	0.227	0.208	0.337	0.412	0.813
2	0.067	0.45	-122.3	113.2	12.3	-3.2	0.174	0.120	0.359	0.435	0.456
3	4.063	4.27	10.7	-6.3	120.7	-116.3	0.239	0.222	0.337	0.412	0.856
4	0.033	0.34	133.7	-126.0	23.7	-16.0	0.197	0.149	0.384	0.456	0.856
Model Node 1	2.352	3.48	-6.88	5.1	116.9	0115.1	0.494	0.453	0.436	0.515	0.782



Table III. Continued

Operating Mode	$\eta_{M1}$	RNR	RNS	R <sub>Nu</sub>	R <sub>Nl</sub>
1	0.876	$6.1 \times 10^6$	$3.3 \times 10^6$	$1.5 \times 10^7$	$1.7 \times 10^7$
2	0.876	$9.1 \times 10^4$	$5.0 \times 10^4$	$2.2 \times 10^5$	$2.5 \times 10^5$
3	0.868	$7.1 \times 10^5$	$3.2 \times 10^5$	$1.3 \times 10^6$	$1.5 \times 10^6$
4	0.868	$7.2 \times 10^4$	$3.3 \times 10^4$	$1.3 \times 10^5$	$1.5 \times 10^5$
Model Mode 1	0.876	$3.2 \times 10^4$	$1.7 \times 10^4$	$7.7 \times 10^4$	$8.6 \times 10^4$



As mentioned earlier, the actual existence of four stable modes is a surprising result. The original expectation, based largely on intuition rather than analysis, was that only one mode would be possible for each direction of shaft rotation. But the absorber is an unusual machine which tends to confound intuitions based on experience with more conventional devices. Consider for example the fact that losses are necessary for the machine to absorb the mechanical energy input. The smaller the loss coefficients, the higher the final equilibrium flow rate will be, and the greater the energy absorption. Thus we are led to the seeming paradox that the lower the loss coefficients the higher the energy lost!

The power curves of Figures 12 and 13 are interesting and significant in that all curves have nearly constant and nearly equal slopes. The power can be expressed in the form

$$\Pi_P = \Pi_{P_{MAX}} \left( \frac{\omega}{\omega_{MAX}} \right)^\eta$$

where the slope of the curve is roughly  $\eta \approx 3$  for all cases.

The horsepower curves of Figure 13 indicate that Mode 1, the design point mode, absorbs the greatest amount of energy. Mode 3, however, is a very close second. Refinement of the analysis should lower the predicted absorption of Mode 3 somewhat. Nevertheless, the favorable comparison of this mode to the design mode is interesting. Figure 13 also shows that the power needed to retract the rotor is reasonably small for Modes 2 and 4, especially in comparison to the power absorbed during arrest.

The question of which mode the absorber will actually operate in under various conditions of use is interesting, but by no means



completely clear at this time. It is thought possibly that if the absorber be started from rest with shaft rotation in the normal direction, Mode 1 should occur. If retraction follows immediately, the retraction mode will probably be Mode 2. This is based on the fact that during arrest the flow will build up a large momentum which will tend to persist in the same sense during the subsequent retraction. If retraction be started after the fluid motion ceased, however, the resulting mode of operation remains uncertain.

Some method of sensing and/or controlling flow direction would be useful to insure that Mode 1 was occurring on all arrests. Mode 3 operation might not have enough absorption capacity to handle large aircraft.

The general question of which mode occurs is an area for further study. Testing of the actual absorber with the idea of definitely determining the operating modes under various conditions would be extremely useful.





## V. CONCLUSIONS AND RECOMMENDATIONS

The development of the problem and the exact solution of the two sets of equations describing normal and reverse flow conditions clearly show that four stable operating modes exist. The analysis adequately predicts the absorption capacity of the proposed device for Mode 1. However, the analysis is not as accurate for the reverse flow or retraction modes.

It is recommended that the retraction problem be further studied to refine loss coefficients and to more accurately predict the power necessary to retract the absorber. It is also recommended that further study be made into the question of predicting which mode occurs under various operating conditions. This study would encompass the unsteady phase of the problem. Actual testing of the absorber should also be conducted with the intention of determining which mode will occur. A method of flow control or sensing would also be useful to guarantee proper performance in that Mode 3 absorption capacity may be insufficient in certain cases.

This turbo-type of energy absorber appears to be completely adequate to meet the demand of carrier operations now and in the foreseeable future. The potential for future development and enlargement is ample.



## APPENDIX A

### DETAILED ANALYSIS OF THE ENERGY ABSORBER WITH THE FLUID CIRCULATING IN THE NORMAL DIRECTION, MODES 1 AND 2.

A one dimensional mean streamline analysis after Vavra (Ref. 2) will be developed with the following assumptions:

- $\beta_2 = \text{constant}$
- $\alpha_2 = \text{constant}$
- Uniform flow at stations 1 to 4 except for blockage factors.
- Blockage factors are independent of the flow.
- The fluid is incompressible.
- Steady state conditions exist.

#### 1.0 Torque and Velocity Relations

The torque  $T_R$  exerted on the fluid by the rotor is positive when acting in the direction of rotation.

$$T_R = \dot{m} [R_2 V_{u2} - R_1 V_{u1}] \quad (1)$$

where  $\dot{m}$  is the mass flow rate.

$$\begin{aligned} \dot{m} &= \rho A \bar{V}_m \\ &= \rho (2\pi R_1 b_R) V_{M1} K_{B1} \\ &= \rho (2\pi R_2 b_R) V_{M2} K_{B2} \end{aligned} \quad (2)$$

The quantity  $2\pi R b_R$  is the flow area,  $V_{m1}$  and  $V_{m2}$  are the meridional velocities at the mean streamline, and  $K_{B1}$  and  $K_{B2}$  are blockage factors which are assumed to be independent of the flow.



By introducing a flow coefficient

$$\phi = \frac{V_{M2}}{U_2} = \frac{V_{M2}}{\omega R_2} \quad (3)$$

all necessary velocity and thrust equations can be written in terms of known geometric parameters and the flow coefficient. An iteration technique is later employed in program NORMAL to calculate  $\phi$ . The following velocity relations are developed now in order to simplify the energy relationships which follow.

The sign convention used is that all peripheral velocity components are positive when in the direction of rotation. From Figures 4 or 5 simple geometric relations are obtained which become, using eq. 3.

$$W_2 = V_{M2} / \cos \beta_2 = \omega R_2 \phi / \cos \beta_2 \quad (4)$$

$$W_{u2} = V_{M2} \tan \beta_2 = \omega R_2 \phi \tan \beta_2 \quad (5)$$

$$V_{u2} = W_{u2} + \omega R_2 = \omega R_2 [1 + \phi \tan \beta_2] \quad (6)$$

Also

$$V_{u2} = V_{M2} \tan \alpha_2 = \omega R_2 \phi \tan \alpha_2 \quad (7)$$

An expression for  $\alpha_2$  in terms of the known relative exit angle can be obtained by equating the previous two equations, or

$$\tan \alpha_2 = \tan \beta_2 + 1/\phi \quad (8)$$

similarly at the rotor inlet

$$W_{u1} = V_{M1} \tan \beta_1 \quad (9)$$

$$V_{u1} = V_{M1} \tan \beta_1 + \omega R_1 \quad (10)$$



The mass flow equation and the definition of the flow coefficient yield

$$V_{M1} = \phi \omega R_2 \frac{R_2}{R_1} \frac{K_{B2}}{K_{B1}} \quad (11)$$

and

$$V_{u1} = \phi \omega R_2 \frac{R_2}{R_1} \frac{K_{B2}}{K_{B1}} \tan \beta_1 + \omega R_1 \quad (12)$$

The mass flow equations must be extended to include flow through the stator.

$$\begin{aligned} \dot{m} &= 2\pi R_2 b_R \rho V_{M2} K_{B2} = 2\pi R_3 b_s \rho V_{M3} K_{B3} \\ &= 2\pi R_4 b_s \rho V_{M4} K_{B4} \end{aligned} \quad (13)$$

From the above relations, the meridional velocity equations are developed.

$$\frac{V_{M1}}{V_{M2}} = \frac{R_2}{R_1} \frac{K_{B2}}{K_{B1}} \quad (14)$$

$$\frac{V_{M3}}{V_{M2}} = \frac{R_2}{R_3} \frac{K_{B2}}{K_{B3}} \frac{b_R}{b_s} \quad (15)$$

$$\frac{V_{M4}}{V_{M2}} = \frac{R_2}{R_4} \frac{K_{B2}}{K_{B4}} \frac{b_R}{b_s} \quad (16)$$

### 1.1 Frictional Losses in Upper Passage

Let  $M_{fu}$  be the frictional moment from forces along the walls of the upper passage from station 2 to 3, acting on the flow opposite to the direction of rotation.

$$\dot{m} R_3 V_{u3} = \dot{m} R_2 V_{u2} - M_{fu} \quad (17)$$





$$\text{Setting } M_{fu} = \lambda_u \dot{m} R_2 V_{u2} \quad (18)$$

$$\text{and } \eta_{Mu} = (1 - \lambda_u) \quad (19)$$

eq. 17 becomes

$$V_{u3} = \eta_{Mu} \frac{R_2}{R_3} V_{u2} \quad (20)$$

From the mass flow equation

$$V_{M3} = \phi \omega R_2 \frac{R_2}{R_3} \frac{K_{B2}}{K_{B3}} \frac{b_R}{b_s} \quad (21)$$

## 1.2 Frictional Losses in Lower Passage

With  $M_{fl}$  being the frictional moment caused by forces along the lower passage walls from station 4 to 1 acting on the flow opposite to the direction of rotation, the equations for the lower passage are developed in a manner similar to the previous development.

$$M_{fl} = \lambda_l \dot{m} R_4 V_{u4} \quad (22)$$

$$\eta_{Ml} = 1 - \lambda_l \quad (23)$$

$$V_{u1} = \eta_{Ml} V_{u4} \frac{R_4}{R_1} \quad (24)$$

$$V_{M4} = \phi \omega R_2 \frac{R_2}{R_4} \frac{K_{B2}}{K_{B4}} \frac{b_R}{b_s} \quad (25)$$

From Figure 4 it can be seen that

$$V_{u4} = V_{M4} \tan \alpha_4 \quad (26)$$

Using the previous three equations gives

$$V_{u1} = \eta_{Ml} \phi \omega R_2 \frac{R_2}{R_1} \frac{K_{B2}}{K_{B4}} \frac{b_R}{b_s} \tan \alpha_4 \quad (27)$$



From Figures 4 or 5, one can relate the absolute inlet angle to absolute velocity components as

$$\tan \alpha_1 = \frac{V_{u1}}{V_{M1}} \quad (28)$$

Using the relations developed for the inlet velocity eqs. 11 and 27, the absolute inlet angle is

$$\tan \alpha_1 = \eta_{M1} \frac{b_R}{b_s} \frac{K_{B1}}{K_{B4}} \tan \alpha_4 \quad (29)$$

Similarly the relative inlet angle is

$$\begin{aligned} \tan \beta_1 &= \frac{V_{u1} - \omega R_1}{V_{M1}} \\ &= \tan \alpha_1 - \frac{\omega R_1}{V_{M1}} \end{aligned}$$

Substituting for  $V_{M1}$  yields

$$\tan \beta_1 = \eta_{M1} \frac{b_R}{b_s} \frac{K_{B1}}{K_{B4}} \tan \alpha_4 - \left( \frac{R_1}{R_2} \right)^2 \frac{K_{B1}}{K_{B2}} \quad 1/\phi \quad (30)$$

The relative and absolute velocities can now be obtained from their respective components by employing the following general equations:

$$V^2 = V_M^2 + V_u^2 \quad (31)$$

$$W^2 = V_M^2 + W_u^2 \quad (32)$$

$$W = V_M / \cos \beta \quad (33)$$



### 1.3 Torque Relations

The torque as defined in eq. 1 can now be expressed in terms of known geometric parameters and the flow coefficient. Using eqs. 37, 6, and 12 in eq. 1 yields

$$T_R = 2\pi R_2^5 \frac{b_R}{R_2} \rho K_{B2} \omega^2 \left[ \phi + \phi^2 \left\{ \tan \beta_2 - \eta_{Ml} \frac{K_{B2}}{K_{B4}} \frac{b_R}{b_s} \tan \alpha_4 \right\} \right] \quad (34)$$

The non-dimensional torque coefficient  $\tau_R$  is now introduced as

$$\tau_R = \frac{T_R}{2\pi(R_2)^5 \frac{b_R}{b_s} \rho K_{B2} \omega^2} = \phi + \phi^2 \left\{ \tan \beta_2 - \eta_{Ml} \frac{K_{B2}}{K_{B4}} \frac{b_R}{b_s} \tan \alpha_4 \right\} \quad (35)$$

The torque  $T_s$  which the stator exerts on the fluid is positive when acting in the direction opposite to rotation

$$T_s = \dot{m} (R_3 V_{u3} - R_4 V_{u4}) \quad (36)$$

Substituting the values for the whirl components gives

$$T_s = 2\pi R_2^5 \left( \frac{b_R}{R_2} \right) \rho \omega^2 K_{B2} \left[ \eta_{Mu} \phi (1 + \phi \tan \beta_2) - \phi^2 \left( \frac{b_R}{b_s} \right) \frac{K_{B2}}{K_{B4}} \tan \alpha_4 \right]$$

Again introducing a non-dimensional torque coefficient

$$\begin{aligned} \tau_s &= \frac{T_s}{2\pi R_2^5 \left( \frac{b_R}{R_2} \right) \rho \omega^2 K_{B2}} \\ &= \eta_{Mu} \phi + \phi^2 \left[ \eta_{Mu} \tan \beta_2 - \frac{b_R}{b_s} \frac{K_{B2}}{K_{B4}} \tan \alpha_4 \right] \end{aligned} \quad (37)$$



The general torque equation is

$$T_R - M_{fu} - M_{f\ell} = T_s$$

The torque exerted on the rotor by the fluid minus frictional moment losses is equal to torque exerted on the fluid by the stator.

The dimensionless torque coefficient introduced earlier is again given as

$$\Pi_T = \frac{T}{\rho \omega_{MAX}^2 R_2^5} \quad (38)$$

## 2.0 Energy Relations

The torque and velocity equations developed in the preceeding section remain in terms of the unknown flow coefficient  $\Phi$ . In this section an algebraic energy equation will be formulated and solved to yield  $\Phi$ .

For the sake of this development, a total head term  $H$  will be defined which differs from the standard definition of total enthalpy  $H_T$  which is

$$H_T = h + \frac{V^2}{2} \quad (39)$$

or

$$H_T = u + \frac{p}{\rho} + \frac{V^2}{2} = u + \frac{P_T}{\rho} \quad (40)$$

where  $h$  is the static enthalpy

$p$  is the static pressure

$u$  is the internal energy

and  $P_T$  is the total pressure.





Since the fluid is treated as incompressible, one can uncouple the thermal effects from the mechanical effects, and define a 'total head'  $H$  which does not include thermal effects. This new term is denoted by

$$H = \frac{P_T}{\rho} = \frac{p}{\rho} + \frac{V^2}{2} \quad (41)$$

Obviously the enthalpies are related by

$$(H_T - u) = H \quad (42)$$

This new definition of total head  $H$  is useful in that constant  $H$  and constant  $P_T$  lines are coincident. Throughout the remainder of the analysis, useful total head  $H$  will be referred to as simply head. Note that this total head has the units of enthalpy (per unit mass).

The process undergone in the absorber is now represented in Figure 8. Obviously the process does not return to the original total enthalpy  $H_{T1}$ , although it does return to the original total pressure and head.

From Figure 8 the energy rise across the rotor is shown to be equal to the energy losses across the stator and through the passages, or

$$\Delta H_R - \Delta H_u - \Delta H_l - \Delta H_S = 0. \quad (43)$$

Therefore,

$$(H_2 - H_1) - (H_2 - H_3) - (H_3 - H_4) - (H_4 - H_1) = 0 \quad (44)$$

where all the above terms are written as positive quantities.



The four terms of eq. 44 will be derived in terms of the flow coefficient and the known geometric parameters as in Section 1.0. Eq. 44 is then straightforwardly solved to yield  $\bar{\phi}$ . Program NORMAL is employed to accomplish this task. Since various loss parameters depend on  $\bar{\phi}$ , an iteration technique must be used.

## 2.1 Conditions in Rotor

The incidence angle of the rotor blading  $i_R$  is defined as

$$i_R = \beta_1 - \beta_{1B} \quad (45)$$

or merely the angle between the tangent to the mean camber line at the leading edge and the relative inlet velocity. The incidence angle  $i_R$  is seen to become more negative in the direction corresponding to a greater lift coefficient for the blade.

The relative velocity  $W_1$  can be resolved into two components respectively tangential and normal to the mean camber line. The energy associated with the tangential component  $W_1'$  is assumed to be largely recoverable. The energy associated with the normal component is assumed to be totally lost.

The useful relative velocity at the rotor inlet is then

$$W_1' = W_1 \cos i_R \quad (46)$$

and the velocity component lost due to incidence is similarly

$$W_{1i} = W_1 \sin i_R \quad (47)$$

The basic energy equation of turbo-machinery is

$$H_{T2} - H_{T1} = U_2 V_{u2} - U_1 V_{u1} \quad (48)$$



which upon expansion becomes

$$H_{T2} - H_{T1} = \frac{V_2^2 + U_2^2 - W_2^2}{2} - \frac{V_1^2 + U_1^2 - W_1^2}{2} \quad (49)$$

Using static enthalpies, regrouping, and cancelling terms in eq. 48 gives

$$h_2 + \frac{W_2^2 - U_2^2}{2} = h_1 + \frac{W_1^2 - U_1^2}{2} \quad (50)$$

Substituting for the static enthalpy and rearranging yields

$$\frac{p_2}{\rho} + \frac{W_2^2}{2} = \frac{p_1}{\rho} + \frac{W_1^2}{2} - \frac{U_2^2 - U_1^2}{2} - (u_2 - u_1) \quad (51)$$

Upon resolving  $W_1^2/2$  into its components and regrouping further, one obtains

$$\left(\frac{p_2}{\rho} + \frac{W_2^2}{2}\right) = \left(\frac{p_1}{\rho} + \frac{W_{1i}^2}{2} + \frac{U_2^2 - U_1^2}{2}\right) - \left(u_2 - u_1 - \frac{W_{1i}^2}{2}\right) \quad (52)$$

This leads naturally to the definition of the "equivalent relative total pressure" as

$$\frac{P_{E2}}{\rho} = \left(\frac{p_2}{\rho} + \frac{W_2^2}{2}\right) \quad (53)$$

and

$$\frac{P_{E1}}{\rho} = \left(\frac{p_1}{\rho} + \frac{W_{1i}^2}{2} + \frac{U_2^2 - U_1^2}{2}\right) \quad (54)$$

and to the definition of the rotor blading losses as

$$\frac{\Delta p_f}{\rho} = \left[(u_2 - u_1) - \frac{W_{1i}^2}{2}\right] = \left(\frac{P_{E1}}{\rho} - \frac{P_{E2}}{\rho}\right) \quad (55)$$



It also proves useful to express this loss in terms of a dimensionless coefficient defined as

$$Y_R = \left( \frac{P_{E1} - P_{E2}}{\frac{\rho}{2} W_2^2} \right) \quad (56)$$

Recalling that

$$H_T = H - u \quad (42)$$

and using the basic energy equation, eq. 48, one obtains the energy rise across the rotor in the form

$$(H_2 - H_1) = U_2 V_{u2} - U_1 V_{u1} - \left\{ \sin^2 i_R \frac{W_1^2}{2} + Y_R \frac{W_2^2}{2} \right\} \quad (57)$$

This equation can be conveniently non-dimensionalized by dividing by  $U_2^2$ . The velocity expressions developed in Section 1.0 can not be utilized to simplify eq. 57, and the dimensionless energy rise across the rotor  $(\Pi \Delta H)_R$  can be written as

$$\begin{aligned} (\Pi_{\Delta H})_R &= \frac{H_2 - H_1}{W_2^2} = 1 - \frac{(\sin^2 i_R)}{2} \left( \frac{R_1}{R_2} \right)^2 \\ &+ \phi \left\{ \tan \beta_2 - \left( \frac{K_{B2}}{K_{B4}} \cdot \frac{b_R}{b_s} \eta_{Ml} \tan \alpha_4 \right) \cos^2 i_R \right\} \\ &- \phi^2 \left\{ \frac{\sin^2 i_R}{2} \left( \frac{R_2}{R_1} \right)^2 \left[ \left( \frac{K_{B2}}{K_{B1}} \right)^2 + \left( \frac{K_{B2}}{K_{B4}} \cdot \frac{b_R}{b_s} \eta_{Ml} \tan \alpha_4 \right)^2 \right] \right. \\ &\left. + \frac{Y_R}{2 \cos^2 \beta_2} \right\} \end{aligned} \quad (58)$$





where the dimensionless head coefficient is defined as

$$\Pi_{\Delta H} = \frac{\Delta H}{\omega^2 R_2^2} \quad (59)$$

The loss coefficient  $Y_R$  of eqs. 56 and 58 is a function of the deflection  $\Delta\beta$ , where

$$\Delta \beta_R = \beta_2 - \beta_1$$

and the aspect ratio  $\Lambda_R$ , defined by

$$\Lambda_R = \frac{b_R}{R_2 - R_1} \quad (60)$$

This will be further discussed in Section 3.0.

## 2.2 Performance of Rotor Blading

The rotor is designed for the maximum useful enthalpy rise across the blades. If this were a frictionless process, the useful energy rise would naturally be greater than in an actual process involving friction. Therefore, the rotor efficiency is defined as

$$\eta_R = \frac{H_2 - H_1}{H_{2Th} - H_1} \quad (61)$$

where the total heads  $H_1$ ,  $H_2$ , and  $H_{2Th}$  are shown on the H-s diagram, Figure 8. Of course the pressure rise through the rotor is related very simply to the corresponding energy rise according to the relation

$$H = \frac{P_T}{\rho} \quad (62)$$



The numerator of eq. 61 is obtained from either eqs. 57 or 58. The denominator of eq. 61 is similarly obtained, but for the theoretical case both the incidence and blading losses are non-existent.

It follows from eq. 58 that

$$\begin{aligned}
 (\Pi_{\Delta H_{Th}})_R &= \left\{ \frac{H_{2Th} - H_1}{\omega^2 R_2^2} \right\} \\
 &= 1 + \Phi \left\{ \tan \beta_2 - \eta_{Ml} \frac{b_R}{b_s} \frac{K_{B2}}{K_{B4}} \tan \alpha_4 \right\}
 \end{aligned} \tag{63}$$

is the theoretical dimensionless energy rise across the rotor. The efficiency can obviously be written as

$$\eta_R = \frac{(\Pi_{\Delta H})_R}{(\Pi_{\Delta H_{Th}})_R} \tag{64}$$

The general definition of power  $\mathcal{P}$  is

$$\mathcal{P} = \dot{m} \Delta H \tag{65}$$

It is convenient to introduce a dimensionless power coefficient as

$$\Pi_{\mathcal{P}} = \frac{\mathcal{P}}{\rho \omega_{MAX}^3 R_2^5} \tag{66}$$

Recalling that

$$\Phi = \frac{V_{M2}}{\omega R_2} \tag{3}$$

$$\dot{m} = 2\pi \rho R_2 b_R V_{M2} K_{B2} \tag{2}$$

and

$$\Pi_{\Delta H} = \frac{\Delta H}{\omega^2 R_2^2} \tag{59}$$



the dimensionless power and head coefficients can now be related as

$$\Pi_D = \left\{ 2\pi \left( \frac{b_R}{R_2} \right) K_B \left( \frac{\omega}{\omega_{MAX}} \right)^3 \right\} \Phi \Pi \Delta H \quad (67)$$

The power is related to the torque by the simple expression

$$\Pi_D = \Pi_{TR} \left( \frac{\omega}{\omega_{MAX}} \right) \quad (68)$$

### 2.3 Energy Losses in the Upper Passage

The energy loss in the upper passage, assumed as only a total pressure loss due to friction between the rotor and stator, is expressed as

$$\Delta H_u = H_2 - H_3 = \frac{P_{T2}}{\rho} - \frac{P_{T3}}{\rho} \quad (69)$$

or

$$\Delta H_u = \left( \frac{p_2}{\rho} + \frac{V_2^2}{2} \right) - \left( \frac{p_3}{\rho} + \frac{V_3^2}{2} \right) \quad (70)$$

In a frictionless process

$$H_2 = (H_3)_{TH} = \frac{p_{3TH}}{2} + \frac{V_3^2}{2} \quad (71)$$

and from eq. 17 with the frictional moment  $M_{fu}$  equal to zero

$$(V_{u3})_{TH} = V_{u2} \frac{R_2}{R_3} = \frac{V_{u3}^2}{\eta_{Mu}^2} \quad (72)$$

Resolving  $V_3^2/2$  into its components, one can write eq. 71 as

$$H_2 = (H_3)_{TH} = \frac{p_{3TH}}{\rho} + \frac{V_{M3}^2}{2} + \frac{1}{2} \frac{V_{u3}^2}{\eta_{Mu}^2} \quad (73)$$



Similarly for an actual process

$$H_3 = \frac{p_3}{\rho} + \frac{V_{M3}^2}{2} + \frac{V_{u3}^2}{2} \quad (74)$$

the energy loss can now be written using the two previous equations as

$$H_2 - H_3 = \frac{p_{3TH} - p_3}{\rho} + \left( \frac{1}{\eta_{Mu}^2} - 1 \right) \frac{V_{u3}^2}{2} \quad (75)$$

A convenient dimensionless pressure loss coefficient can now be denoted as

$$C_u = \frac{p_{3TH} - p_3}{\rho \left( \frac{V_{M3}^2}{2} \right)} \quad (76)$$

where  $C_u$  will be shown to depend primarily on the radius ratio  $\frac{r_o}{r_i}$  of the upper passage in Figure 2. This is similar to energy loss coefficients developed for bends in smooth pipes.

Eq. 75 is non-dimensionalized, and using eq. 76 one obtains

$$(\Pi \Delta H)_u = \frac{C_u}{2} \frac{V_{M3}^2}{\omega^2 R_2^2} + \frac{1}{2} \left( \frac{1}{\eta_{Mu}^2} - 1 \right) \frac{V_{u3}^2}{\omega^2 R_2^2} \quad (77)$$

Using previously developed expressions for  $V_M$  one obtains an equation similar in form to eq. 58 or

$$\begin{aligned} (\Pi \Delta H)_u &= \frac{H_2 - H_3}{\omega^2 R_2^2} \\ &= \frac{1 - \eta_{Mu}^2}{2} \left( \frac{R_2}{R_3} \right)^2 + \phi \left\{ \left( \frac{R_2}{R_3} \right)^2 (1 - \eta_{Mu}^2) \tan \beta_2 \right\} \\ &\quad + \phi^2 \left\{ \frac{C_u}{2} \left( \frac{R_2}{R_3} \right)^2 \frac{b_R}{b_s} \frac{K_{B2}}{K_{B3}} + \frac{(1 - \eta_{Mu}^2)}{2} \left( \frac{R_2}{R_3} \right)^2 \tan \beta_2 \right\} \end{aligned} \quad (78)$$





## 2.4 Performance of Stator Blading

From Figure 4 the stator incidence angle  $i_s$  is

$$i_s = \alpha_3 - \alpha_3^B \quad (79)$$

and the useful inlet velocity  $V_3'$  is

$$V_3' = V_3 \cos i_s \quad (80)$$

The total head ahead of stator blades is given by

$$H_3 = \frac{p_3}{\rho} + \frac{V_3^2}{2} = \frac{P_{T3}}{\rho} \quad (81)$$

while the useful head is

$$H_3' = \frac{p_3}{\rho} + \frac{(V_3')^2}{2} = \frac{P_{T3}'}{\rho} \quad (82)$$

The above three equations combine to yield

$$\begin{aligned} H_3' &= H_3 + \frac{(V_3')^2 - (V_3)^2}{2} \\ &= H_3 - \frac{V_3^2}{2} (\sin^2 i_s) \end{aligned} \quad (83)$$

Similar to rotor blading losses, stator blading losses will be defined as

$$Y_s = \frac{P_{T3}' - P_{T4}}{\frac{\rho}{2} V_4^2} = \frac{H_3' - H_4}{(V_4^2/2)} \quad (84)$$

or

$$H_4 = H_3' - Y_s \frac{V_4^2}{2} = H_3 (\sin^2 i_s) \frac{V_3^2}{2} - Y_s \frac{V_4^2}{2} \quad (85)$$



Subtracting  $H_1$  from both sides yields

$$H_4 - H_1 = H_3 - H_1 - (\sin^2 i_s) \frac{V_3^2}{2} - Y_s \frac{V_4^2}{2} \quad (86)$$

The same non-dimensionalizing technique used in Sections 2.1, and 2.3 is again employed and the energy loss in the lower passage is now available in the general form as

$$\begin{aligned} \frac{H_4 - H_1}{\omega^2 R_2^2} &= \frac{H_3 - H_1}{\omega^2 R_2^2} - \frac{\eta_{Mu}^2}{2} \left( \frac{R_2}{R_3} \right)^2 \left\{ (\sin^2 i_s) \right. \\ &+ \Phi \left[ (\sin^2 i_s) 2 \tan \beta_2 \right] + \Phi^2 \left\{ (\sin^2 i_s) \left[ \left( \frac{1}{\eta_{Mu}} \frac{b_R}{b_s} \frac{K_{B2}}{K_{B3}} \right)^2 + \tan^2 \beta_2 \right] \right. \\ &\left. \left. + \frac{Y_s}{\eta_{Mu}^2} \left[ \frac{R_3}{R_4} \frac{b_R}{b_s} \frac{K_{B2}}{K_{B4}} \frac{1}{\cos \alpha_4} \right]^2 \right\} \right\} \end{aligned} \quad (87)$$

The above equation is actually

$$\frac{H_4 - H_1}{\omega^2 R_2^2} = \frac{H_3 - H_1}{\omega^2 R_2^2} - \frac{H_3 - H_4}{\omega^2 R_2^2}$$

This can be further reduced to give

$$\frac{H_4 - H_1}{\omega^2 R_2^2} = \frac{H_2 - H_1}{\omega^2 R_2^2} - \frac{H_2 - H_3}{\omega^2 R_2^2} - \frac{H_3 - H_4}{\omega^2 R_2^2} \quad (88)$$

which gives the energy losses in the lower passage in terms of the energy changes throughout the remainder of the system. The next step is to find the energy loss in the lower passage and solve eq.



Again the loss coefficient  $Y_s$  is a function of deflection and the aspect ration, where

$$\Delta\beta_s = \alpha_3 - \alpha_4 \quad (89)$$

and

$$\Lambda_s = \frac{b_s}{R_3 - R_4} \quad (90)$$

## 2.5 Losses in Lower Passage

The development of the energy loss in the lower passage closely follows the technique of Section 2.3.

The energy loss in the lower passage is

$$\Delta H_\ell = H_4 - H_1 = \frac{p_4}{\rho} + \frac{V_4^2}{2} - \left( \frac{p_1}{\rho} + \frac{V_1^2}{2} \right) \quad (91)$$

for a frictionless process

$$(V_{u1})_{Th} = V_{u4} \frac{R_4}{R_1} \quad (92)$$

or relating theoretical to actual velocities yields

$$(V_{u1})_{Th} = \frac{V_{u1}}{\eta_{M\ell}} \quad (93)$$

Therefore,

$$H_4 = (H_1)_{Th} = \frac{(p_1)_{Th}}{\rho} + \frac{V_{M1}^2}{2} + \frac{1}{2} \left( \frac{V_{u1}}{\eta_{M\ell}} \right)^2 \quad (94)$$

while

$$H_1 = \frac{p_1}{\rho} + \frac{V_{M1}^2}{2} + \frac{V_{u1}^2}{2} \quad (95)$$



the pressure loss coefficient is

$$\frac{(p_1)_{Th} - p_1}{\rho} = C_\ell \frac{V_{M1}^2}{2} \quad (96)$$

The expressions for  $H_1$  and  $H_4$  are now substituted into eq. 1, along with eq. 6 to yield

$$H_4 - H_1 = C_\ell \frac{V_{M1}^2}{2} + (1 - \eta_{M\ell}^2) \left( \frac{R_4}{R_1} \right)^2 V_{u4}^2 \quad (97)$$

This is easily put into the dimensionless form used previously or

$$(\Pi\Delta H)_\ell = \frac{\phi^2}{2} \left( \frac{R_2}{R_1} \right)^2 \left[ C_\ell \left( \frac{K_{B2}}{K_{B1}} \right)^2 + (1 - \eta_{M\ell}^2) \left( \frac{b_R}{b_s} \frac{K_{B2}}{K_{B4}} \tan \alpha_4 \right)^2 \right] \quad (98)$$

Eq. 97 can now be substituted into eq. 88 and  $\phi$  can be solved for straightforwardly. Iteration is necessary, however, since all loss coefficients depend on  $\phi$ .

### 3.0 Loss Coefficient in Rotor

Vavra (3) gives a relation for the losses in axial turbine bladings as

$$\Psi = 0.99 - \frac{2.28}{10^4} \Delta \beta - \frac{4.97}{180 - \Delta \beta} \quad (99)$$

where  $\Delta \beta$  is the flow deflection angle in degrees. The quantity  $\Psi$  is the velocity coefficient defined as the ratio of the actual and theoretical discharge velocities, which for the rotor is

$$\Psi_R = \frac{W_2}{W_{2Th}} \quad (100)$$

and

$$\Delta \beta_R = \beta_2 - \beta_1 \quad (101)$$





The theoretical case occurs for  $Y_R$  equal zero which in accordance to eq. 56 gives  $P_{E1} = P_{E2Th}$ . Substituting eq. 100 into eq. 53 yields

$$\frac{P_{E1}}{\rho} = \frac{P_{E2Th}}{\rho} = \frac{p_2}{\rho} + \frac{1}{2} \frac{W_2^2}{\psi^2} \quad (102)$$

The actual rotor blading losses using eq. 102 can now be written as

$$Y_R = \frac{\left(\frac{p_2}{\rho} + \frac{W_2^2}{2\psi^2}\right) - \left(\frac{p_2}{\rho} + \frac{W_2^2}{2}\right)}{W_2^2/2} = \frac{1}{\psi^2} - 1 \quad (103)$$

In accordance with Horlock (Ref. 4) the loss coefficients depend on Reynolds numbers  $R_{NR}$  and aspect ratio  $\Lambda_R$  of eq. 60. Hence let  $Y_R$  of eq. 103 now denoted as  $Y_R^*$  be the loss coefficient across the rotor blading for  $\Lambda_R = 3$  and  $R_{NR} = 10^5$ . The latter term is defined as

$$R_{NR} = \frac{D_{hR} W_2}{\nu} \quad (104)$$

where  $D_{hR}$  is the hydraulic diameter of the discharge area of the flow channel between adjacent blades. If  $\Delta_R$  is the rotor blade spacings at the radius  $R_2$ , and  $a_R$  is the opening at the discharge as shown in Figure 3, an approximation of the discharge opening is given by

$$a_R \approx \Delta_R \cos \beta_2 \quad (105)$$

then

$$D_{hR} = \frac{4 \text{ (flow area)}}{\text{wetted perimeter}} = \frac{4 a_R b_R}{2 (a_R + b_R)} \quad (106)$$



Substituting for  $a_R$  and rearranging yields

$$D_{hR} = \frac{2b_R}{1 + \frac{b_R}{a'_R \cos \beta_2}} \quad (107)$$

The blade spacing  $a'_R$  can be found with respect to the radial extension  $R_2 - R_1$  by using the blade loading criterion of Zweifel (Ref. 5). For axial bladings this approximation is

$$\frac{a'_R}{R_2 - R_1} \approx \frac{0.425}{(\tan \beta_2 - \tan \beta_{1B}) \cos^2 \beta_2} \quad (108)$$

Substituting this equation into the expression for the hydraulic diameter yields

$$\frac{D_{hR}}{R_2} = \frac{2\left(\frac{b_R}{R_2}\right)}{1 + \frac{(b_R/R_2)(\tan \beta_2 - \tan \beta_{1B}) \cos^2 \beta_2}{0.425(1 - R_1/R_2)}} \quad (109)$$

Placing the above equation into the expression for the Reynolds number and recalling that

$$W_2 = \frac{\omega R_2 \phi}{\cos \beta_2} \quad (4)$$

one obtains

$$R_{NR} = \frac{2\left(\frac{b_R}{R_2}\right) \phi \omega R_2^2}{\left[ \cos \beta_2 + \frac{(b_R/R_2)(\tan \beta_2 - \tan \beta_{1B}) \cos^2 \beta_2}{0.425 (1 - R_1/R_2)} \right]} \quad (110)$$



The loss coefficient is dependent on the aspect ratio and Reynolds number through the following relations after Horlock (Ref. 4).

$$Y_R^* = \frac{1}{\Psi^2} - 1 \quad (111)$$

$$Y_R' = \frac{1}{\Psi^2} \left( .975 + \frac{.075}{\Lambda_R} \right) - 1 \quad (112)$$

and

$$Y_R = Y_R' \left( \frac{10^5}{R_{NR}} \right)^{.25} \quad (113)$$

where the coefficient  $Y_R'$  holds for the actual aspect ration only at a Reynolds number equal to  $10^5$ . By combining the above equations the generalized loss coefficient is simply

$$Y_R = \left\{ \frac{1}{\Psi^2} \left( .975 + \frac{.075}{\Lambda_R} \right) - 1 \right\} \left( \frac{10^5}{R_{NR}} \right)^{.25} \quad (114)$$

These relations allow the actual loss coefficient of the energy absorber to be determined under varied conditions.

Obviously the Reynolds number is not totally specified by geometric parameters, but depends on the flow coefficient  $\Phi$ . In iterating for  $\Phi$ , the process must be assumed to begin at  $Y_R'$ , or a Reynolds number of  $10^5$ , and subsequently correct the loss coefficient as improved values of  $\Phi$  and  $R_{NR}$  are calculated. This procedure must also be employed for the velocity coefficient  $\Psi$  which is dependent on  $\Phi$  through a dependence on the actual inlet angle  $\beta_1$ . The iteration must be continued until convergence is achieved for all values dependent on  $\Phi$ .



### 3.1 Loss Coefficient in Stator

This section follows closely the development in Section 3.0.

Eq. 99 is again used with

$$\Psi_s = \frac{V_4}{V_{4Th}} \quad (115)$$

and

$$\Delta\beta_s = \alpha_3 - \alpha_4 \quad (116)$$

For a frictionless process in the stator, the total pressure  $(P_{T4})_{Th}$  at stator exit would equal total useful inlet pressure  $P_{T3}'$ ,  
or

$$\frac{(P_{T4})_{Th}}{\rho} = \frac{P_{T3}'}{\rho} = \frac{p_4}{\rho} + \frac{(V_4)_{Th}^2}{2} \quad (117)$$

Substituting eq. 115 into eq. 117 yields

$$\frac{P_{T3}}{\rho} = \frac{p_4}{\rho} + \frac{1}{\Psi_s^2} \frac{V_4^2}{2} \quad (118)$$

For an actual flow

$$H_4 = \frac{P_{T4}}{\rho} = \frac{p_4}{\rho} + \frac{V_4^2}{2} \quad (119)$$

which yields through eq. 84

$$Y_s = \frac{1}{\Psi_s^2} - 1 = Y_s^* \quad (120)$$

This was as expected from Section 3.0. The loss coefficient can now be written after eqs. 112, 113, and 114 as

$$Y_s' = \frac{1}{\Psi^2} \left( .975 + \frac{.075}{\Lambda_R} \right) - 1 \quad (121)$$





$$Y_s = Y_s' \left( \frac{10^5}{R_{Ns}} \right)^{.25} \quad (122)$$

and finally

$$Y_s = \left\{ \frac{1}{\Psi^2} \left( .975 + \frac{.075}{\Lambda_s} \right) - 1 \right\} \left( \frac{10^5}{R_{Ns}} \right)^{.25} \quad (123)$$

where the aspect ratio is defined by eq. 90 as

$$\Lambda_s = \frac{b_s}{R_3 - R_4}$$

The Reynolds number for the stator is

$$R_{Ns} = \frac{D_{hs} V_4}{\nu} \quad (124)$$

where for  $a_s \approx \mathcal{A}_s \cos \alpha_4$ , the hydraulic diameter is

$$D_{hs} = \frac{2b_s}{1 + \frac{b_s/\mathcal{A}_s}{\cos \alpha_4}} \quad (125)$$

The blade spacing according to Zweifel (Ref. 5) is

$$\frac{\mathcal{A}_s}{R_3 - R_4} = \frac{0.425}{(|\tan \alpha_4 - \tan \alpha_{3B}|) \cos^2 \alpha_4} \quad (126)$$

and from eqs. 25 and 26

$$V_4 = \Phi \omega R_2 \frac{R_2}{R_4} \frac{b_R}{b_s} \frac{K_{B2}}{K_{B4}} \frac{1}{\cos \alpha_4} \quad (127)$$

The Reynolds number can now be expressed using the above four equations as



$$R_{Ns} = \frac{2 \left( \frac{b_R}{R_4} \right) \frac{K_{B2}}{K_{B4}} \phi \omega R_2^2}{v \left[ \cos \alpha_4 + \frac{b_s}{R_2} (| \tan \alpha_4 - \tan \alpha_{3B} |) \cos^2 \alpha_4 \right.} \quad (128)$$

$$\left. \frac{0.425 (R_3/R_2) \left( 1 - \frac{R_4}{R_3} \right)}{\left. \right]} \right]$$

A series of iterations is again needed to insure proper convergence of all parameters.

#### 4.0 Pressure Loss Coefficients in Upper and Lower Passages

In accordance with eq. 76 the pressure losses in the upper passage are expressed by

$$\frac{(p_3)_{Th} - p_3}{\rho} = C_u \frac{V_{M3}^2}{2} \quad (129)$$

and similarly for the lower passage by eq. 96 as

$$\frac{(p_1)_{Th} - p_1}{\rho} = C_\ell \frac{V_{M1}^2}{2} \quad (130)$$

With  $\Delta p_b$  being the pressure drop in the bend, the loss coefficients of these bends defined as

$$\xi = \frac{\Delta p_b}{\frac{\rho}{2} V^2} \quad (131)$$

are shown in Figure 15 as functions of the Reynolds number  $R_N$ , where similar to eqs. 104 and 124

$$R_N = \frac{V \cdot D_n}{\nu} \quad (132)$$

Vavra (Ref. 2) has developed the set of curves shown in Figure 15.

These curves are based on the data of Sprenger (Ref. 6). Interpolation



was to obtain values for ratios of  $r_i/b$  different than those found in Sprenger.

The hydraulic diameter  $D_h$  is again

$$D_h = \frac{4 \text{ flow area}}{\text{wetted perimeter}} \quad (133)$$

For a ring channel with flow area of  $2\pi R b$  the wetted perimeter is  $2(2\pi R)$ , or

$$D_h = \frac{4(2\pi R)b}{2(2\pi R)} = 2b \quad (134)$$

Hence at the rotor inlet there is

$$D_h = 2b_R \quad (135)$$

and at the stator inlet

$$D_h = 2b_s \quad (136)$$

These above two values are introduced into eq. 132, with  $V$  equal to the corresponding value of  $V_M$ , that is,  $V_{M1}$  before the rotor and  $V_{M3}$  before the stator. The result is

$$R_{Nu} = \frac{V_{M3} 2b_s}{\nu} \quad (137)$$

$$R_{Nl} = \frac{V_{M1} 2b_R}{\nu} \quad (138)$$

The Reynolds number is then used to obtain the loss coefficients  $\xi$  of Figure 15.

The loss coefficients  $\xi$  of Figure 15 have been obtained from the measured pressure drops by subtracting the pressure drops that would



occur in a straight duct at the corresponding Reynolds number and surface roughness.

There are several conclusions which can be drawn from Figure 15 and from additional data in Sprenger (Ref. 6). In general, the loss coefficients for bends made up of two concentric radii increase with decreasing  $r_i/b$  ratios. The curves  $\xi$  versus  $R_N$  that exhibit a minimum indicate the flow separations occur at the inner radius, and should be avoided. Finally, Sprenger (Ref. 6) shows that two bends with  $r_i/b = 0.5$  arranged in series to form a  $180^\circ$  bend have a loss coefficient of  $1.66\xi$  at  $R_N = 10^5$  where  $\xi$  is the loss coefficient of one of the  $90^\circ$  bends. This data will be a first approximation in choosing the loss coefficient for the  $180^\circ$  bends in the energy absorber.

#### 4.1 Estimate of the Pressure Loss Coefficients in the Upper and Lower Passage

The losses in the upper and lower passages will be assumed due to two components, passage bending and friction. The losses due to duct bending were discussed in the previous section. An arbitrary assumption is to take these loss coefficients equal to 2.0 and 2.5 for the upper and lower passage respectively. The values of  $\xi$  are given in Figure 15 for various value of  $r_i/b$ . It is recommended that  $r_i/b$  be chosen between 0.5 and 1.0. Any bend with a value of  $r_i/b$  larger than 1.0 will be assumed to have the same losses as a bend with  $r_i/b$  equal 1.0.

To the above losses must be added the frictional losses in a straight duct of hydraulic diameter  $D_h$  and average length  $L$ , where

$$L = \frac{L_i + L_o}{2} \quad (139)$$





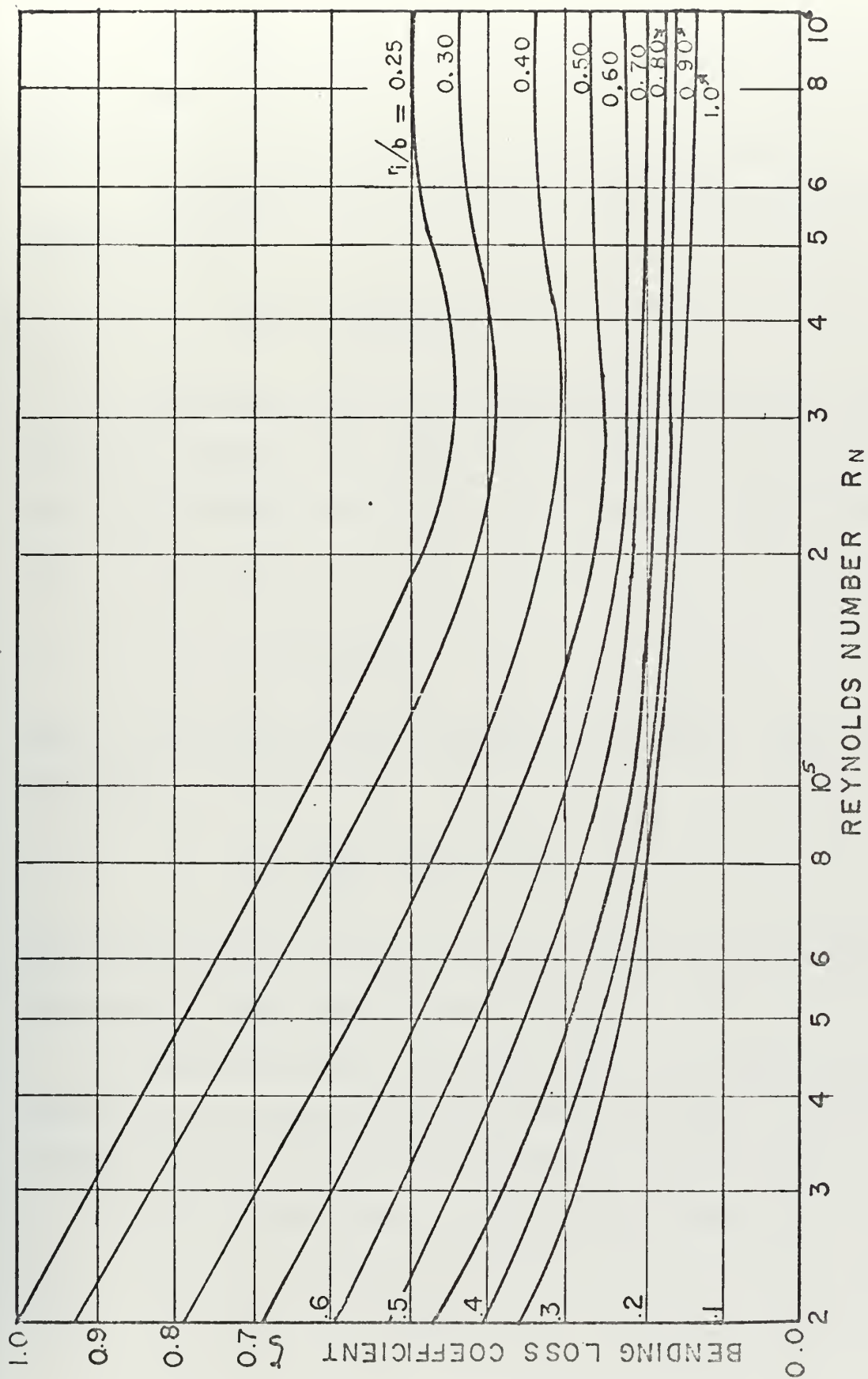


Figure 15 Estimate of Loss Coefficient  $\xi$  (Vavra Ref. 2)



and  $L_i$  is the distance along the inner contour and  $L_o$  that along the outer contour in the meridional plane from the trailing edges of one blade row to the leading edges of the other row. (See Figure 2)

In accordance with eqs. 132 and 136 this general frictional pressure loss is

$$\Delta p_f' = \lambda_f \frac{L}{2b} \frac{\rho}{2} V_M^2 \quad (140)$$

The friction factor  $\lambda_f$  is a function of both Reynolds number and surface roughness. The value of  $\lambda_f$  is obtained from the curve of Figure 16, also from Vavra (Ref. 2), for a relative surface roughness of

$$\frac{K_r}{D_h} = \frac{1}{10^4} \quad (141)$$

where  $K_r$  is the peak-to-valley roughness of the surface. Hence, for this case

$$K_r = \frac{2b}{10^4} = 200 \text{ b } \mu\text{-in.} \quad (142)$$

If it is assumed that the rms roughness be one-half  $K_r$ , the surface finish must be better than 100 b micro-inches.

The applicability of this data to the three dimensional flow channels of the energy absorbed is obviously questionable. The losses defined below must, at best, be considered as first estimates only.

The loss coefficient  $C_u$  of eq. 129 will be taken as

$$C_u = 2.0 \xi + \frac{L_u}{2b_R} \lambda_f \quad (143)$$



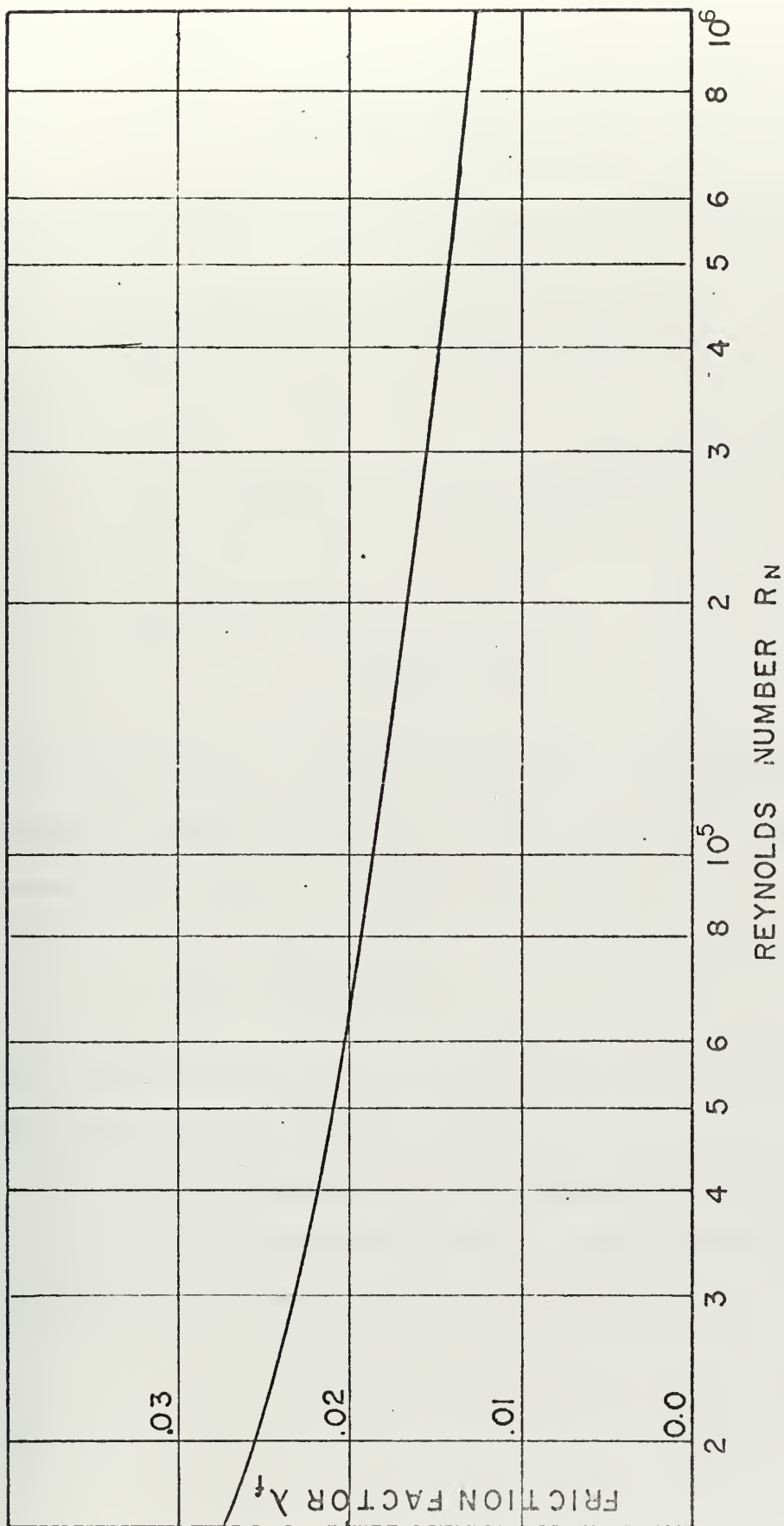


Figure 16 Estimated Channel Wall Friction Factor  $\lambda_f$  (Vavra Ref. 2)



and  $C_\ell$  of eq. 130 is

$$C_\ell = 2.5 \xi + \frac{L_\ell}{2b_s} \lambda_f \quad (144)$$

where  $\xi$  is obtained from Figure 15 and  $\lambda_f$  from Figure 16 for

$$R_{Nu} = \frac{2b_s V_{M3}}{v} = \left( \phi \omega R_2 \frac{R_2}{R_3} \frac{K_{B2}}{K_{B3}} \frac{b_R}{b_s} \right) \frac{2b_s}{v} \quad (145)$$

and

$$R_{N\ell} = \frac{2b_R V_{M1}}{v} = \left( \phi \omega R_2 \frac{R_2}{R_1} \frac{K_{B2}}{K_{B1}} \right) \frac{2b_R}{v} \quad (146)$$

In eq. 4 the length  $L_u$  is given by

$$L_u = \frac{(L_u)_i + (L_u)_o}{2}$$

where  $(L_u)_i$  and  $(L_u)_o$  are the lengths of the inner and outer meridional contours, respectively, of the walls of the upper passage between stations 2 and 3. Similarly in eq. 133

$$L_\ell = \frac{(L_\ell)_i + (L_\ell)_o}{2} \quad (147)$$

where  $(L_\ell)_i$  and  $(L_\ell)_o$  are the counterparts of  $(L_i)_u$  and  $(L_u)_o$  for the lower passage between stations 4 and 1.

## 5.0 Losses of Angular Momentum in Upper and Lower Passages

The frictional moments along the upper and lower passages were introduced by eqs. 18 and 22 respectively as

$$M_{fu} = \lambda_u \dot{m} R_2 V_{u2} \quad (148)$$

and

$$M_{f\ell} = \lambda_\ell \dot{m} R_4 V_{u4} \quad (149)$$





No data is presently available for the losses of angular momentum in passages of the type needed between the rotor and stator of the present absorber. A very crude approximation of these moments is obtained, however, by assuming that the shear stresses  $\Psi_o$  on the walls are merely those acting on a flat plate with a peripheral velocity  $V_u$  at R being the velocity outside the boundary layer. This oversimplification ignores the effect of the meridional velocity components which may cause large increases in the frictional moments.

For fully turbulent boundary layers along rough walls the shear stress is

$$\Psi_o = c_f \frac{\rho}{2} V_u^2 \quad (150)$$

where  $c_f$  is assumed to be invariant with the Reynolds number of the flow. On the element of wall area  $2\pi R dL$  of Figure 2 there acts a frictional moment

$$dM_f = 2\pi R dL \Psi_o R$$

which becomes when using eq. 3

$$dM_f = \pi \rho c_f (R V_u)^2 dL \quad (151)$$

It is assumed that the passages have been designed such that the flow is not separated from the walls, and all stresses external to the boundary layer are an order of magnitude smaller than stresses along the walls, and therefore negligible. This results in the product  $(R V_u)$  being constant outside of the boundary layers and equal to  $R_2 V_{u2}$ , the value at the rotor discharge, for the upper passage. Integrating eq. 151 from station 2 to station 3 yields



$$M_{fu} = \int_{(2)}^{(3)} \pi \rho c_f (R_2 V_{u2})^2 dL \quad (152)$$

$$M_{fu} = \pi \rho c_f (R_2 V_{u2})^2 [(L_u)_i + (L_u)_o] \quad (153)$$

where the inner wall is of length  $(L_u)_i$  and the outer wall is of length  $(L_u)_o$ . Hence by eq. 148

$$\lambda_u = \frac{\pi \rho c_f R_2 V_{u2} [(L_u)_i + (L_u)_o]}{m} \quad (154)$$

Substitution of the mass flow equation and velocity relations into eq. 154 gives

$$\lambda_u = c_f \frac{1 + \phi \tan \beta_2}{\phi} \frac{[(L_u)_i + (L_u)_o]}{2 b_R K_{B2}} \quad (155)$$

from eq. 19

$$\eta_{Mu} = 1 - c_f \frac{1 + \phi \tan \beta_2}{\phi} \frac{[(L_u)_i + (L_u)_o]}{2 b_R K_{B2}} \quad (156)$$

For the lower passage a similar procedure and derivation leads to

$$\lambda_\ell = \frac{c_f \tan \alpha_4}{K_{B4}} \frac{[(L_\ell)_i + (L_\ell)_o]}{2 b_s} \quad (157)$$

and

$$\eta_{M\ell} = 1 - \frac{c_f \tan \alpha_4 [(L_\ell)_i + (L_\ell)_o]}{2 K_{B4} b_s} \quad (158)$$



In eqs. 155 through 158, the absolute value of the flow angles must be introduced since the loss is a function of absolute deflection.

For fully turbulent boundary layers, as in the present case, the local skin friction coefficients  $c_f$  depend on the surface roughness ratio  $K_s/x$ , where  $K_s$  is the peak to average value roughness and  $x$  is length along the plate.

$$c_f \approx .004 \text{ for } K_s/x = 10^{-4}$$

and

$$c_f \approx .006 \text{ for } K_s/x = 10^{-3}$$

Since there will be flow irregularities and possible flow separations, it is advisable to use a larger value for  $c_f$ . A  $c_f = .016$  was chosen since it gives best agreement with M-21 test data.



## APPENDIX B

### DETAILED ANALYSIS OF THE ENERGY ABSORBER WITH THE FLUID CIRCULATING IN THE REVERSE DIRECTION, MODES 3 AND 4

A separate set of equations must be derived for the reverse flow modes. The reason, mentioned earlier, is that the relative flow exit angles which are assumed constant are now different.

This development follows very closely to the previous analysis. Therefore, the intermediate steps of this derivation are omitted.

#### 1. Assumptions

a.  $\beta_1 = \text{constant}$

$$\alpha_3 = \text{constant}$$

The remaining assumptions are identical to the normal flow case.

#### 2. Analysis

The geometric relations employed are obtainable from Figures 6 and 7. A new flow coefficient  $\phi'$  is conveniently defined as

$$\phi' = \frac{V_{M1}}{\omega R_1} = \phi \left( \frac{V_{M1}}{V_{M2}} \right) \left( \frac{R_2}{R_1} \right) \quad (1)$$

The torque exerted on the fluid by the rotor when acting in the direction of rotation is

$$T_R = \dot{m} (R_1 V_{u1} - R_2 V_{u2}) \quad (2)$$

where the mass flow equations are identical to those for the normal case.





The frictional moments acting from stations 1 to 4 and stations 3 to 2 are respectively

$$M_{f\ell} = \lambda_{\ell} \dot{m} R_1 V_{u1} \quad (3)$$

$$M_{fu} = \lambda_u \dot{m} R_3 V_{u3}$$

where

$$\dot{m} R_4 V_{u4} = \dot{m} R_1 V_{u1} - M_{f\ell} \quad (4)$$

$$\dot{m} R_2 V_{u2} = \dot{m} R_3 V_{u3} - M_{fu}$$

The relative flow inlet angles are

$$\tan \beta_2 = \eta_{Mu} \frac{b_R}{b_s} \frac{K_{B2}}{K_{B3}} \tan \alpha_3 - \left( \frac{R_2}{R_1} \right)^2 \frac{K_{B2}}{K_{B1}} 1/\phi' \quad (5)$$

and

$$\tan \alpha_4 = \frac{\eta_{M\ell} (1 + \phi' \tan \beta_1)}{\phi' \frac{K_{B1}}{K_{B4}} \frac{b_R}{b_s}} \quad (6)$$

The torque is now reduced to

$$T_R = 2 \pi \rho R_1^5 \left( \frac{b_R}{R_1} \right) K_{B1} \omega^2 \tau_R \quad (7)$$

where

$$\tau_R = \phi + \phi'^2 \left[ \tan \beta_1 - \frac{K_{B1}}{K_{B3}} \frac{b_R}{b_s} \eta_{Mu} \tan \alpha_3 \right] \quad (8)$$



Proceeding to the rotor, one can write,

$$W_2' = W_2 \cos i_R$$

$$i_R = \beta_{2B} - \beta_2$$

$$Y_R = \frac{P_{E2} - P_{E1}}{\frac{\rho}{2} W_1^2}$$

and finally

$$\begin{aligned} \frac{\Delta H_R}{\omega_{R1}^2} \frac{H_1 - H_2}{\omega_{R1}^2} &= 1 - \frac{\sin^2 i_R}{2} \left( \frac{R_2}{R_1} \right) \\ &+ \phi' \left\{ \tan \beta_1 - \left( \frac{K_{B1}}{K_{B3}} \frac{b_R}{b_s} \eta_{Mu} \tan \alpha_3 \right) \cos^2 i_R \right\} \\ &- \phi'^2 \left\{ \frac{\sin^2 i_R}{2} \left( \frac{R_1}{R_2} \right)^2 \left[ \left( \frac{K_{B1}}{K_{B2}} \right)^2 + \left( \frac{K_{B1}}{K_{B3}} \frac{b_R}{b_s} \eta_{Mu} \tan \alpha_3 \right)^2 \right] + \frac{Y_R}{2 \cos^2 \beta_1} \right\} \end{aligned} \quad (9)$$

where

$$\Delta \beta_R = \beta_1 - \beta_2$$

$$\Lambda_R = \frac{b_R}{R_2 - R_1}$$

for this case

$$\Pi_{\Delta H} = \frac{\Delta H}{\omega_{R1}^2} \quad (10)$$

In the lower passage

$$C_\ell = \frac{P_{lTh} - P_l}{\frac{\rho}{2} V_{M4}^2} \quad (11)$$



and the energy drop is

$$\begin{aligned}
 \frac{H_1 - H_4}{\omega^2 R_1^2} &= \frac{(1 - \eta_{Ml}^2)}{2} \left( \frac{R_1}{R_4} \right)^2 \\
 &+ \Phi' \left\{ (1 - \eta_{Ml}^2) \left( \frac{R_1}{R_4} \right)^2 \tan \beta_1 \right\} \\
 &+ \Phi'^2 \left\{ \frac{C_l}{2} \left( \frac{K_{B1}}{K_{B4}} \frac{b_R}{b_s} \frac{R_1}{R_4} \right)^2 + \frac{(1 - \eta_{Ml}^2)}{2} \left( \frac{R_1}{R_4} \right)^2 \tan^2 \beta_1 \right\}
 \end{aligned} \tag{12}$$

Nor for the stator

$$V_4' = V_4 \cos i_s$$

$$i_s = \alpha_{4B} - \alpha_4$$

$$Y_s = \frac{P_{T4} - P_{T3}}{\frac{\rho}{2} V_3^2}$$

$$\Lambda_s = \frac{b_s}{R_3 - R_4}$$

$$\Delta\beta_s = \alpha_3 - \alpha_4$$

and the energy drop across the stator is

$$\begin{aligned}
 \frac{H_4 - H_3}{\omega^2 R_1^2} &= \frac{\sin^2 i_s}{2} \eta_{Ml}^2 \left( \frac{R_1}{R_4} \right)^2 + \Phi' \left\{ (\sin^2 i_s) \eta_{Ml}^2 \left( \frac{R_1}{R_4} \right)^2 \tan \beta_1 \right\} \\
 &+ \Phi'^2 \frac{\sin^2 i_s}{2} \left( \frac{R_1}{R_4} \eta_{Ml} \right)^2 \left\{ \left( \frac{1}{\eta_{Ml}} \frac{K_{B1}}{K_{B4}} \frac{b_R}{b_s} \right)^2 + \tan^2 \beta_1 \right\} \\
 &+ \frac{\Phi'^2}{2 \cos^2 \alpha_3} Y_s \left( \frac{R_1}{R_3} \frac{b_R}{b_s} \frac{K_{B1}}{K_{B3}} \right)^2
 \end{aligned} \tag{13}$$



In the upper passage

$$C_u = \frac{p_{2Th} - p_2}{\rho \frac{V_{M2}}{2}} \quad (14)$$

and

$$\frac{H_3 - H_2}{\omega^2 R_1^2} = \frac{\phi'^2}{2} \left( \frac{R_1}{R_2} \right)^2 \left\{ C_u \left( \frac{K_{B1}}{K_{B2}} \right)^2 + (1 - \eta_{Mu}^2) \left( \frac{b_R}{b_s} \frac{K_{B1}}{K_{B3}} \tan \alpha_3 \right)^2 \right\} \quad (15)$$

The loss coefficients are now given as

$$C_u = 2.0 \xi + \frac{L_u}{2b_s} \lambda_f \quad (16)$$

$$C_\ell = 2.5 \xi + \frac{L_\ell}{2b_R} \lambda_f$$

$$\lambda_u = c_f \tan \alpha_3 \frac{L_u}{b_s \frac{K_{B4}}{K_{B1}}} \quad (17)$$

$$\lambda_\ell = c_f \tan \beta_1 \frac{L_\ell}{b_R \frac{K_{B1}}{K_{B4}}}$$

The Reynolds numbers to obtain  $\xi$  and  $\lambda_f$  graphically are

$$R_{Nu} = \frac{2b_s}{\nu} \left( \phi' \omega \frac{R_1^2}{R_3} \frac{K_{B1}}{K_{B3}} \right) \quad (18)$$

$$R_{N\ell} = \frac{2b_R}{\nu} \phi' \omega_R R_1$$

The expressions for  $\Psi$ ,  $Y_R$ , and  $Y_s$  remain the same as in the previous analysis, but the Reynolds numbers are now





$$R_{NR} = \frac{2\left(\frac{b_R}{R_1}\right) \frac{\bar{\phi}' \omega R_1^2}{v}}{\cos\beta_1 + \frac{(b_R/R_1) [\tan \beta_1 - \tan \beta_{2B}] \cos^2 \beta_1}{0.425 \left(\frac{R_2}{R_1} - 1\right)}}$$

(19)

$$R_{NS} = \frac{2\left(\frac{b_R}{R_3}\right) \left(\frac{K_{B1}}{K_{B3}}\right) \frac{\bar{\phi}' \omega R_1^2}{v}}{\cos\alpha_3 + \frac{\frac{b_s}{R_1} [\tan \alpha_{4B} - \tan \alpha_3] \cos^2 \alpha_3}{0.425 \left(\frac{R_4}{R_1}\right) \left(\frac{R_3}{R_4} - 1.0\right)}}$$

The equation which is finally solved to obtain  $\bar{\phi}$  is

$$\Delta H_R = \Delta H_u + \Delta H_s + \Delta H_\ell$$

or

$$H_1 - H_2 - (H_4 - H_3) - (H_3 - H_2) - (H_1 - H_4) = 0 \quad (20)$$

The equation is solved by the program. An iteration technique must be carried out until all parameters dependent on  $\bar{\phi}'$  converge.



## APPENDIX C

### PROGRAM NORMAL

Program NORMAL is essentially a modification of the program developed by NAEC.

Program NORMAL solves the equations governing normal circulation, Modes 1 and 2, for a given design. The solution is based on an iteration technique which is repeated until the flow coefficient  $\Phi$  converges to within a specific accuracy. A starting value of  $\Phi$  is picked as are initial values of the various Reynolds numbers which are also  $\Phi$  dependent. The initial iteration step occurs with all losses based on standard initial Reynolds numbers. This subsequent value of  $\Phi$  is then used to improve the estimates of the Reynolds numbers and consequential losses. The technique is carried out until  $\Phi$  converges to the proper value.

If the design parameters and angular speed are input data, the program will compute the flow coefficient, torque, velocities, losses, energy changes over each component, and the dimensionless torque, power, speed, and energy. The flow chart of Table IV depicts this process.

The method of data input is clearly indicated in the program itself. The program is felt to be self-explanatory in that comment cards have been extensively used. The Fortran symbols employed are given in the list of symbols.

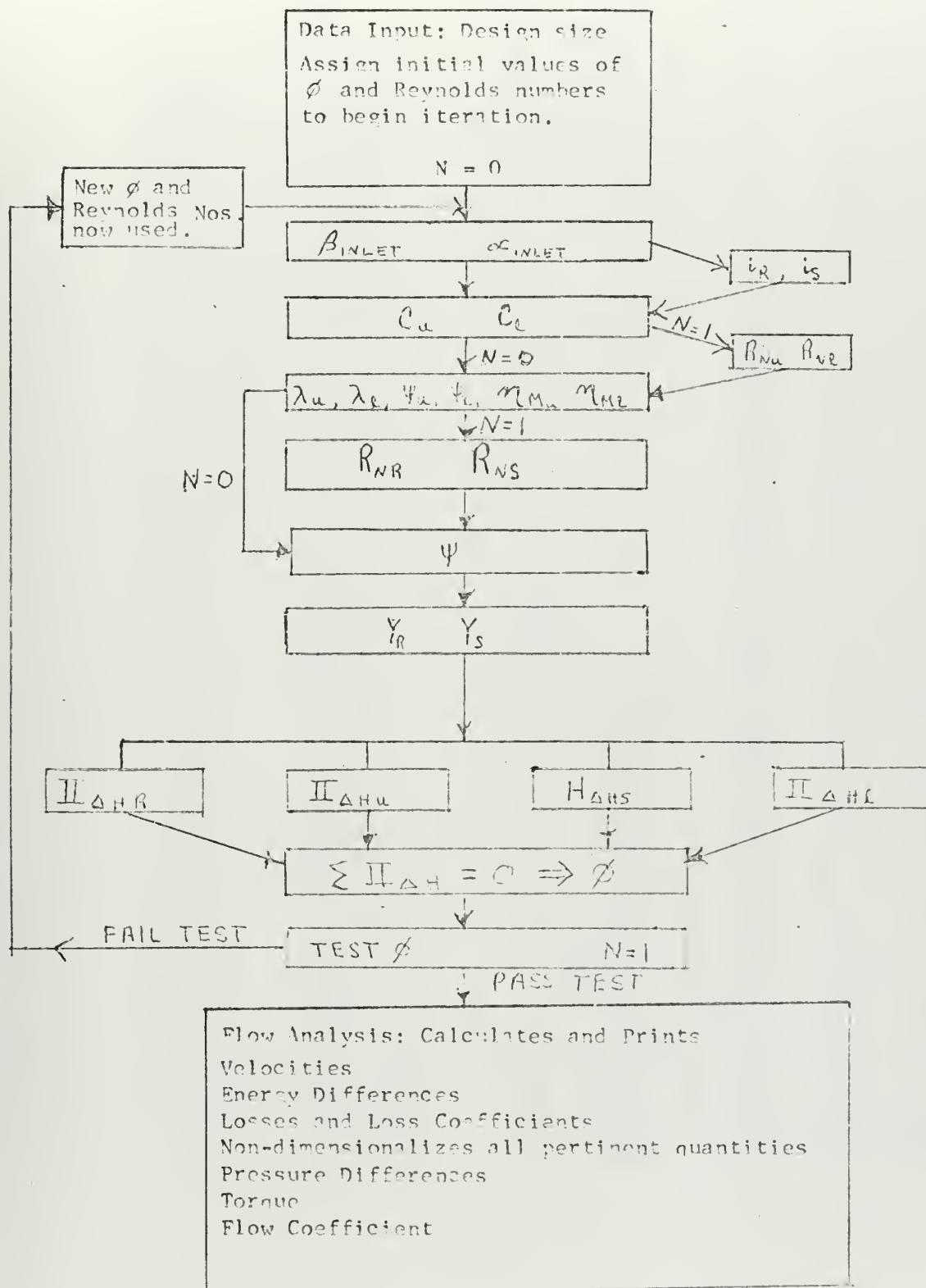
Subroutines have been used liberally. Each subroutine accomplishes one individual task such as determining a loss coefficient, or



enthalpy change across the stator, etc. The subroutines Fig. 15 and Fig. 16 are closest point approximations of the curves depicted in Figures 15 and 16 of the analysis. Thses points are given by Block data which is called by each subroutine.



Table IV FLOW CHART FOR COMPUTER PROGRAMS NORMAL AND REVERSE







# PROGRAM NORMAL

THIS PROGRAM SOLVES THE SET OF EQUATIONS PRESENTED IN APPENDIX A. AN ITERATION TECHNIQUE IS NECESSARY TO SOLVE FOR PHI SINCE VARIOUS LOSS COEFFICIENTS ARE PHI DEPENDENT. A STRAIGHT QUADRATIC EQUATION SOLVES THE ENERGY BALANCE EQUATION GIVEN BY EQUATION A44. AFTER CONVERGENCE IS ACHIEVED, THE FLOW ANALYSIS AND NON-DIMENSIONALIZATION WILL BE ACCOMPLISHED.

IT MUST BE REMEMBERED THAT THIS SOLUTION IS ONLY VALID FOR THE CONDITION OF NORMAL CIRCULATION, MODES 1 OR 2. THE ACTUAL DIFFERENCE BETWEEN THE MODES IS THE DIRECTION OF SHAFT ROTATION. THE FLOW EXIT ANGLES AT THE ROTOR AND STATOR MUST REMAIN CONSTANT, HOWEVER, THE SIGNS WILL BE CHANGED DUE TO THE SIGN CONVENTION EMPLOYED IN THE ANALYSIS. THAT IS ALL ANGLES ARE POSITIVE IF THEIR PERIPHERAL COMPONENT OF VELOCITY IS IN THE DIRECTION OF ROTATION.

THE DATA IS INPUTTED ON SEVEN(7) DATA CARDS.

CARD ONE: THE MONTH, DAY, AND YEAR ARE PLACED IN COLUMNS 1-5, 6-10, AND 11-15 RESPECTIVELY. NOTE THAT THESE INTEGERS MUST BE RIGHT HAND ADJUSTED

CARD TWO: COLUMNS 1-5 THE RUN NUMBER, RIGHT ADJUSTED. COLUMNS 6-15 AND 16-25, THE RADIUS OF THE ROTOR INLET AND OUTLET (IN INCHES), RESPECTIVELY. COLUMNS 26-35, THE INCREMENT OF ANGULAR SPEED (RAD/SECOND). COLUMNS 36-45, VALUE OF PHI TO BEGIN ITERATIONS. COLUMNS 46-55, THE INITIAL ANGULAR SPEED.

CARD THREE: THE BLOCKAGE FACTORS AT STATIONS 1, 2, 3, AND 4 ARE PLACED IN COLUMNS 1-10, 11-20, 21-30, 31-40.

CARD FOUR: THE RELATIVE EXIT ANGLES AT ROTOR AND STATOR (IN DEGREES) GO IN COLUMNS 1-10, AND 11-20. THE ANGLE TO THE MEAN CAMBER LINE (IN DEGREES) FOR ROTOR AND STATOR GO IN COLUMNS 21-30, AND 31-40, RESPECTIVELY.

CARD FIVE: IN COLUMNS 1-10, 11-20, 21-30, AND 31-40 ARE PLACED THE COEFFICIENT OF FRICTION, THE SPECIFIC HEAT OF THE FLUID, THE FLUID DENSITY (SLUGS PER CUBIC FOOT), AND THE KINEMATIC VISCOSITY (FEET<sup>2</sup> PER SECOND). CARD SIX: THE RATIO OF THE AVERAGE LENGTH OF THE UPPER PASSAGE TO ROTOR BLADE HEIGHT, THE RATIO OF THE AVERAGE LENGTH OF THE LOWER PASSAGE TO STATOR BLADE HEIGHT, THE RATIO OF THE INNER CONTOUR TO ROTOR BLADE HEIGHT, AND THE RATIO OF THE ROTOR TO STATOR BLADE HEIGHT GO IN COLUMNS 1-10, 11-20, 21-30, AND 31-40, RESPECTIVELY.

CC







```

498 FORMAT(3I5)
499 FFORMAT(15,5F10.3)
500 FFORMAT(3F10.5,F10.8)
501 FFORMAT(1H,4F10.3)
509 FFORMAT(1H1,DATE=,3I5)
510 FFORMAT(1H0,7X,KB2,7X,KB3,7X,KB4)
513 FFORMAT(1H0,7X,KB1,7X,ALPHA4,7X,B16,7X,A3B)
514 FFORMAT(1H0,5X,BETA2,4X,CP,7X,RHO,13X,NU)
515 FFORMAT(1H0,8X,CF,8X,CP,7X,RHO,13X,NU)
516 FFORMAT(1H0,6X,R1R2,6X,R3R2,6X,R4R2,6X,BRR2)
517 FFORMAT(1H0,6X,LUBR,6X,LLBS,6X,R1BR,6X,BRBS)
521 FFORMAT(1H0,3X,IRUN,8X,R1,9X,R2,9X,DELOM,8X,PHIO,6X,OMO)
523 FFORMAT(1H0,15,5F12.3)
530 FFORMAT(1H0,2F10.3,F15.5,F15.8)
540 FFORMAT(1H0,10X,EXITS AT STATION 2, NORMAL ROTATION)
550 FFORMAT(1H0,7X,R1,8X,R2,8X,R3,8X,R4,8X,BR,8X,BS)
551 FFORMAT(1H0,6F10.3)

C****
C
C INITIALIZATION

R1R2 = R1/R2
R3R2 = R3/R2
R4R2 = R4/R2
BR1 = BR/R2
R1INCH = R1
R2INCH = R2
R3INCH = R3
R4INCH = R4
BRINCH = BR
BSINCH = BS
PRINT 516, R1R2, R3R2, R4R2, BRR2
PRINT 550
PRINT 551, R1INCH, R2INCH, R3INCH, R4INCH, BRINCH, BSINCH
CMAX = 800.*3.1416/30.0
OM = R1/12.0
R2 = R2/12.0
BR = BR/12.0
BS = BR/BRBS
AB2 = BR/BETA2
AA4 = ALPHA4
BETA2 = 3.1416/180.*BETA2
ALPHA4 = 3.1416/180.*ALPHA4
B1B = 3.1416/180.*B1B
A3B = 3.1416/180.*A3B
R2R1 = 1./R1R2

```



```

R2R3 = 1./R3R2
R2R4 = 1./R4R2
R4R2 = R4R2 * R2R3
BSR2 = BRR2/BRB5
BSR3 = BSR2*R2R3
ARR = BRR2/(1.-R1R2)
ARS = BSR3/(1.-R4R3)
C      THE VALUE OF R1BR IS INITIALIZED HERE AND WILL BE USED IN SUBROUTINE FIG TO
C      OBTAIN VALUES OF THE BENDING LOSSES FROM FIGURE 15.
IZ = 0
IF (R1BR .LE. 0.25) IZ=1
IF (R1BR .GE. 1.0) IZ=9
IF (IZ .NE. 0) GO TO 22
REALIZ = R1BR*10.0 - 1.0
IZ = REALIZ

C      INITIAL VALUES OF THE REYNOLDS NUMBERS ARE GIVEN TO BEGIN THE ITERATIONS.
22  RER = 10.0**5
    RES = 10.0**5
    REU = 10.0**5
    REL = 10.0**5
    PHI = PHI0
    TORREF = RHO*(OMMAX**2)*(R2**5)
    POWREF = TORREF * OMMAX
    PRINT 410, TORREF
410  PRINT 415, TORREF
415  FORMAT(IH0,6X, 'THE REFERENCE POWER IS',F13.3)
    FORMAT(IH0,6X, 'THE REFERENCE TORQUE IS',F13.3)
    IF ( PHI .GT. 0.0 ) GO TO 30

C
IR=C.
IS = 0.0
BETAL = B1B
ALPHA3 = A3B
GO TO 40

C*****      CALCULATE PHI
C 25  RER = ENRER ( PHI )
    RES = ENRES ( PHI )

C 30  CALL EQG1
    CALL EQG2
    CALL EQH5
    CALL EQH6
    TANB1 = (ETAML*KB1/KB4*TAN(ALPHA4))- (R1R2**2)*(KB1/KB2)/PHI
    BETAL = ATAN(TANB1)
    IR = BETAL - B1B

```





```

C 40  TAN A3 = ETAMU*(1. + PHI*TAN(BETA2))/((PHI*KB2/KB3)
      ALPHA3 = ATAN(TANA3)
      IS = ALPHA3 - A3B
      YR = EQI8(RER,ARR,BETA2,BETA1)
      YS = EQI8(RES,ARS,ALPHA4,ALPHA3)
      CALL EQE28
      CALL EQF12
      CALL EQE13A
      CALL EQD9
      CALL PHITES
C***
C      TESTING PHI
C 100  IF ( K .GE. 1 ) GO TO 110
      K=2
      PHIO = PHI
      GO TO 25
C 110  TEST = ABS( (PHI - PHIO)/((PHI + PHIO)/2.) )
      IF ( TEST .LE. 0.0005 ) GO TO 120
C
      K = K + 1
      SAFETY OUTLET
C***
      IF ( K .GT. 20 ) GO TO 120
      PHIO = PHI
      GO TO 25
C*****
C      OUTPUT AND FLOW CALCULATIONS
C 120  TAU = EQB19( PHI )
      CALL EQB20
      DELBET = BETA2-BETA1
      DELALP = ALPHA4-ALPHA3
      DELBET = DELBET*180./3.1416
      DELALP = DELALP*180./3.1416
      DBETA1 = BETA1*180./3.1416
      CALPH3 = ALPHA3*180./3.1416
      DIR = IR*180./3.1416
      DIS = IS*180./3.1416
      PRINT 300
      PRINT 299,K,PHI,TORQUE,TAUR,OM
      PRINT 311
      PRINT 302,DBETA1,DALPH3,DIR,DIS
      PRINT 312
      PRINT 313,DELBET,DELALP
      PRINT 325
      PRINT 308

```



```

PRINT 302,YR,YS,CU,CL
PRINT 309
PRINT 302,ETAMU,ETAML,PSIU,PSIL
PRINT 310
PRINT 303,RER,RES,REU,REL

C
CALL NONDEM
CALL VALUE
DELOM = OMMAX * 0.1
OM = OM + DELOM
PHIO = PHI
K = 1
IF ( OM.LE. OMMAX ) GO TO 25

C
299 FORMAT(1H,8X,I5,F15.4,F15.2,F15.5,F15.2)
300 FORMAT(1H,11X,K,1,10X,PHI,1,10X,TORQUE,1,10X,TAUR,1,10X,OM)
302 FORMAT(1H,13X,4F15.3)
303 FORMAT(1H,13X,4E15.5)
308 FORMAT(1H,26X,YR,13X,YS,13X,CU,13X,CL)
309 FORMAT(1H,23X,ETAMU,11X,ETAML,11X,PSIU,11X,PSIL)
310 FORMAT(1H,25X,RER,12X,RES,12X,REU,12X,REL)
311 FORMAT(1H,22X,BETA,1,11X,ALPHA3,1,10X,IR,1,10X,IS)
312 FORMAT(1H,22X,DELTA BETA,3X,DELTA ALPHA)
313 FORMAT(1H,12X,2F15.3)
325 FORMAT(1H,30X,FLOW LOSS COEFFICIENTS)
STOP
END

SUBROUTINE EOGL
FINDS CU AND REU

REAL KB1,KB2,KB3,KB4,IR,IS,NU,LAMDAU,LAMDAL,LUBR,LLBS,LMBDU,LMBDL
COMMON R1,R2,R3,R4,KB1,KB2,KB3,KB4,RHO,ETAMU,ETAML,PHIO,B1B,A3B,
BETA1,BETA2,ALPHA1,ALPHA2,ALPHA3,ALPHA4,B2B,A4B,BR,BS,
IR,IS,PSIU,PSIL,RER,RES,REU,REL,PHI,ARR,ARS,YR,YS,CU,CL,
CH2MH1,CH2MH3,CH3MH3,CH4MH1,CH4MH4,AH2MH1,AH2MH3,AH3MH4,AH4MH1,
BH2MH1,BH2MH3,BH3MH4,BH4MH1,CSUM,BSUM,ASUM,ROOT,PHIPR,PHIMR
COMMON R2R1,R2R2,R4R2,BRR2,BRBS,NU,R1R2,R2R3,R2R4,R4R3,BSR2,BSR3,
TORQUE,TAUR,OM,DELOM,LAMDAU,LAMDAL,LMBDU,LMBDL,LLBS,LUBR,
ZETAU,ZETAL
CP,CF
COMMON JJ,JJJ,K
COMMON/ ZETARE / YZ(9,11),XRZ(11),YSTRZ,NZR,IZ
COMMON/ LMDARE / YL(12),XRL(12),YSTRL,NRL

C
REU = 2.*BS*R2R3*KB2/KB3*PHI*R2*OM/NU

```



```

ZETAU = FIG(REU)
LMBDU = FIG2(REU)
CU = 2.0*ZETAU+ .5*LUBR*LMBDU
RETURN
END

```

# SUBROUTINE EQG2

```

C*****
C      CALCULATES CL AND REL
C
REAL KB1,KB2,KB3,KB4,IR,IS,NU,LAMDAU,LAMDAL,LUBR,LLBS,LMBDU,LMBDL
COMMON
1  R1,R2,R3,R4,KB1,KB2,KB3,KB4,RHO,ETAMU,ETAML,PHIO,B1B,A3B,
2  BETAI,BETA2,ALPHA1,ALPHA2,ALPHA3,ALPHA4,B2B,A4B,BR,BS,
3  IR,IS,PSIU,PSIL,RES,REU,REL,PHI,ARR,ARS,YR,YS,CU,CL,
4  CH2MH1,CH2MH3,CH3MH4,CH4MH1,AH2MH3,AH3MH4,AH4MH1,
COMMON BH2MH1,BH2MH3,BH3MH4,BH4MH1,CSUM,BSUM,ROOT,PHIPR,PHIMR
1  R2R1,R3R2,R4R2,BRR2,BRBS,NU,R1R2,R2R3,B2R3,B2R4,R4R3,BSR3,
2  TORQUE,TAUR,OM,DELOM,LAMDAU,LAMDAL,LMBDU,LMBDL,LLBS,LUBR,
COMMON ZETAU,ZETAL
COMMON CP,CF
COMMON JJ,JJ,K
COMMON ZETARE / YZ(9,11),XRZ(11),YSTRZ,NZR,IZ
COMMON LMDARE / YL(12),XRL(12),YSTRL,NRL
REL = 2.*BRR2R2R1*KB2/KB1*PHI*R2*OM/NU
LMBDL = FIG2(REL)
ZETAL = FIG(REL)
CL = 2.5*ZETAL+ .5 * LLBS * LMBDL
RETURN
END

```

# SUBROUTINE EQH5

```

C*****
C      FINDS LAMBDA, ETA, AND PSI FOR THE LOWER PASSAGES
C
REAL KB1,KB2,KB3,KB4,IR,IS,NU,LAMDAU,LAMDAL,LUBR,LLBS,LMBDU,LMBDL
COMMON
1  R1,R2,R3,R4,KB1,KB2,KB3,KB4,RHO,ETAMU,ETAML,PHIO,B1B,A3B,
2  BETAI,BETA2,ALPHA1,ALPHA2,ALPHA3,ALPHA4,B2B,A4B,BR,BS,
3  IR,IS,PSIU,PSIL,RES,REU,REL,PHI,ARR,ARS,YR,YS,CU,CL,
4  CH2MH1,CH2MH3,CH3MH4,CH4MH1,AH2MH3,AH3MH4,AH4MH1,
COMMON BH2MH1,BH2MH3,BH3MH4,BH4MH1,CSUM,BSUM,ROOT,PHIPR,PHIMR
1  R2R1,R3R2,R4R2,BRR2,BRBS,NU,R1R2,R2R3,B2R3,B2R4,R4R3,BSR3,
2  TORQUE,TAUR,OM,DELOM,LAMDAU,LAMDAL,LMBDU,LMBDL,LLBS,LUBR,
COMMON ZETAU,ZETAL
COMMON CP,CF
COMMON JJ,JJ,K

```



```

C***** TAKING INTO ACCOUNT ABSOLUTE VALUE
AAAA4 = ABS(ALPHA4)
LAMDA4 = CF*TAN(AAAA4)*LLBS/KB4
ETAML = 1.0 - LAMDA4
PSIL = 1.0 -(ETAML**2)
RETURN
END

SUBROUTINE EQH6
C***** FINDS LAMBDA, ETA, AND PSI FOR THE UPPER PASSAGES.
C
REAL KB1,KB2,KB3,KB4,IR,IS,NU,LAMDAU,LAMDAL,LUBR,LLBS,LMBDU,LMBDL
COMMON R1,R2,R3,R4,KB1,KB2,KB3,KB4,RHO,ETAMU,ETAML,PHIO,B1B,A3B,
1 BETAI,BETA2,ALPHA1,ALPHA2,ALPHA3,ALPHA4,B2B,A4B,BR,BS,
2 IR,IS,PSIU,PSIL,RER,RES,REU,REL,PHI,ARR,ARS,YR,YS,CU,CL,
3 CH2MH1,CH2MH3,CH3MH4,CH4MH1,AH2MH1,AH2MH3,AH3MH4,AH4MH1,
4 BH2MH1,BH2MH3,BH3MH4,BH4MH1,CSUM,BSUM,ROOT,PHIPR,PHIMR
COMMON R2R1,R3R2,R4R2,BRR2,BRRS,NU,R1R2,R2R3,R2R4,R4R3,BSR2,BSR3,
1 TORQUE,TAUR,OM,DELOM,LAMDAU,LAMDAL,LMBDU,LMBDL,LLBS,LUBR,
2 ZETAU,ZETAL
COMMON CP,CF
COMMON JJ,JJJ,K
C***** ACCOUNTING FOR SIGNS BY ASSIGNING ABSOLUTE VALUES
B8BB2 = ABS(BETA2)
LAMDAU = (CF*(1 + PHI*TAN(B8BB2)) * LUBR)/(PHI *KB2)
ETAMU = 1.0 - LAMDAU
PSIU = 1.0 -(ETAMU**2)
RETURN
END

FUNCTION EQI8 (RE,AR,ANG1,ANG2)
C
C CALCULATES THE LOSS COEFFICIENTS YR AND YS.
C
REAL KB1,KB2,KB3,KB4,IR,IS,NU,LAMDAU,LAMDAL,LUBR,LLBS,LMBDU,LMBDL
COMMON R1,R2,R3,R4,KB1,KB2,KB3,KB4,RHO,ETAMU,ETAML,PHIO,B1B,A3B,
1 BETAI,BETA2,ALPHA1,ALPHA2,ALPHA3,ALPHA4,B2B,A4B,BR,BS,
2 IR,IS,PSIU,PSIL,RER,RES,REU,REL,PHI,ARR,ARS,YR,YS,CU,CL,
3 CH2MH1,CH2MH3,CH3MH4,CH4MH1,AH2MH1,AH2MH3,AH3MH4,AH4MH1,
4 BH2MH1,BH2MH3,BH3MH4,BH4MH1,CSUM,BSUM,ROOT,PHIPR,PHIMR
COMMON R2R1,R3R2,R4R2,BRR2,BRRS,NU,R1R2,R2R3,R2R4,R4R3,BSR2,BSR3,
1 TORQUE,TAUR,OM,DELOM,LAMDAU,LAMDAL,LMBDU,LMBDL,LLBS,LUBR,
2 ZETAU,ZETAL
COMMON CP,CF

```





```

C*****
COMMON JJ,JJJ,K
TAKING INTO ACCOUNT ABSOLUTE VALUE
DELANG = ABS((ANG1 -ANG2))
DELANE = DELANG*180./3.1416
PSI = .99 -2.28*DELANE/(10.0**4) -4.97/(180.- DELBE)
EQI8 = ((.975+.075/AR)/(PSI**2)-1.) * (((10.**5)/RE)**.25)
RETURN
END

C
C
FUNCTION ENRER (PHII)
CALCULATES THE REYNOLDS NUMBER OF THE ROTOR

REAL KB1,KB2,KB3,KB4,IR,IS,NU,LAMDAU,LAMDAL,LUBR,LLBS,LMBDU,LMBDL
COMMON
R1,R2,R3,R4,KB1,KB2,KB3,KB4,RHO,ETAMU,ETAML,PHIO,B1B,A3B,
BETA1,BETA2,ALPHA1,ALPHA2,ALPHA3,ALPHA4,B2B,A4B,BR,BS,
IR,IS,PSIU,PSIL,RER,RES,REU,REL,PHI,ARR,ARS,YR,YC,CL,
CH2MH1,CH2MH3,CH3MH4,CH4MH1,AH2MH3,AH3MH4,AH4MH1,
BH2MH1,BH2MH3,BH3MH4,BH4MH1,CSUM,BSUM,ROOT,PHIPR,PHIMR
COMMON R2R1,R3R2,R4R2,BRR2,BRBS,NU,R1R2,R2R3,R4R3,BSR2,BSR3,
TORQUE,TAU,OM,DELOM,LAMDAU,LAMDAL,LMBDU,LMBDL,LLBS,LUBR,
ZETAU,ZETA
COMMON CP,CF
COMMON JJ,JJJ,K
C*****
TAKING INTO ACCOUNT ABSOLUTE VALUE
ADELB2 = ABS(TAN(BETA2) - TAN(B1B))
X1 = BRR2*ADELB2*COS(BETA2)**2
X2 = 0.425*(1.-R1R2)
X3 = PHII*OM*(R2**2)/NU
ENRER = X3*(2.0*BRR2) / (COS(BETA2) + X1/X2)
RETURN
END

C
C
FUNCTION ENRES (PHII)
CALCULATES THE REYNOLDS NUMBER OF THE STATOR

REAL KB1,KB2,KB3,KB4,IR,IS,NU,LAMDAU,LAMDAL,LUBR,LLBS,LMBDU,LMBDL
COMMON
R1,R2,R3,R4,KB1,KB2,KB3,KB4,RHO,ETAMU,ETAML,PHIO,B1B,A3B,
BETA1,BETA2,ALPHA1,ALPHA2,ALPHA3,ALPHA4,B2B,A4B,BR,BS,
IR,IS,PSIU,PSIL,RER,RES,REU,REL,PHI,ARR,ARS,YR,YC,CL,
CH2MH1,CH2MH3,CH3MH4,CH4MH1,AH2MH3,AH3MH4,AH4MH1,
BH2MH1,BH2MH3,BH3MH4,BH4MH1,CSUM,BSUM,ROOT,PHIPR,PHIMR
COMMON R2R1,R3R2,R4R2,BRR2,BRBS,NU,R1R2,R2R3,R4R3,BSR2,BSR3,
TORQUE,TAU,OM,DELOM,LAMDAU,LAMDAL,LMBDU,LMBDL,LLBS,LUBR,

```



```

2 COMMON ZETAU, ZETAU
COMMON CP, CF
COMMON JJ, JJJ, K
C***** TAKING INTO ACCOUNT ABSOLUTE VALUE
C ADELA4 = ABS(TAN(A3B) - TAN(ALPHA4))
C
X1 = BSR2 * ADELA4 * (COS(ALPHA4)**2)
X2 = 0.425 * R3R2 * (1. - R4R3)
X3 = PHI * OM * (R2**2) / NU
ENRES = X3 * (2. * BRR2 / R4R2 * KB2 / KB4) / (COS(ALPHA4) + X1 / X2)
RETURN
END

```

```

SUBROUTINE EQE28
C***** CALCULATES COEFFICIENTS OF (H2 - H1) / (OMEGA * R2)**2
C
REAL KB1, KB2, KB3, KB4, IR, IS, NU, LAMDAU, LAMDAL, LUBR, LLBS, LMBDU, LMBDL
COMMON R1, R2, R3, R4, KB1, KB2, KB3, KB4, RHO, ETAMU, ETAML, PHI, B1B, A3B,
BETA1, BETA2, ALPHA1, ALPHA2, ALPHA3, ALPHA4, B2B, A4B, BR, BS,
1 IR, IS, PSIU, PSIL, REU, REL, PHI, ARR, ARS, YR, YS, CU, CL,
2 CH2MH1, CH2MH3, CH3MH4, CH4MH1, AH2MH3, AH3MH4, AH4MH1,
3 BH2MH1, BH2MH3, BH3MH4, BH4MH1, CSUM, BSUM, ROOT, PHIPR, PHIMR
4 COMMON R2R1, R3R2, R4R2, BRR2, BRBS, NU, R1R2, R2R3, R2R4, R4R3, BSR2, BSR3,
1 TORQUE, TAUR, OM, DELOM, LAMDAU, LAMDAL, LMBDU, LMBDL, LLBS, LUBR,
2 ZETAU, ZETAU
COMMON CP, CF
COMMON JJ, JJJ, K
X1 = COS(IR)**2
X2 = (1. - X1) / 2.
X3 = (KB2 / KB4 * ETAML * TAN(ALPHA4))
CH2MH1 = 1. - X2 * ((R1R2)**2)
BH2MH1 = TAN(BETA2) - (X1 * X3)
AH2MH1 = -X2 * ((R2R1)**2) * (((KB2 / KB1)**2) + (X3**2)) - YR / (2. * (
1 RETURN
END

```

```

SUBROUTINE EQF12
C***** CALCULATES COEFFICIENTS OF (H2 - H3) / (OMEGA * R2)**2
C
REAL KB1, KB2, KB3, KB4, IR, IS, NU, LAMDAU, LAMDAL, LUBR, LLBS, LMBDU, LMBDL
COMMON R1, R2, R3, R4, KB1, KB2, KB3, KB4, RHO, ETAMU, ETAML, PHI, B1B, A3B,
1 BETA1, BETA2, ALPHA1, ALPHA2, ALPHA3, ALPHA4, B2B, A4B, BR, BS,
2 IR, IS, PSIU, PSIL, REU, REL, PHI, ARR, ARS, YR, YS, CU, CL,

```



```

3      CH2MH1, CH2MH3, CH3MH4, CH4MH1, AH2MH1, AH2MH3, AH3MH4, AH4MH1,
4      BH2MH1, BH2MH3, BH3MH4, BH4MH1, CSUM, BSUM, ASUM, ROOT, PHI, PR, PHIMR
COMMON R2R1, R3R2, R4R2, BRR2, BRBS, NU, R1R2, R2R3, R2R4, R4R3, BSR2, BSR3,
1      TORQUE, TAUR, OM, DELOM, LAMDAU, LAMDAL, LMBDU, LMBDL, LLBS, LUBR,
2      ZETAU, ZETAL
COMMON CP, CF
COMMON JJ, JJJ, K
      X1 = (R2R3)**2
      CH2MH3 = PSIUX1/2.
      BH2MH3 = PSIUX1*TAN(BETA2)
      AH2MH3 = X1/2. * (PSIU*(TAN(BETA2)**2) + CU*((KB2/KB3)**2))
      RETURN
      END

```

C

#### SUBROUTINE EQE13A

CALCULATES COEFFICIENTS OF  $(H3 - H4)/(OMEGA * R2)**2$

C  
C  
C

```

      REAL KB1, KB2, KB3, KB4, IR, IS, NU, LAMDAU, LAMDAL, LUBR, LLBS, LMBDU, LMBDL
COMMON R1, R2, R3, R4, KB1, KB2, KB3, KB4, RHIO, ETAMU, ETAML, PHI, A3B,
1      BETA1, BETA2, ALPHA1, ALPHA2, ALPHA3, ALPHA4, B2B, A4B, BR, BS,
2      IR, IS, PSIUX1, REP, RES, REL, PHI, ARR, ARS, YR, YS, CU, CL,
3      CH2MH1, CH2MH3, CH3MH4, CH4MH1, AH2MH1, AH2MH3, AH3MH4, AH4MH1,
4      BH2MH1, BH2MH3, BH3MH4, BH4MH1, CSUM, BSUM, ASUM, ROOT, PHI, PR, PHIMR
COMMON R2R1, R3R2, R4R2, BRR2, BRBS, NU, R1R2, R2R3, R2R4, R4R3, BSR2, BSR3,
1      TORQUE, TAUR, OM, DELOM, LAMDAU, LAMDAL, LMBDU, LMBDL, LLBS, LUBR,
2      ZETAU, ZETAL
COMMON CP, CF
COMMON JJ, JJJ, K
      X1 = ((1. - (COS((IS)**2))/2.)*((R2R3)**2)
      X2 = (R2R4*(COS(KB1/KB4))/(COS(ALPHA4)))**2
      CH3MH4 = X1*(ETAMU**2)
      BH3MH4 = CH3MH4*2.*TAN(BETA2)
      AH3MH4 = X1*((KB2/KB3)**2) + ((ETAMU*TAN(BETA2))**2) ÷ YS*X2*.5
      RETURN
      END

```

#### SUBROUTINE EQD9

CALCULATES COEFFICIENTS OF  $(H4 - H1)/(OMEGA * R2)**2$

C  
C  
C

```

      REAL KB1, KB2, KB3, KB4, IR, IS, NU, LAMDAU, LAMDAL, LUBR, LLBS, LMBDU, LMBDL
COMMON R1, R2, R3, R4, KB1, KB2, KB3, KB4, RHIO, ETAMU, ETAML, PHI, A3B,
1      BETA1, BETA2, ALPHA1, ALPHA2, ALPHA3, ALPHA4, B2B, A4B, BR, BS,
2      IR, IS, PSIUX1, PSIL, PER, RES, REL, PHI, ARR, ARS, YR, YS, CU, CL,

```



```

3      CH2MH1,CH2MH3,CH3MH4,CH4MH1,AH2MH1,AH3MH4,AH4MH1,
4      BH2MH1,BH3MH4,BH4MH1,CSUM,BSUM,ASUM,ROOT,PHIPR,PHIMR
COMMON R2R1,R3R2,R4R2,BRBS,NU,R1R2,R2R3,R2R4,R4R3,BSR2,BSR3,
1      TORQUE,TAUR,OM,DELOM,LAMDAU,LMBDL,LLBS,LUBR,
2      ZETAU,ZETAL
COMMON CP,CF
COMMON JJ,JJJ,K
C
X1 = KB2/KB4*TAN(ALPHA4)
CH4MH1 = 0.0
BH4MH1 = 0.0
AH4MH1 = .5*((R2R1)**2)*( CL*((KB2/KB1)**2) + PSIL*(X1**2))
RETURN
END

```

#### SUBROUTINE PHITES

ACCOMPLISHES THE FINAL ITERATION STEP IN DETERMINING PHI

```

REAL KB1,KB2,KB3,KB4,IR,IS,NU,LAMDAU,LAMDAL,LUBR,LLBS,LMBDU,LMBDL
COMMON R1,R2,R3,R4,KB1,KB2,KB3,KB4,RHO,ETAMU,ETAML,PHIO,B1B,A3B,
1      BETAL,BETA2,ALPHA1,ALPHA2,ALPHA3,ALPHA4,B2B,A4B,BR,BS,
2      IR,IS,PSIU,PSIL,RER,RES,REU,REL,PHI,ARR,ARS,YR,YS,CU,CL,
3      CH2MH1,CH2MH3,CH3MH4,CH4MH1,AH2MH1,AH3MH4,AH4MH1,
4      BH2MH1,BH2MH3,BH3MH4,BH4MH1,CSUM,BSUM,ASUM,ROOT,PHIPR,PHIMR
COMMON R2R1,R3R2,R4R2,BRBS,NU,R1R2,R2R3,R2R4,R4R3,BSR2,BSR3,
1      TORQUE,TAUR,OM,DELOM,LAMDAU,LMBDL,LLBS,LUBR,
2      ZETAU,ZETAL
COMMON CP,CF
COMMON JJ,JJJ,K

```

THE PREVIOUS FOUR SUBROUTINES ARE NOW ADDED

```

CSUM = CH2MH1 - CH2MH3 - CH3MH4 - CH4MH1
BSUM = BH2MH1 - BH2MH3 - BH3MH4 - BH4MH1
ASUM = AH2MH1 - AH2MH3 - AH3MH4 - AH4MH1

```

THE QUADRATIC EQUATION IS NOW SOLVED TO YIELD THE NEW VALUE OF PHI.

```

ROOT = SQRT((BSUM**2) - 4.0*ASUM*CSUM)
PHIPR = (-BSUM + ROOT)/(2.0*ASUM)
PHIMR = (-BSUM - ROOT)/(2.0*ASUM)
JJ = 0
JJJ = 0

```

DETERMINING THE PROPER ROOT

```

IF (PHIMR.LT. 0.0) GO TO 2
IF ( PHIMR.GT. 0.0) GO TO 5
IF ( PHIPR.LT. 0.0 ) GO TO 15

```







```

5 IF (PHIPR.GT. 0.0 ) GO TO 6
  PHI = PHIMR
  GO TO 80
15 PRINT 20
  PHI = PHIPR
20 FORMAT(1H0,' BOTH ROOTS OF PHI ARE NEGATIVE, AND THE PROGRAM WILL BE
  1 DUMPED*****')
80 IF ( PHI.LT. 0.0 ) JJ = 1
  IF ( JJ.EQ. 1 ) GO TO 10
  IF (JJJ.EQ. 1 ) GO TO 10
  RETURN
10 PRINT 11,JJ,JJJ
11 FORMAT(1H0,'JJ = ',I5,'JJJ = ',I5)
  RETURN
  END

```

```

FUNCTION EQB19( PHI )
REAL KB1,KB2,KB3,KB4,IR,IS,NU,LAMDAU,LAMDAL,LUBR,LLBS,LMBDU,LMBDL
COMMON
  1 R1,R2,R3,R4,KB1,KB2,KB3,KB4,RHO,ETAMU,ETAML,PHIO,B1B,A3B,
  2 BETAI,BETA2,ALPHA1,ALPHA2,ALPHA3,ALPHA4,B2B,A4B,BR,BS,
  3 IR,IS,PSIU,PSIL,RER,RES,REU,REL,PHI,ARR,ARS,YR,YS,CU,CL,
  4 CH2MH1,CH2MH3,CH3MH4,CH4MH1,AH2MH3,AH3MH4,AH4MH1,
  5 BH2MH1,BH2MH3,BH3MH4,BH4MH1,CSUM,BSUM,ASUM,ROOT,PHIPR,PHIMR
COMMON R2R1,R3R2,R4R2,BRR2,BRR3,NU,R1R2,R2R3,R4R3,BSR2,BSR3,
  1 TORQUE,TAUR,OM,DELOM,LAMDAU,LAMDAL,LMBDU,LLBS,LUBR,
  2 ZETAU,ZETAL
COMMON CP,CF
COMMON JJ,JJJ,K

```

```

  X1 = TAN(BETA2) - ETAML*(KB2/KB4)*TAN(ALPHA4)
  EQB19 = PHII + (PHII**2)*X1
  RETURN
  END

```

C

```

SUBROUTINE EQB20
REAL KB1,KB2,KB3,KB4,IR,IS,NU,LAMDAU,LAMDAL,LUBR,LLBS,LMBDU,LMBDL
COMMON
  1 R1,R2,R3,R4,KB1,KB2,KB3,KB4,RHO,ETAMU,ETAML,PHIO,B1B,A3B,
  2 BETAI,BETA2,ALPHA1,ALPHA2,ALPHA3,ALPHA4,B2B,A4B,BR,BS,
  3 IR,IS,PSIU,PSIL,RER,RES,REU,REL,PHI,ARR,ARS,YR,YS,CU,CL,
  4 CH2MH1,CH2MH3,CH3MH4,CH4MH1,AH2MH3,AH3MH4,AH4MH1,
  5 BH2MH1,BH2MH3,BH3MH4,BH4MH1,CSUM,BSUM,ASUM,ROOT,PHIPR,PHIMR
COMMON R2R1,R3R2,R4R2,BRR2,BRR3,NU,R1R2,R2R3,R4R3,BSR2,BSR3,
  1 TORQUE,TAUR,OM,DELOM,LAMDAU,LAMDAL,LMBDU,LLBS,LUBR,
  2 ZETAU,ZETAL
COMMON CP,CF
COMMON JJ,JJJ,K

```



```
TORQUE = 2.*3.1416*RHO*(R2**5)*BRR2*KB2*TAUR*(OM**2)
RETURN
END
```

```
SUBROUTINE NONDEM
```

```
ACCOMPLISHES THE NON-DIMENSIONALIZATION
```

```
REAL KB1,KB2,KB3,KB4,IR,IS,NU,LAMDAU,LAMDAL,LUPR,LLBS,LMBDU,LMBDL
COMMON R1,R2,R3,R4,KB1,KB2,KB3,KB4,RHO,ETAMU,ETAML,PHIO,B1B,A3B,
BETA1,BETA2,ALPHA1,ALPHA2,ALPHA3,ALPHA4,B2B,A4B,BR,BS,
IR,IS,PSIU,PSIL,RER,RES,REU,REL,PHI,ARR,ARS,YR,YC,CL,
CH2MH1,CH2MH3,CH3MH4,CH4MH1,AH2MH1,AH3MH4,AH4MH1,
BH2MH1,BH2MH3,BH3MH4,BH4MH1,CSUM,BSUM,ASUM,FOOT,PHIPR,PHIMR
COMMON R2R1,R3R2,R4R2,BRR2,BRBS,NU,R1R2,R2R3,R2R4,R4R3,BSR2,BSR3,
TORQUE,TAUR,OM,DELOM,LAMDAU,LAMDAL,LMBDU,LMBDL,LLBS,LUBR,
ZETAU,ZETAL
COMMON CP,CF
COMMON JJ,JJ,K
COMMON TORREF,POWREF,PIOM,PITORQ,PIPOWR,OMMAX
```

```
PIGM = OM/OMMAX
PITORQ = TORQUE/TORREF
PIPOWR = (OM*TORQUE)/POWREF
PIPHI = PHI*PIOM
PRINT 600,PIOM
PRINT 605,PIPOWR
PRINT 609,PITORQ
PRINT 611,PIPHI
600 FORMAT(1H0,15X,'THE DIMENSIONLESS ROTATIONAL SPEED=',F6.3)
605 FORMAT(1H0,15X,'THE DIMENSIONLESS POWER =',F16.3)
609 FORMAT(1H0,15X,'THE DIMENSIONLESS TORQUE =',F15.3)
611 FORMAT(1H0,15X,'THE REVISED FLOW COEFFICIENT =',F9.3)
RETURN
END
```

```
FUNCTION FIG( RE )
```

```
THE BENDING LOSS COEFFICIENT IS APPROXIMATED FOR IN THIS SUBROUTINE
AN ALTERNATE CHOICE TO EMPLOY WOULD BE TO USE A CURVE FIT ON FIGURE 15.
```

```
COMMON/ ZETARE / YZ(9,11),XRZ(11),YSTRZ,NZR,IZ
```

```
J = 1
IF(RE.LE. XRZ(J)) GO TO 20
J = NZR
```



```

10 IF(RE .GE. XRZ(J)) GO TO 20
   J=1
   IF(RE .EQ. XRZ(J)) GO TO 20
   IF(RE .LT. XRZ(J+1)) GO TO 25
   J=J+1
   IF( J .LT. NZR ) GO TO 10
   Y = YZ(IZ,J)
20 GO TO 30
25 Y = YZ(IZ,J) + (YZ(IZ,J+1) - YZ(IZ,J))*(RE - XRZ(J))/
   (XRZ(J+1) - XRZ(J))
30 FIG = Y*YSTRZ
   RETURN
   END

```

#### FUNCTION FIG2( RE )

THE FRICTION FACTOR IS APPROXIMATED IN THIS SUBROUTINE. THE VALUES ARE GIVEN IN THE BLOCK DATA OBTAINED FROM FIGURE 16. THIS IS APPROXIMATE SINCE IT IS ONLY TO THE NEAREST VALUE OF REYNOLDS NUMBERS. AN ALTERNATE CHOICE TO EMPLOY WOULD BE TO USE A CURVE FIT ON FIGURE 16.

COMMON/ LMDARE / YL(12),XRL(12),YSTRL,NRL

```

10 J=1
   IF(RE .LE. XRL(J)) GO TO 20
   J=NRL
   IF(RE .GE. XRL(J)) GO TO 20
   J=1
   IF(RE .EQ. XRL(J)) GO TO 20
   IF(RE .LT. XRL(J+1)) GO TO 25
   J=J+1
   IF( J .LT. NRL ) GO TO 10
   Y = YL(J)
20 GO TO 30
25 Y = YL(J) + (YL(J+1) - YL(J))*(RE - XRL(J))/(XRL(J+1) - XRL(J))
30 FIG2 = Y*YSTRL
   RETURN
   END

```

#### SUBROUTINE VALUE

THIS SUBROUTINE ACCOMPLISHES THE FLOW ANALYSIS. ANY MODIFICATIONS TO THE DESIRED OUTPUT SHOULD PROBABLY BE MADE IN THIS SUBROUTINE. SINCE THE FLOW COEFFICIENT IS ALREADY KNOWN, ANY VALUES IN TERMS OF PHI OR GEOMETRIC PARAMETERS CAN NOW BE EVALUATED



```

REAL KB1,KB2,KB3,KB4,IR,IS,NU,LAMDAU,LAMDAL,LUBR,LLBS,LMBDU,LMBDL
COMMON R1,R2,R3,R4,KB1,KB2,KB3,KB4,RHO,ETAMU,ETAML,PHIO,B1B,A3B,
      BETAI,BETA2,ALPHA1,ALPHA2,ALPHA3,ALPHA4,B2B,A4B,BR,BS,
      IR,IS,PSIU,PSIL,RER,RES,REU,REL,PHI,ARR,ARS,YR,YS,CU,CL,
      CH2MH1,CH2MH3,CH3MH4,CH4MH1,AH2MH1,AH2MH3,AH3MH4,AH4MH1,
      BH2MH1,BH2MH3,BH3MH4,BH4MH1,CSUM,BSUM,ROOT,PHIPR,PHIMR
COMMON R2R1,R3R2,R4R2,BRBS,NU,R1R2,R2R3,R2R4,R4R3,BSR2,BSR3,
      TORQUE,TAUR,OM,DELOM,LANDAU,LAMDAL,LMBDU,LLBS,LUBR,
      ZETAU,ZETAL
COMMON CP,CF
COMMON JJ,JJJ,K
COMMON TORREF,POWREF,PIOM,PITORQ,PIPOWR,OMMAX

```

# VELOCITIES

```

VM2 = PHI*OM*R2
VU2 = VM2 * TAN(BETA2) + (R2*OM)
V2 = SQRT(VU2**2 + VM2**2)
VM1 = VM2 * R2R1 * KB2/KB1
VU1 = VM1 * TAN(BETA1) + OM * R1
V1 = SQRT(VU1**2 + VM1**2)
VM3 = VM2 * R2R3 * BRBS * KB2/KB3
VU3 = VU2 * R2R3 * ETAMU
V3 = SQRT(VU3**2 + VM3**2)
VM4 = VM2 * R2R4 * BRBS * KB2/KB4
VU4 = VM4 * TAN(ALPHA4)
V4 = SQRT(VU4**2 + VM4**2)
W1 = VM1/COS(BETA1)
W2 = VM2/COS(BETA2)

```

# ENERGY DIFFERENCES

```

ABSOLUTE ENERGY CHANGES
ROM = (R2**2)*(OM**2)
H2M1 = (CH2MH1 + PHI*BH2MH1 + (PHI**2)*AH2MH1)*ROM
H2M3 = (CH2MH3 + PHI*BH2MH3 + (PHI**2)*AH2MH3)*ROM
H3M4 = (CH3MH4 + PHI*BH3MH4 + (PHI**2)*AH3MH4)*ROM
H4M1 = (CH4MH1 + PHI*BH4MH1 + (PHI**2)*AH4MH1)*ROM

```

# DIMENSIONLESS ENERGY CHANGES AND INPUT

```

H2M1N = (CH2MH1 + PHI*BH2MH1 + (PHI**2)*AH2MH1)
H2M3N = (CH2MH3 + PHI*BH2MH3 + (PHI**2)*AH2MH3)
H3M4N = (CH3MH4 + PHI*BH3MH4 + (PHI**2)*AH3MH4)
H4M1N = (CH4MH1 + PHI*BH4MH1 + (PHI**2)*AH4MH1)
ENERJN = OM *(R2*VU2 - R1*VU1)
H2M1TH = ENERJN/ROM
ROTLOS = H2M1TH - H2M1N

```





CCC

# TOTAL PRESSURE DIFFERENCES

```

RHOIN = RHO/144.
TP2M1 = H2M1*RHOIN
TP2M3 = H2M3*RHOIN
TP3M4 = H3M4*RHOIN
TP4M1 = H4M1*RHOIN

```

CCC

# STATIC PRESSURE DIFFERENCES

```

SP2M1 = TP2M1 + ((V1**2) - (V2**2))*RHOIN/2.
SP2M3 = TP2M3 + ((V3**2) - (V2**2))*RHOIN/2.
SP3M4 = TP3M4 + ((V4**2) - (V3**2))*RHOIN/2.
SP4M1 = TP4M1 + ((V1**2) - (V4**2))*RHOIN/2.

```

CCC

# LOSSES ENCOUNTERED

```

ENLYR = YR*(W2**2)/(2.*ENERIN)
ENLIR = (1.-(COS(IR)**2))*ENERIN
ENLCU = CU*(VM3**2)/(2.*ENERIN)
ENLEU = ((1./(ETAMU**2))-1.)*(VU3**2)/(2.*ENERIN)
ENLIS = YS*(V4**2)/(2.*ENERIN)
ENLIS = (1.-(COS(IS)**2))*ENERIN
ENLCL = CL*(VM1**2)/(2.*ENERIN)
ENLEL = ((1./(ETAML**2))-1.)*(VU1**2)/(2.*ENERIN)

```

C

```

PRINT 700
PRINT 701, VM1, VM2, VM3, VM4
PRINT 702, VU1, VU2, VU3, VU4
PRINT 703, V1, V2, V3, V4
PRINT 704, W1, W2
PRINT 750, ENERIN
PRINT 752
PRINT 755
PRINT 756, H2M1, H2M3, H3M4, H4M1
PRINT 757
PRINT 758, H2M1N
PRINT 759, H2M3N
PRINT 760, H3M4N
PRINT 761, H4M1N
PRINT 763, H2M1TH
PRINT 764, ROTLOS
PRINT 770
PRINT 772
PRINT 774, TP2M1, TP2M3, TP3M4, TP4M1
PRINT 776
PRINT 778

```







```

C
C
C
C
BLOCK DATA
THIS DATA IS OBTAINED FROM FIGURE 16, AND ARE THE VALUES OF THE FRICTION
FACTOR AT VARIOUS REYNOLDS NUMBERS.
COMMON/ LMDARE / YL(12),XRL(12),YSTRL,NRL
DATA YL/.0265,.0233,.0218,.0204,.0193,.0185,.0173,.0165,.0155,
1 .0148,.0141,.0137/,XRL/2.E04,3.E04,4.E04,6.E04,8.E04,
2 1.E05,1.5E05,2.E05,3.E05,4.E05,6.E05,8.E05/,
3 YSTRL/1.0/,NRL/12/
END

```



## APPENDIX D

### PROGRAM REVERSE

Program REVERSE solves the equations for reverse circulation, Modes 3 and 4. The program is very similar to program NORMAL, and the flow chart of Table IV is the same. Further discussion would be mere repetition of Appendix C.





# PROGRAM REVERSE

THIS PROGRAM SOLVES THE SET OF EQUATIONS PRESENTED IN APPENDIX B. AN ITERATION TECHNIQUE IS NECESSARY TO SOLVE FOR PHI SINCE VARIOUS LOSS COEFFICIENTS ARE PHI DEPENDENT. A STRAIGHT QUADRATIC EQUATION SOLVES THE ENERGY BALANCE EQUATION GIVEN BY EQUATION B2C. AFTER CONVERGENCE IS ACHIEVED, THE FLOW ANALYSIS AND NON-DIMENSIONALIZATION WILL BE ACCOMPLISHED.

IT MUST BE REMEMBERED THAT THIS SOLUTION IS ONLY VALID FOR THE CONDITION OF REVERSE CIRCULATION, MODES 3 AND 4. THE ACTUAL DIFFERENCE BETWEEN THE MODES IS THE DIRECTION OF SHAFT ROTATION. THE FLOW EXIT ANGLES AT THE ROTOR AND STATOR MUST REMAIN CONSTANT, HOWEVER, THE SIGNS WILL BE CHANGED DUE TO THE SIGN CONVENTION EMPLOYED IN THE ANALYSIS. THAT IS ALL ANGLES ARE POSITIVE IF THEIR PERIPHERAL COMPONENT OF VELOCITY IS IN THE DIRECTION OF ROTATION.

THE DATA IS INPUTTED ON SEVEN(7) DATA CARDS.

CARD ONE: THE MONTH, DAY, AND YEAR ARE PLACED IN COLUMNS 1-5, 6-10, AND 11-15 RESPECTIVELY. NOTE THAT THESE INTEGERS MUST BE RIGHT HAND ADJUSTED.

CARD TWO: COLUMNS 1-5 THE RUN NUMBER, RIGHT ADJUSTED. COLUMNS 6-15 AND 16-25, THE RADIUS OF THE ROTOR INLET AND OUTLET (IN INCHES), RESPECTIVELY. COLUMNS 26-35, THE INCREMENT OF ANGULAR SPEED (RAD/SECOND). COLUMNS 36-45, VALUE OF PHI TO BEGIN ITERATIONS. COLUMNS 46-55, THE INITIAL ANGULAR SPEED.

CARD THREE: THE BLOCKAGE FACTORS AT STATIONS 1, 2, 3, AND 4 ARE PLACED IN COLUMNS 1-10, 11-20, 21-30, 31-40.

CARD FOUR: THE RELATIVE EXIT ANGLES AT ROTOR AND STATOR (IN DEGREES) GO IN COLUMNS 1-10, AND 11-20. THE ANGLE TO THE MEAN CAMBER LINE (IN DEGREES) FOR ROTOR AND STATOR GO IN COLUMNS 21-30, AND 31-40, RESPECTIVELY.

CARD FIVE: IN COLUMNS 1-10, 11-20, 21-30, AND 31-40 ARE PLACED THE COEFFICIENT OF FRICTION, THE SPECIFIC HEAT OF THE FLUID, THE FLUID DENSITY (SLUGS PER CUBIC FOOT), AND THE KINEMATIC VISCOSITY (FEET\*\*2 PER SECOND)

CARD SIX: THE RATIO OF THE AVERAGE LENGTH OF THE UPPER PASSAGE TO ROTOR BLADE HEIGHT, THE RATIO OF THE AVERAGE LENGTH OF THE LOWER PASSAGE TO STATOR



BLADE HIEGHT, THE RADIUS OF THE INNER CONTOUR TO ROTOR BLADE HIEGHT, AND THE  
 RATIO OF THE ROTOR TO STATOR BLADE HIEGHT GO IN COLUMNS 1-10,11-20,21-30,  
 AND 31-40, RESPECTIVELY.

CARD SEVEN: THE RADIUS OF STATIONS 3 AND 4 AND THE BLADE HIEGHT OF THE  
 ROTOR AND STATOR(ALL VALUES ARE IN INCHES) ARE PLACED IN COLUMNS 1-10,11-20,  
 21-30,AND 31-40, RESPECTIVELY.

BLOCK DATA IS USED FOR CONVENIENCE DUE TO THE LARGE NUMBER OF SUBROUTINES.

```

REAL KB1,KB2,KB3,KB4,IR,IS,NU,LAMDAU,LAMDAL,LUBS,LLBR,LMBDU,LMBDL
COMMON R1,R2,R3,R4,KB1,KB2,KB3,KB4,RHO,ETAMU,ETAML,PHIO,
  BETAI,BETA2,ALPHA1,ALPHA2,ALPHA3,ALPHA4,B2B,A4B,BR,BS,
  IR,IS,PSIU,PSIL,REU,RES,REL,PHI,ARR,ARS,YR,YS,CU,CL,
  CH1MH2,CH3MH2,CH4MH3,CH1MH4,AH1MH2,AH3MH2,AH4MH3,AH1MH4,
  BH1MH2,BH3MH2,BH4MH3,8H1MH4,CSUM,BSUM,ROOT,PHIPR,PHIMR
COMMON R2R1,R3R1,R4R1,BRBS,NU,R1R2,R1R3,R1R4,R3R4,BSR1,BSR4,
  TORQUE,TAUR,OM,DELOM,LAMDAU,LAMDAL,LUBS,LLBR,ZETAU,ZETAL,
  LMBDU,LMBDL
COMMON CP,CF
COMMON JJ,JJJ,K
COMMON TORREF,PIOM,PITORQ,PIPUWR,OMMAX
COMMON/ ZETARE / YZ(9,11),XRZ(11),YSTRZ,NZR,IZ
COMMON/ LMDARE / YL(12),XRL(12),YSTRL,NRL

```

\*\*\*\*DATA INPUT\*\*\*

```

READ 498,IMON,IDAY,IYEAR
READ 499,IRUN,R1,R2,DELOM,PHIO,OMO
READ 500,KB1,KB2,KB3,KB4
READ 500,BETAI,ALPHA3,B2B,A4B
READ 500,CF,CP,RHO,NU
READ 500,LUBS,LLBR,R1BR,BRBS
READ 500,R3,R4,BR,BS
K = 0

```

LIST DATA INPUT

```

PRINT 509
PRINT 540
PRINT 510,IMON,IDAY,IYEAR
OM = OMO
PRINT 524
PRINT 521
PRINT 523,IRUN,R1,R2,DELOM,PHIO,OMO
PRINT 513

```

20



```

PRINT 501,KB1,KB2,KB3,KB4
PRINT 514
PRINT 501,BETA1,ALPHA3,B2B,A4B
PRINT 515
PRINT 530,CF,CP,RHO,NU
PRINT 517
PRINT 501,LUBS,LLBR,RIBR,BRBS
PRINT 518
C 498
498 FORMAT(3I5)
499 FORMAT(I5,5F10.2)
500 FORMAT(3F10.5,F10.8)
501 FORMAT(IH,4F10.3)
503 FORMAT(IH,4F10.4)
509 FORMAT(IH1,'DATA =',3I5)
510 FORMAT(IH0,7X,KB1,7X,KB2,7X,KB3,7X,KB4)
513 FORMAT(IH0,5X,BETA1,4X,ALPHA3,7X,B2B,7X,A4B)
514 FORMAT(IH0,5X,CF,8X,CP,7X,RHO,13X,NU)
515 FORMAT(IH0,6X,R2R1,6X,R3R1,6X,R4R1,6X,BRR1)
516 FORMAT(IH0,6X,LUBS,6X,LLBR,6X,RIBR,6X,BRBS)
517 FORMAT(IH0,6X,LMBDF,6X,ZETA,6X,BR,6X,BS)
518 FORMAT(IH0,3X,IRUN,8X,R1,9X,R2,9X,DELOM,8X,PHIO,6X,OMO)
521 1)
523 FORMAT(IH0,I5,5F12.2)
524 FORMAT(IH0,'CASE A.. FLOW IS RADially INWARD AT ROTOR ')
530 FORMAT(IH0,2F10.3,F15.5,F15.8)
540 FORMAT(IH0,10X,'FLOW EXITS ROTOR AT STATION 1, RETRACTION:')
550 FORMAT(IH0,7X,R1,9X,R2,9X,R3,9X,R4,9X,BR,9X,BS)
551 FORMAT(IH0,6F12.2)
C****
C INITIALIZATION
C
R2/R1 = R2/R1
R3/R1 = R3/R1
R4/R1 = R4/R1
BR/R1 = BR/R1
R1 INCH = R1
R2 INCH = R2
R3 INCH = R3R1*R1 INCH
R4 INCH = R4R1*R1 INCH
BR INCH = BR
BS INCH = BR INCH/BRBS
PRINT 516
PRINT 503,R2R1,R3R1,R4R1,BRR1
PRINT 550
PRINT 551,R1 INCH,R2 INCH,R3 INCH,R4 INCH,BR INCH,BS INCH
OMWAX = 800.*3.1416/30.0

```



THE VALUE OF RIBR IS INITIALIZED HERE AND WILL BE USED IN SUBROUTINE FIG TO OBTAIN VALUES OF THE BENDING LOSSES FROM FIGURE 15.

INITIAL VALUES OF THE REYNOLDS NUMBERS ARE GIVEN TO BEGIN THE ITERATIONS.

```

OM = OMMAX*C.O.1
R1 = R1/12.O
R2 = R2/12.O
BR = BR/12.O
BS = BR/BRBS
AB1 = BR/BETA1
AA3 = BETA1
ALPHA3 = 3.1416/180.*BETA1
B2B = 3.1416/180.*B2B
A4B = 3.1416/180.*A4B
R1R2 = 1./R2R1
R1R4 = 1./R4R1
R3R4 = 1./R3R1
BSR1 = BR/BRBS
BSR4 = BR/BRBS
ARR = BSR1/(R2R1-1.O)
THE VALUE OF RIBR IS INITIALISED
OBTAIN VALUES OF THE BENDING LOSS
IZ = 0
IF (RIBR.LE. 0.25) IZ=1
IF (RIBR.GE. 1.O) IZ=9
IF (IZ.NE. 0) GO TO 22
REALIZ = RIBR*10.O - 1.O
IZ = REALIZ

INITIAL VALUES OF THE REYNOLDS N
22 IRER = 10.O**5
RES = 10.O**5
REU = 10.O**5
REH = 10.O**5
PHI = PHI
TCRREF = RHO*(OMMAX**2)*(R2**5)
POWEREF = TORREF * OMMAX
PRINT 410, POWEREF
PRINT 415, TORREF
FORMAT(1H0,6X, 'THE REFERENCE TO
410 FORMAT(1H0,6X, 'THE REFERENCE TO
415 IF ( PHI .GT. 0.O ) GO TO 30
IR=0.
IS=0.0
BETA2= .82B
ALPHA4= .A4B
GO TO 30

```





```

C*****      CALCULATE PHI
C
  25  RER = ENRER ( PHI )
  30  RES = ENRES ( PHI )
      CALL EQG1
      CALL EQG2
      CALL EQH5
      CALL EQH6
      IF (PHI .LE. 0.0) GO TO 40
      TANB2 = (ETAMU**KB2/KB3*TAN(ALPHA3)) - (R2R1**2)*(KB2/KB1)/PHI
      BETA2 = ATAN(TANB2)
      IR = B2B - BETA2
      TANA4 = (ETAML/(PHI*(KB1/KB4)))*(1. + PHI*TAN(BETA1))
      ALPHA4 = ATAN(TANA4)
      IS = A4B - ALPHA4
C
  40  YR = EQI8(RER,ARR,BETA1,BETA2)
      YS = EQI8(RES,ARS,ALPHA3,ALPHA4)
      CALL EQE28
      CALL EQF12
      CALL EQE13A
      CALL EQD9
      CALL PHITES
C
C***** TESTING PHI
C
  100 IF ( K .GE. 1 ) GO TO 110
      K = 2
      PHIO = PHI
      GO TO 25
C
  110 TEST = ABS( (PHI - PHIO)/( (PHI + PHIO)/2. ) )
      IF ( TEST .LE. .0005 ) GO TO 120
C
      K = K + 1
      SAFETY OUTLET
      IF ( K .GT. 20 ) GO TO 120
      PHIO = PHI
      GO TO 25
C
C***** OUTPUT AND FLOW CALCULATIONS
C
  120 TAUR = EQB19( PHI )
      CALL EQB20
      DELBET = BETA1 - BETA2
      DELALP = ALPHA3 - ALPHA4
      DELALP = DELALP*180./3.1416
      DELBET = DELBET*180./3.1416

```



```

DBETA2 = BETA2 *180.0/3.1416
DALPHA4 = ALPHA4 *180.0/3.1416
DIR = IR *180.0/3.1416
DIS = IS *180.0/3.1416
PRINT 300
PRINT 299,K,PHI,TORQUE,TAUR,OM
PRINT 325
PRINT 308
PRINT 302,YR,YS,CU,CL
PRINT 309
PRINT 302,ETAMU,ETAML,PSIU,PSIL
PRINT 310
PRINT 303,RER,RES,REU,REL
PRINT 307
PRINT 305,DBETA2,DALPHA4,DIR,DIS
PRINT 312
PRINT 313,DELBET,DELALP
CALL NONDEM
CALL VALUE
DELOM = OMMAX * 0.1
OM = OM + DELOM
PHIO = PHI
K = 1
IF ( OM .LE. OMMAX ) GO TO 25
FORMAT(1H,8X,I5,F15.4,F15.2,F15.5,F15.2)
FORMAT(1H,11X,10X,PHI,10X,TORQUE,10X,TAUR,10X,OM)
FORMAT(1H,13X,4F15.3)
FORMAT(1H,20X,4F15.5)
FORMAT(1H,22X,F10.4,10X,F10.4,10X,F10.4)
FORMAT(1H,22X,BETA2,11X,ALPHA4,10X,DIR,11X,DIS)
FORMAT(1H,26X,YR,13X,YS,13X,CU,13X,CL)
FORMAT(1H,23X,ETAMU,11X,ETAML,11X,PSIU,11X,PSIL)
FORMAT(1H,25X,RER,12X,RES,12X,REU,12X,REL)
FORMAT(1H,20X,DELTA,BETA,3X,DELTA,ALPHA)
FORMAT(1H,12X,2F15.3)
FORMAT(1H,30X,FLOW,LOSS,COEFFICIENTS)
STOP
END

```

SUBROUTINE EQG1

FINDS CU AND REU

```

REAL KB1,KB2,KB3,KR4,IR,IS,NU,LAMDAU,LAMDAL,LUBS,LLBR,LMBDU,LMBDL
COMMON
  P1,R2,R3,R4,KB1,KB2,KB3,KR4,RHO,ETAMU,ETAML,PHIO,
  BETA1,BETA2,ALPHA1,ALPHA2,ALPHA3,ALPHA4,B2B,A4B,BR,BS,
  IR,IS,PSIU,PSIL,RER,RES,REU,REL,PHI,ARR,ARS,YR,YS,CU,CL,

```

1  
2



```

3      CH1MH2,CH3MH2,CH4MH3,CH1MH4,AH1MH2,AH3MH2,AH4MH3,AH1MH4,
4      BH1MH2,BH3MH2,BH4MH3,BH1MH4,CSUM,BSUM,ASUM,ROOT,PHIPR,PHIMR
1      COMMON R2R1,R3R1,R4R1,BRR1,BRR2,BRR3,R1R2,R1R3,R1R4,R3R4,BSR1,BSR4,
2      TORQUE,TAUR,OM,DELOM,LAMDAU,LAMDAL,LUBS,LLBR,ZETAU,ZETAL,
3      LMBDU,LMBDL
4      COMMON CP,CF
1      COMMON JJ,JJJ,K
2      COMMON/ ZETARE / YZ(9,11),XRZ(11),YSTRZ,NZR,IZ
3      COMMON/ LMDARE / YL(12),XRL(12),YSTRL,NRL
4      REU = (2.*BS/NU)*R1R3*(KB1/KB3)*OM*R1*PHI
1      ZETAU = FIG(REU)
2      LMBDU = FIG2(REU)
3      CU = 2.0*ZETAU+.5*LUBS*LMBDU
4      RETURN
END

```

C

```

SUBROUTINE EQG2
FINDS CL AND REL
REAL KB1,KB2,KB3,KB4,IR,IS,NU,LAMDAU,LAMDAL,LUBS,LLBR,LMBDU,LMBDL
COMMON R1,R2,R3,R4,KB1,KB2,KB3,KB4,RHO,ETAMU,ETAML,PHIO,
1      BETA1,BETA2,ALPHA1,ALPHA2,ALPHA3,ALPHA4,B2B,A4B,BR,BS,
2      IR,IS,PSIU,PSIL,RES,REU,REL,PHI,ARR,ARS,YR,YS,CU,CL,
3      CH1MH2,CH3MH2,CH4MH3,CH1MH4,AH1MH2,AH3MH2,AH4MH3,AH1MH4,
4      BH1MH2,BH3MH2,BH4MH3,BH1MH4,CSUM,BSUM,ASUM,ROOT,PHIPR,PHIMR
1      COMMON R2R1,R3R1,R4R1,BRR1,BRR2,BRR3,R1R2,R1R3,R1R4,R3R4,BSR1,BSR4,
2      TORQUE,TAUR,OM,DELOM,LAMDAU,LAMDAL,LUBS,LLBR,ZETAU,ZETAL,
3      LMBDU,LMBDL
4      COMMON CP,CF
1      COMMON JJ,JJJ,K
2      COMMON/ ZETARE / YZ(9,11),XRZ(11),YSTRZ,NZR,IZ
3      COMMON/ LMDARE / YL(12),XRL(12),YSTRL,NRL
4      REL = (2.*BR/NU)*OM*R1*PHI
1      LMBDL = FIG2(REL)
2      ZETAL = FIG(REL)
3      CL = 2.5*ZETAL+.5 * LLBR * LMBDL
4      RETURN
END

```

C  
C  
C

C



```

SUBROUTINE EQH5
C****
C      FINDS LAMBDA, ETA, AND PSI FOR THE LOWER PASSAGES
C
REAL KB1,KB2,KB3,KB4,IR,IS,NU,LAMDAU,LAMDAL,LUBS,LLBR,LMBDU,LMBDL
COMMON
1  BETAI,BETA2,ALPHA1,ALPHA2,ALPHA3,ALPHA4,B2B,A4B,BR,BS,
2  IR,IS,PSIU,PSIL,RER,RES,REU,REL,PHI,ARR,ARS,YR,YS,CU,CL,
3  CH1MH2,CH3MH2,CH4MH3,CH1MH4,CH1MH4,CH3MH2,AH4MH3,AH1MH4,
4  BH1MH2,BH3MH2,BH4MH3,BH1MH4,CSUM,BSUM,ROOT,PHIPR,PHIMR
COMMON R2R1,R3R1,R4R1,BRR1,BRBS,NU,R1R2,R1R3,R1R4,R3R4,BSR1,BSR4,
1  TORQUE,TAUR,OM,DELOM,LAMDAU,LAMDAL,LUBS,LLBR,ZETAU,ZETAL,
2  LMBDU,LMBDL
COMMON CP,CF
COMMON JJ,JJJ,K
C**** TAKING INTO ACCOUNT ABSOLUTE VALUE
BBBI = ABS(BETAI)
LAMDAL = CF*(TAN(BBBI))*LLBR/KB1
ETAML = 1.0 - LAMDAL
PSIL = 1.0 - (ETAML**2)
RETURN
END

```

```

SUBROUTINE EQH6
C****
C      FINDS LAMBDA, ETA, AND PSI FOR THE UPPER PASSAGES
C
REAL KB1,KB2,KB3,KB4,IR,IS,NU,LAMDAU,LAMDAL,LUBS,LLBR,LMBDU,LMBDL
COMMON
1  BETAI,BETA2,ALPHA1,ALPHA2,ALPHA3,ALPHA4,B2B,A4B,BR,BS,
2  IR,IS,PSIU,PSIL,RER,RES,REU,REL,PHI,ARR,ARS,YR,YS,CU,CL,
3  CH1MH2,CH3MH2,CH4MH3,CH1MH4,CH1MH4,CH3MH2,AH4MH3,AH1MH4,
4  BH1MH2,BH3MH2,BH4MH3,BH1MH4,CSUM,BSUM,ROOT,PHIPR,PHIMR
COMMON R2R1,R3R1,R4R1,BRR1,BRBS,NU,R1R2,R1R3,R1R4,R3R4,BSR1,BSR4,
1  TORQUE,TAUR,OM,DELOM,LAMDAU,LAMDAL,LUBS,LLBR,ZETAU,ZETAL,
2  LMBDU,LMBDL
COMMON CP,CF
COMMON JJ,JJJ,K
C**** TAKING INTO ACCOUNT ABSOLUTE VALUE
BBBI = ABS(BETAI)
LAMDAL = CF*(TAN(BBBI))*LLBR/KB1
ETAML = 1.0 - LAMDAL
PSIL = 1.0 - (ETAML**2)
RETURN
END

```





```

C
C
FUNCTION EQI8 (RE,AR,ANG1,ANG2)
CALCULATES THE LOSS COEFFICIENTS YR AND YS

REAL KB1,KB2,KB3,KB4,IR,IS,NU,LAMDAU,LAMDAL,LUBS,LLBR,LMBDU,LMBDL
COMMON R1,R2,R3,R4,KB1,KB2,KB3,KB4,RHO,ETAMU,ETAML,PHIO,BS,
BETA1,BETA2,ALPHA1,ALPHA2,ALPHA3,ALPHA4,B2B,A4B,BR,BS,
IR,IS,PSIU,PSIL,RER,RES,REU,REL,PHI,ARR,ARS,YR,YS,CU,CL,
CH1MH2,CH3MH2,CH4MH3,CH1MH4,CH2MH4,CH3MH4,CH4MH4,AH1MH2,AH3MH2,AH4MH3,AH1MH4,
BH1MH2,BH3MH2,BH4MH3,BH1MH4,CSUM,BSUM,ASUM,ROOT,PHIPR,PHIMR
COMMON R2R1,R3R1,R4R1,BRR1,BRR2,R1R2,R1R3,R1R4,R3R4,BSR1,BSR4,
TORQUE,TAUR,OM,DELOM,LAMDAU,LAMDAL,LUBS,LLBR,ZETAU,ZETAL,
LMBDU,LMBDL
COMMON CP,CF
COMMON JJ,JJJ,K

C**** TAKING INTO ACCOUNT ABSOLUTE VALUE
DELANG = ABS(ANG1 - ANG2)
DELBE = DELANG*180./3.1416
PSI = .99 - 2.28 * DELBE/(10.0**4) - 4.97/(180. - DELBE)
EQI8 = ((.975+.075/AR)/(PSI**2)-1.) * (((10.0**5)/RE)**.25)
RETURN
END

```

```

C
C
FUNCTION ENRER (PHI1)
CALCULATES THE REYNOLDS NUMBER OF THE ROTOR

REAL KB1,KB2,KB3,KB4,IR,IS,NU,LAMDAU,LAMDAL,LUBS,LLBR,LMBDU,LMBDL
COMMON R1,R2,R3,R4,KB1,KB2,KB3,KB4,RHO,ETAMU,ETAML,PHIO,BS,
BETA1,BETA2,ALPHA1,ALPHA2,ALPHA3,ALPHA4,B2B,A4B,BR,BS,
IR,IS,PSIU,PSIL,RER,RES,REU,REL,PHI,ARR,ARS,YR,YS,CU,CL,
CH1MH2,CH3MH2,CH4MH3,CH1MH4,CH2MH4,CH3MH4,CH4MH4,AH1MH2,AH3MH2,AH4MH3,AH1MH4,
BH1MH2,BH3MH2,BH4MH3,BH1MH4,CSUM,BSUM,ASUM,ROOT,PHIPR,PHIMR
COMMON R2R1,R3R1,R4R1,BRR1,BRR2,R1R2,R1R3,R1R4,R3R4,BSR1,BSR4,
TORQUE,TAUR,OM,DELOM,LAMDAU,LAMDAL,LUBS,LLBR,ZETAU,ZETAL,
LMBDU,LMBDL
COMMON CP,CF
COMMON JJ,JJJ,K

C
C
X1 = (2.*BRR1*PHI1*OM*R1**2)/NU
TAKING INTO ACCOUNT ABSOLUTE VALUE
ABB1 = ABS(TAN(BETA1) - TAN(B2B))
X2 = BRR1*ABB1 * (COS(BETA1)**2)
X3 = .425*(R2R1 - 1.0)
ENRER = X1/(COS(BETA1) + X2/X3)
RETURN

```



END

FUNCTION ENRES (PHI1)

CALCULATES THE REYNOLDS NUMBER OF THE STATOR

```

REAL KB1,KB2,KB3,KB4,IR,IS,NU,LAMDAU,LAMDAL,LUBS,LLBR,LLBDU,LMBDL
COMMON R1,R2,R3,R4,KB1,KB2,KB3,KB4,RHO,ETAMU,ETAML,PHIO,
      BETAI,BETA2,ALPHA1,ALPHA2,ALPHA3,ALPHA4,B2B,A4B,BR,BS,
      IR,IS,PSIU,PSIL,REU,REL,PHI,ARR,ARS,YR,YS,CU,CL,
      CH1MH2,CH3MH2,CH4MH3,CH1MH4,AH1MH2,AH3MH2,AH4MH3,AH1MH4,
      BH1MH2,BH3MH2,BH4MH3,BH1MH4,CSUM,BSUM,ASUM,ROOT,PHIPR,PHIMR
COMMON R2R1,R3R1,R4R1,BRRI,BRBS,NU,R1R2,R1R3,R1R4,R3R4,BSR1,BSR4,
      TORQUE,TAUR,OM,DELOM,LAMDAU,LAMDAL,LUBS,LLBR,ZETAU,ZETAL,
      LMBDU,CP,CF
COMMON JJ,JJJ,K

```

```

X1 = (2.*BS*CN*PHI1*R1*R1R3*KB1/KB3)/NU
      TAKING INTO ACCOUNT ABSOLUTE VALUE
AA43B = ABS(TAN(A4B) - TAN(ALPHA3))
X2 = BS*AA43B*(COS(ALPHA3)**2)
X3 = .425*R4R1*R1*(R3R4-1.0)
ENRES = X1/(COS(ALPHA3) + X2/X3)
      RETURN
      END

```

SUBROUTINE EQE28

CALCULATES COEFFICIENTS OF (H1 - H2)/(OMEGA \* R1)\*\*2

```

REAL KB1,KB2,KB3,KB4,IR,IS,NU,LAMDAU,LAMDAL,LUBS,LLBR,LLBDU,LMBDL
COMMON R1,R2,R3,R4,KB1,KB2,KB3,KB4,RHO,ETAMU,ETAML,PHIO,
      BETAI,BETA2,ALPHA1,ALPHA2,ALPHA3,ALPHA4,B2B,A4B,BR,BS,
      IR,IS,PSIU,PSIL,REU,REL,PHI,ARR,ARS,YR,YS,CU,CL,
      CH1MH2,CH3MH2,CH4MH3,CH1MH4,AH1MH2,AH3MH2,AH4MH3,AH1MH4,
      BH1MH2,BH3MH2,BH4MH3,BH1MH4,CSUM,BSUM,ASUM,ROOT,PHIPR,PHIMR
COMMON R2R1,R3R1,R4R1,BRRI,BRBS,NU,R1R2,R1R3,R1R4,R3R4,BSR1,BSR4,
      TORQUE,TAUR,OM,DELOM,LAMDAU,LAMDAL,LUBS,LLBR,ZETAU,ZETAL,
      LMBDU,CP,CF
COMMON JJ,JJJ,K

```

```

X1 = (1.0 - (COS(IR)**2))/(COS(BETA2)**2)
CH1MH2 = 1.0
BH1MH2 = TAN(BETAI) - (KB1/KB3)*ETAMU*TAN(ALPHA3)

```



```

AH1MH2 = -YR/(2.*COS(BETA1)**2) - ((R1R2*KB1/KB2)**2)*X1*0.5
RETURN
END

```

# SUBROUTINE EQF12

CALCULATES COEFFICIENTS OF (H3 - H2)/(OMEGA \* R1)\*\*2

```

REAL KB1,KB2,KB3,KB4,IR,IS,NU,LAMDAU,LAMDAL,LUBS,LLBR,LMBDU,LMBDL
COMMON R1,R2,R3,R4,KB1,KB2,KB3,KB4,RHO,ETAMU,ETAML,PHIO,
1 BETAL,BETA2,ALPHA1,ALPHA2,ALPHA3,ALPHA4,B2B,A4B,BR,BS,
2 IR,IS,PSIU,PSIL,RES,REU,REL,PHI,ARR,ARS,YR,YS,CU,CL,
3 CH1MH2,CH3MH2,CH4MH3,CH1MH4,AH1MH2,AH3MH2,AH4MH3,AH1MH4,
4 BH1MH2,BH3MH2,BH4MH3,BH1MH4,CSUM,BSUM,ASUM,ROOT,PHIPR,PHIMR
1 COMMON R2R1,R3R1,R4R1,BRR1,BRRS,NU,R1R2,R1R3,R1R4,R3R4,BSR1,BSR4,
2 TORQUE,TAUR,OM,DELON,LAMDAU,LAMDAL,LUBS,LLBR,ZETAU,ZETAL,
3 LMBDU,LMBDL
COMMON CP,CF
COMMON JJ,JJJ,K
X1 = (KB1/KB3)*TAN(ALPHA3)
CH3MH2 = 0.0
BH3MH2 = 0.0
AH3MH2 = 0.5*((R1R2**2)*(CU * ((KB1/KB2)**2)+PSIU*(X1**2))
RETURN
END

```

# SUBROUTINE EQE13A

CALCULATES COEFFICIENTS OF (H4 - H3)/(OMEGA \* R1)\*\*2

```

REAL KB1,KB2,KB3,KB4,IR,IS,NU,LAMDAU,LAMDAL,LUBS,LLBR,LMBDU,LMBDL
COMMON R1,R2,R3,R4,KB1,KB2,KB3,KB4,RHO,ETAMU,ETAML,PHIO,
1 BETAL,BETA2,ALPHA1,ALPHA2,ALPHA3,ALPHA4,B2B,A4B,BR,BS,
2 IR,IS,PSIU,PSIL,RES,REU,REL,PHI,ARR,ARS,YR,YS,CU,CL,
3 CH1MH2,CH3MH2,CH4MH3,CH1MH4,AH1MH2,AH3MH2,AH4MH3,AH1MH4,
4 BH1MH2,BH3MH2,BH4MH3,BH1MH4,CSUM,BSUM,ASUM,ROOT,PHIPR,PHIMR
1 COMMON R2R1,R3R1,R4R1,BRR1,BRRS,NU,R1R2,R1R3,R1R4,R3R4,BSR1,BSR4,
2 TORQUE,TAUR,OM,DELON,LAMDAU,LAMDAL,LUBS,LLBR,ZETAU,ZETAL,
3 LMBDU,LMBDL
COMMON CP,CF
COMMON JJ,JJJ,K
X1 = ((1.-(COS( IS)**2))/2.)* ((R1R4)**2)
X2 = (R1R3*(KB1/KB3)/(COS(ALPHA3))**2)

```



```

CH4MH3 = X1*(ETAML**2)
BH4MH3 = X1*2.*TAN(BETA1)*(ETAML**2)
AH4MH3 = X1*((KB1/KB4)**2)+(TAN(BETA1)**2))+.5*YS*X2
RETURN
END

```

#### SUBROUTINE EQD9

CALCULATES COEFFICIENTS OF  $(H1 - H4)/(\Omega * R1)**2$

```

REAL KB1,KB2,KB3,KB4,IR,IS,NU,LAMDAU,LAMDAL,LUBS,LLBR,LMBDU,LMBDL
COMMON R1,R2,R3,R4,KB1,KB2,KB3,KB4,RHO,ETAMU,ETAML,PHIO,
      BETA1,BETA2,ALPHA1,ALPHA2,ALPHA3,ALPHA4,B2B,A4B,BR,BS,
      IR,IS,PSIU,PSIL,RER,RES,REU,REL,PHI,ARR,ARS,YR,YS,CU,CL,
      CH1MH2,CH3MH2,CH4MH3,CH1MH4,AH1MH2,AH3MH2,AH4MH3,AH1MH4,
      BH1MH2,BH3MH2,BH4MH3,BH1MH4,CSUM,BSUM,ASUM,ROOT,PHIPR,PHIMR
COMMON R2R1,R3R1,R4R1,BRBS,NU,R1R2,R1R3,R1R4,R3R4,BSR1,BSR4,
      TORQUE,TAUR,OM,DELOM,LAMDAU,LAMDAL,LUBS,LLBR,ZETAU,ZETAL,
      LMBDU,LMBDL
COMMON CP,CF
COMMON JJ,JJJ,K
X1 = (R1R4)**2
CH1MH4 = .5*PSIL*X1
BH1MH4 = PSIL*X1*TAN(BETA1)
AH1MH4 = X1*.5*((CL*((KB1/KB4)**2)+PSIL*(TAN(BETA1)**2)))
RETURN
END

```

#### SUBROUTINE PHITES

ACCOMPLISHES THE FINAL ITERATION STEP IN DETERMINING PHI

```

REAL KB1,KB2,KB3,KB4,IR,IS,NU,LAMDAU,LAMDAL,LUBS,LLBR,LMBDU,LMBDL
COMMON R1,R2,R3,R4,KB1,KB2,KB3,KB4,RHO,ETAMU,ETAML,PHIO,
      BETA1,BETA2,ALPHA1,ALPHA2,ALPHA3,ALPHA4,B2B,A4B,BR,BS,
      IR,IS,PSIU,PSIL,RER,RES,REU,REL,PHI,ARR,ARS,YR,YS,CU,CL,
      CH1MH2,CH3MH2,CH4MH3,CH1MH4,AH1MH2,AH3MH2,AH4MH3,AH1MH4,
      BH1MH2,BH3MH2,BH4MH3,BH1MH4,CSUM,BSUM,ASUM,ROOT,PHIPR,PHIMR
COMMON R2R1,R3R1,R4R1,BRBS,NU,R1R2,R1R3,R1R4,R3R4,BSR1,BSR4,
      TORQUE,TAUR,OM,DELOM,LAMDAU,LAMDAL,LUBS,LLBR,ZETAU,ZETAL,
      LMBDU,LMBDL
COMMON CP,CF
COMMON JJ,JJJ,K

```

THE PREVIOUS FOUR SUBROUTINES ARE NOW ADDED







```

C      CSUM = CH1MH2 - CH3MH2 - CH4MH3 - CH1MH4
C      BSUM = BH1MH2 - BH3MH2 - BH4MH3 - BH1MH4
C      ASUM = AH1MH2 - AH3MH2 - AH4MH3 - AH1MH4
C      THE QUADRATIC EQUATION IS NOW SOLVED TO YIELD THE NEW VALUE OF PHI.
C      ROOT = SQRT((BSUM**2) - 4.0*ASUM*CSUM)
C      PHIPR = (-BSUM + ROOT)/(2.0*ASUM)
C      PHIMR = (-BSUM - ROOT)/(2.0*ASUM)
C      IF PHI IS NEGATIVE, CASE A IS NOT TAKING PLACE
C      TESTING FOR THE PROPER ROOT
C      JJ = 0
C      JJJ = 0
C      IF (PHIMR.LT. 0.0) GO TO 2
C      IF (PHIMR.GT. 0.0) GO TO 5
C      IF (PHIPR.LT. 0.0) GO TO 15
C      IF (PHIPR.GT. 0.0) GO TO 6
C      PHI = PHIMR
C      GO TO 80
C      PRINT 20
C      PHIPR = PHIPR
C      PRINT 90, PHI, PHIMR, PHIPR
C      FORMAT(IH0,3X,'PHI=',F10.5,3X,'PHIMR=',F10.5,' PHIPR =',F10.5)
C      20 FORMAT(IH0,' BOTH ROOTS OF PHI ARE NEGATIVE, AND THE PROGRAM WILL BE
1      CUMPED*****')
1      IF (PHI.LT. 0.0) JJJ = 1
1      IF (JJJ.EQ. 1) GO TO 10
1      IF (JJJ.EQ. 1) GO TO 10
1      RETURN
10      PRINT 11, JJ, JJJ
11      FORMAT(IH0,'JJ = ',15,'JJJ = ',15)
11      RETURN
11      END

C*****
C      FUNCTION EQ219.(PHI)
C      CALCULATES TAUR COEFFICIENTS
C
REAL KB1, KB2, KB3, KB4, IR, IS, NU, LAMDAU, LAMDAL, LUBS, LLBR, LMBDU, LMBDL
COMMON R1, R2, R3, R4, KB1, KB2, KB3, KB4, RHO, ETAMU, ETAML, PHIO,
BETA1, BETA2, ALPHA1, ALPHA2, ALPHA3, ALPHA4, B2B, A4B, BR, BS,
IR, IS, PSI, PSI, PSI, PSI, REU, RES, REU, REL, PHI, ARR, ARS, YR, YS, CU, CL,
CH1MH2, CH3MH2, CH4MH3, CH1MH4, CSUM, BSUM, ASUM, ROOT, PHIPR, PHIMR,
BH1MH2, BH3MH2, BH4MH3, BH1MH4, CSUM, BSUM, ASUM, ROOT, PHIPR, PHIMR,
COMMON R2R1, R3R1, R4R1, BR1, BR2, BR3, NU, R1R2, R1R3, R1R4, R3R4, BSR1, BSR4,
TORQUE, TAUR, OM, DELOM, LAMDAU, LAMDAL, LUBS, LLBR, ZETAU, ZETAL,
LMEDU, LMBDL
COMMON CP, CF
COMMON JJ, JJJ, K
C

```



```
EQB19 = PHII + (PHII**2)*(TAN(BETA1)- ETAMU * KB1/KB3*TAN(ALPHA3))
RETURN
END
```

```
C*****
SUBROUTINE EQB20
CALCULATES TORQUE
```

```
REAL KB1,KB2,KB3,KB4,IR,IS,NU,LAMDAU,LAMDAL,LUBS,LLBR,LMBDU,LMBDL
COMMON
1 BETAI,BETA2,ALPHA1,ALPHA2,ALPHA3,ALPHA4,B2B,A4B,BR,BS,
2 IR,IS,PSIU,PSIL,RER,RES,REU,REL,PHI,AH3MH2,AH4MH3,AH1MH4,
3 CH1MH2,CH3MH2,CH4MH3,BH1MH2,BH3MH2,BH4MH3,CSUM,BSUM,ASUM,ROOT,PHIPR,PHIMR
4 COMMON R2R1,R3R1,R4R1,BRR1,BRRS,NU,R1R2,R1R3,R1R4,R3R4,BSR1,BSR4,
1 TORQUE,TAUR,OM,DELOM,LAMDAU,LAMDAL,LUBS,LLBR,ZETAU,ZETAL,
2 LMBDU,LMBDL
COMMON CP,CF
COMMON JJ,JJ,K
```

```
C
TORQUE = 2.*3.1416*RHO*(OM**2)*(R1**5)*(BRR1)* TAUR
RETURN
END
```

```
SUBROUTINE NONDEM
```

```
ACCOMPLISHES THE NON-DIMENSIONALIZATION
```

```
REAL KB1,KB2,KB3,KB4,IR,IS,NU,LAMDAU,LAMDAL,LUBS,LLBR,LMBDU,LMBDL
COMMON
1 BETAI,BETA2,ALPHA1,ALPHA2,ALPHA3,ALPHA4,B2B,A4B,BR,BS,
2 IR,IS,PSIU,PSIL,RER,RES,REU,REL,PHI,AH3MH2,AH4MH3,AH1MH4,
3 CH1MH2,CH3MH2,CH4MH3,BH1MH2,BH3MH2,BH4MH3,CSUM,BSUM,ASUM,ROOT,PHIPR,PHIMR
4 COMMON R2R1,R3R1,R4R1,BRR1,BRRS,NU,R1R2,R1R3,R1R4,R3R4,BSR1,BSR4,
1 TORQUE,TAUR,OM,DELOM,LAMDAU,LAMDAL,LUBS,LLBR,ZETAU,ZETAL,
2 LMBDU,LMBDL
```

```
COMMON JJ,JJ,K
COMMON TORREF,PIOM,PITORQ,PIPOWR,OMMAX
PIOM = CN/OMMAX
PITORQ = TORQUE/TORREF
PIPOWR = (OM*TORQUE)/POWREF
PIPHI = PHI*PIOM
PRINT 600,PIOM
PRINT 605,PIPOWR
PRINT 609,PITORQ
```



```

600 PRINT 611, PIPHI, 'THE DIMENSIONLESS ROTATIONAL SPEED=', F6.3)
605 FORMAT(1H0,15X, 'THE DIMENSIONLESS POWER =', F16.3)
609 FORMAT(1H0,15X, 'THE DIMENSIONLESS TORQUE =', F15.3)
611 FORMAT(1H0,15X, 'THE REVISED FLOW COEFFICIENT =', F9.3)
      RETURN
      END

      FUNCTION FIG( RE )

      COMMON/ ZETARE / YZ(9,11),XRZ(11),YSTRZ,NZR,IZ

      THE BENDING LOSS COEFFICIENT IS APPROXIMATED FOR IN THIS SUBROUTINE
      AN ALTERNATE CHOICE TO EMPLOY WOULD BE TO USE A CURVE FIT ON FIGURE 15.

```

```

C      FUNCTION FIG( RE )
C
C      COMMON/ ZETARE / YZ(9,11),XRZ(11),YSTRZ,NZR,IZ
C
C      THE BENDING LOSS COEFFICIENT IS APPROXIMATED FOR IN THIS S
C      AN ALTERNATE CHOICE TO EMPLOY WOULD BE TO USE A CURVE FIT
C
10    J=1
        IF(RE .LE. XRZ(J)) GO TO 20
        J=NZR
        IF(RE .GE. XRZ(J)) GO TO 20
        J=1
        IF(RE .EQ. XRZ(J)) GO TO 20
        IF(RE .LT. XRZ(J+1)) GO TO 25
        J=J + 1
        IF( J .LT. NZR ) GO TO 10
        GO TO 30
20    Y = YZ( IZ,J) + (YZ( IZ,J+1) - YZ( IZ,J))*(RE - XRZ(J))/
25    (XRZ(J+1) - XRZ(J))
30    FIG = Y*YSTRZ
        RETURN
        END

```

```

C C C C C C C C
FUNCTION FIG2( RE )

THE FRICTION FACTOR IS APPROXIMATED IN THIS SUBROUTINE. THE VALUES ARE
GIVEN IN THE BLOCK DATA OBTAINED FROM FIGURE 16. THIS IS APPROXIMATE
SINCE IT IS ONLY TO THE NEAREST VALUE OF REYNOLDS NUMBERS.
AN ALTERNATE CHOICE TO EMPLOY WOULD BE TO USE A CURVE FIT ON FIGURE 16.

COMMON/ LMDARE / YL(12), XRL(12), YSTRL,NRL

J = 1
IF(RE .LE. XRL(J)) GO TO 20
J = NRL
IF(RE .GE. XRL(J)) GO TO 20

```



```

10 J=RE
    IF(RE .EQ. XRL(J)) GO TO 20
    IF(RE .LT. XRL(J+1)) GO TO 25
    J=J+1
    IF(J .LT. NRL) GO TO 10
    Y=YL(J)
    GO TO 30
25 Y=YL(J) + (YL(J+1) - YL(J))*(RE - XRL(J))/(XRL(J+1) - XRL(J))
30 FIG2=Y*YSTRL
    RETURN
    END

```

#### SUBROUTINE VALUE

THIS SUBROUTINE ACCOMPLISHES THE FLOW ANALYSIS. ANY MODIFICATIONS TO THE DESIRED OUTPUT SHOULD PROBABLY BE MADE IN THIS SUBROUTINE. SINCE THE FLOW COEFFICIENT IS ALREADY KNOWN, ANY VALUES IN TERMS OF PHI OR GEOMETRIC PARAMETERS CAN NOW BE EVALUATED.

```

COMMON R1,R2,R3,KB1,KB2,KB3,KB4,IR,IS,NU,LAMDAU,LAMDAL,LUBS,LLBR,LMBDU,LMBDL
      BETAI,BETA2,ALPHA1,ALPHA2,ALPHA3,ALPHA4,B2B,A4B,BR,BS,
      IR,IS,PSIU,PSIL,RER,RES,REU,REL,PHI,ARR,ARS,YR,YS,CU,CL,
      CH1MH2,CH3MH2,CH4MH3,CH1MH4,CH1MH2,AH3MH2,AH4MH3,AH1MH4,
      BH1MH2,BH3MH2,BH4MH3,BH1MH4,CSUM,BSUM,ROOT,PHIPR,PHIMR,
      COMMON R2R1,R3R1,R4R1,BRR1,BRRS,NU,R1R2,R1R3,R1R4,R3R4,BSR1,BSR4,
      TORQUE,TAUR,OM,DELOM,LAMDAU,LAMDAL,LUBS,LLBR,ZETAU,ZETAL,
      LMBDU,LMBDL

```

#### VELOCITIES

```

R2R3 = R2R1*R1R3
R3R2 = 1./R2R3
VM1 = OM*R1*PHI + PHI*TAN(BETAI)
VU1 = OM*R1*(1.**2 + VM1**2)
VM4 = VM1*R1R4**BRBS**KB1/KB4
VU4 = ETAML*R1R4**VU1
V4 = SQRT(VU4**2 + VM4**2)
VM3 = VM1*PIR2*BRBS**KB1*R2R3/K33
VU3 = VM3*TAN(ALPHA3)
V3 = SQRT(VU3**2 + VM3**2)
VM2 = VM1*R1R2**KB1/KB2
VU2 = ETAMU*R3R2**VU3
V2 = SQRT(VU2**2 + VM2**2)
W1 = VM1/COS(BETAI)
W2 = VM2/COS(BETA2)

```









```

757 FORMAT(1H0,' THE DIMENSIONLESS ENERGY CHANGES OVER EACH COMPONENT
1T,')
758 FORMAT(1H0,' (H1-H2)/(OM*R2)**2 = ', F13.2)
759 FORMAT(1H0,' (H1-H4)/(OM*R2)**2 = ', F13.2)
760 FORMAT(1H0,' (H4-H3)/(OM*R2)**2 = ', F13.2)
761 FORMAT(1H0,' (H3-H2)/(OM*R2)**2 = ', F13.2)
763 FORMAT(1H0,' DIMENSIONLESS ENERGY INPUT = ', F6.2)
764 FORMAT(1H0,' DIMENSIONLESS ROTOR LOSS = ', F9.2)
      RETURN
      END

```

# BLOCK DATA

THIS DATA IS OBTAINED FROM FIGURE 15. IT REPRESENTS THE VALUE OF THE BENDING LOSS COEFFICIENT FOR VARIOUS VALUES OF TURNING RATIOS AND REYNOLDS NUMBERS

COMMON/	ZETARE	/	YZ(0,11)	XRZ(11)	YSTRZ	NZR	IZ
DATA YZ/1.00,	925,	780,	680,	600,	530,	470,	410,
1	844,	760,	624,	540,	450,	384,	333,
2	747,	663,	532,	455,	375,	321,	275,
3	680,	595,	472,	394,	330,	285,	243,
4	632,	542,	429,	350,	296,	260,	225,
5	545,	456,	364,	289,	250,	227,	201,
6	483,	415,	330,	264,	235,	213,	195,
7	445,	390,	309,	250,	225,	204,	185,
8	450,	400,	315,	258,	225,	200,	180,
9	490,	430,	332,	270,	230,	200,	180,
A	500,	440,	340,	272,	232,	200,	180,
B	XRZ/2,	EO4,	4.6,	EO4,	8.8,	EO4,	1.5,
C	4.6,	EO5,	8.8,	EO5,	7.1,	EO5,	1.5,
END							

# BLOCK DATA

THIS DATA IS OBTAINED FROM FIGURE 16, AND ARE THE VALUES OF THE FRICTION FACTOR AT VARIOUS REYNOLDS NUMBERS.

COMMON/	LMDARE	/	YL(12)	XRL(12)	YSTRL	NRL
DATA YL/	0.265,	0.233,	0.218,	0.204,	0.193,	0.185,
1	0.148,	0.141,	0.137,	0.137,	0.137,	0.137,
2	1.5,	EO5,	2.2,	EO5,	3.3,	EO5,
3	YSTRL/1.0,	NRL/12/				
END						



## REFERENCES

1. Naval Air Engineering Center, Engineering Department (SI) Report Misc-08998, Theoretical Performance of Programmed Drum Arresting Gear, by William Clark, 1 July 1970.
2. Vavra, M. H., Energy Absorber, April 1970.
3. Vavra, M. H., Aero-Thermodynamics and Flow in Turbomachines. New York: John Wiley and Sons, 1960.
4. Horlock, J.H., Journal of the Institute of Mechanical Science, Vol. 2, p. 48-75, 1960.
5. Zweifel, O., "The Spacing of Turbomachine Bladings", Brown Boveri Company Review, December, 1945.
6. Sprenger, H., Schweiz Bauzeitung, 87th year, no. 13, p. 223-231, 1969.
7. Biolley, A., Schweiz Bauzeitung, Vol. 118, no. 8, p. 85-86, 1941.



# INITIAL DISTRIBUTION LIST

	No. Copies
1. Defense Documentation Center Cameron Station Alexandria, Virginia 22314	2
2. Library, Code 0212 Naval Postgraduate School Monterey, California 93940	2
3. Professor T. H. Gawain, Code 57Gn Department of Aeronautics Naval Postgraduate School Monterey, California 93940	2
4. Chairman, Code 57 Department of Aeronautics Naval Postgraduate School Monterey, California 93940	1
5. Assoc. Professor R. D. Zucker, Code 57Zu Department of Aeronautics Naval Postgraduate School Monterey, California 93940	1
6. Professor M. H. Vavra, Code 57Va Department of Aeronautics Naval Postgraduate School Monterey, California 93940	5
7. ENS Leo S. Rolek, Jr. USN 9808 Avenue J Chicago, Illinois 60617	1





## DOCUMENT CONTROL DATA - R &amp; D

(Security classification of title, body of abstract and indexing annotation must be entered when the overall report is classified)

ORIGINATING ACTIVITY (Corporate author)

Naval Postgraduate School  
Monterey, California 93940

2a. REPORT SECURITY CLASSIFICATION

Unclassified

2b. GROUP

REPORT TITLE

Performance Analysis of a Turbo-Type Energy Absorber for an Aircraft Carrier  
Arresting Gear

DESCRIPTIVE NOTES (Type of report and, inclusive dates)

Master's Thesis; June 1971

AUTHOR(S) (First name, middle initial, last name)

Leo S. Rolek, Jr.

REPORT DATE

June 1971

7a. TOTAL NO. OF PAGES

132

7b. NO. OF REFS

7

CONTRACT OR GRANT NO.

9a. ORIGINATOR'S REPORT NUMBER(S)

PROJECT NO.

9b. OTHER REPORT NO(S) (Any other numbers that may be assigned  
this report)

DISTRIBUTION STATEMENT

Approved for public release; distribution unlimited.

SUPPLEMENTARY NOTES

12. SPONSORING MILITARY ACTIVITY

Naval Postgraduate School  
Monterey, California 93940

ABSTRACT

The increasing weight and speed of carrier based aircraft are taxing the limit of conventional piston type energy absorbers which are used for arresting gear. Turbo-type absorbers have been proposed as an alternative. This study investigates a turbo-type energy absorber for an aircraft arresting gear under development by the Naval Air Engineering Center. A mathematical analysis, computer simulation and performance prediction are given for each mode of operation. It was initially expected that the absorber could operate in just two modes, forward and reverse, but the analysis shows that four distinct modes are possible, since not only shaft rotation but the path of fluid flow can be reversed. Theoretical performance predictions are also compared with test data from an existing smaller scale version of the absorber. The agreement is excellent. An approximation of scaling effects on power absorption is also presented. It is concluded that the turbo-type absorber is basically adequate to meet the demands of carrier operation for the foreseeable future.



### KEY WORDS

turbo-type energy absorber

resting gear

[illegible]



Thesis  
R68945  
c.1

Rolek

Performance analysis  
of a turbo-type energy  
absorber for an air-  
craft carrier arresting  
gear.

128616

Thesis  
R68945  
c.1

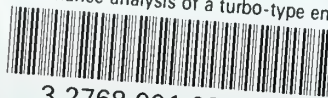
Rolek

Performance analysis  
of a turbo-type energy  
absorber for an air-  
craft carrier arresting  
gear.

128616

thesR68945

Performance analysis of a turbo-type ene



3 2768 001 98109 5

DUDLEY KNOX LIBRARY